

Carbon quantum dots for bioimaging cells and tissues

A thesis submitted in fulfillment of the requirements for the
degree of

Doctor of Philosophy

By

Karthiga Anpalagan

College of Engineering and Science

Victoria University

January 2023



**VICTORIA
UNIVERSITY**

MELBOURNE AUSTRALIA

College of Engineering and Science

Abstract

Bioimaging is an innovative technique in research and clinical settings that has a lot of significance in today's world. It is an optical form of biosensing used to create visual representations of biological processes in cells, tissues, and anatomy that enable more accurate diagnosis and treatment of diseases. The fluorescent probes such as organic fluorophores, which include dyes and proteins are commercially in use. For example, Rhodamine 6G is one of the better ones which exhibits a quantum yield value of 80%. The photoluminescence efficiency is termed as quantum yield, and it is defined by the ratio of the number of photons emitted to the number of photons absorbed. Although quantum yield is high, fluorescent dyes are prone to photobleaching and have less photostability. As a result, their brightness degrades with time, and they possess very low resistance to change under the influence of light. Moreover, the biocompatibility of organic fluorophores is very low, and they are toxic to live cells. These shortcomings make them inappropriate for long-term bioimaging. Therefore, research is now focused on discovering new fluorescent probes with better biocompatibility, good photostability, and low cytotoxicity. As commercial fluorescent probes are expensive, non-environment-friendly, and require professional handling, new fluorescent probes fabricated via facile, cost-effective, and green synthesis routes are fast becoming appealing alternatives.

One such emerging technology platform is carbon quantum dots (CQDs), which are increasingly used in cell bioimaging. These fascinating nanoscale semiconductors possess useful characteristics, such as tunable photoluminescence, biocompatibility, solubility, chemical stability, photostability, and resistance to photobleaching, which potentially make them better fluorescent probes. Generally, CQDs are fabricated from

chemical-based precursors and natural resources through various fabrication methods that involve multiple steps for neutralization, surface passivation, and doping. The long fabrication processes consume a lot of energy, time, and cost. The addition of organic and inorganic chemicals during the fabrication process is very common and this is mainly for the purpose of obtaining better quantum yield. However, the usage of chemicals curtails the biocompatibility of the CQDs and limits their application in bioimaging.

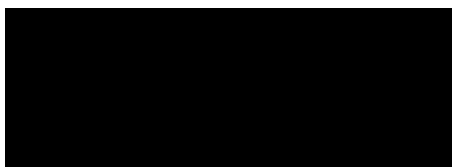
In order to overcome the above-mentioned gaps, this research focused on the fabrications of biocompatible CQDs from a very common edible resource, namely bread. Bread is the third-highest food wastage contributor to climate change. In this study all the fabrications of CQDs were performed completely chemical-free. A novel thermolysis synthesis route namely the toasting method was introduced for the first time to derive CQDs from bread. Our CQDs exhibited excitation tunable emission and low cytotoxicity. These biocompatible CQDs were successfully utilized in bioimaging C2C12 mouse muscle myoblasts cell lines and differentiated myotubes. This study verified that fluorescent CQDs with bioimaging capabilities can be fabricated in the absence of chemicals. When the C2C12 myotubes were allowed to differentiate in the presence of CQDs at 1mg/mL concentration, a delay in myotube formation was observed. This effect was tracked by bioimaging the differentiation at various time points and studied using western blotting. The alteration of the transcription factors and myosin heavy chain (MHC) in the presence of CQDs confirmed the influence. The cytotoxicity was assessed prior to the bioimaging and observed more than 95 % of cell viability even at 1.5 mg/mL concentration. This concentration was nearly 1000 times higher than the concentration, required for cell labelling and generally used in cell viability assays. Hence, it was shown that the CQDs from edible precursors are safe for

bioimaging even at high concentrations. However, our observation suggested further work is required to study the impact of CQDs on cellular functions prior to long-term live cell or *in vivo* bioimaging.

The efficacy of the toasting method was compared with the standard and commonly used hydrothermal technique. The experiment was expanded in this chapter by including two more types of bread. White bread, whole meal bread, and mixed grain bread were used to produce CQDs through two fabrication routes. The CQDs fabricated from both techniques were able to cross cell membranes and were capable of bioimaging colon cancer cell lines, namely CT-26 and HT-29, derived from mice and humans, respectively. The facile, cost-effective, and time-efficient toasting method doesn't require sophisticated equipment but produced comparable CQDs to the hydrothermal technique. Even though all the CQDs were fluorescent, CQDs derived from whole-meal bread displayed the highest quantum yield of 0.81%. This quantum yield was achieved via a sustainable and chemical-free synthesis route. To further enhance this quantum yield and improve its performance, green routes were used instead of traditional methods that include chemicals. Soybean flour and lemon juice were adequate to enhance the quantum yield up to 2.31%. It is an approximately fourfold increment that was achieved without any chemical additives. This study evidently improved the application of CQDs in bioimaging via sustainable production with a focus on green engineering.

Declaration by author

I, Karthiga Anpalagan, declare that the Ph.D. thesis entitled “Carbon quantum dots for bioimaging of cells and tissues” is no more than 80,000 words in length including quotes and exclusive of tables, figures, appendices, bibliography, references, and footnotes. This thesis contains no material that has been submitted previously, in whole or in part, for the award of any other academic degree or diploma. Except where otherwise indicated, this thesis is my own work. I have conducted my research in alignment with the Australian Code for the Responsible Conduct of Research and Victoria University’s Higher Degree by Research Policy and Procedures.

A solid black rectangular box used to redact the author's signature.

Signature

21/01/2023

Date

Acknowledgments

I would like to express my sincere gratitude to my principal supervisor A/Prof. Daniel T H Lai for his professional guidance and constant encouragement throughout this doctoral research. This thesis would not have been possible without his amazing mentoring, motivation, and prompt feedback. I am also thankful to my associate supervisor Prof. Kulmira Nurgali for her support and advice. My sincere appreciation goes to Dr. Jimsheena Valyakath Karakkat for her valuable assistance in cell culture and imaging. Thanks also due to Prof. Paul Joseph for his expert advice and timely help.

I greatly acknowledge the technical team consists of Stacey Llyod, Melinda Tagiwasa, Larruceo Bautista, Nishantha Illangantilaka, Charmaine DiQuattro, Chathuri Piyadasa, Mary Marshall, and Valentina Jovanovska for providing me with laboratory inductions, equipment training, and technical support during my research. I'm grateful to my collaborators Prof. Ivan Cole, Adam Truskewycz, and Hong Yin from RMIT University and Tian Zhang from Monash University for their support in characterization facilities.

I express my profound gratefulness for my past and present teachers from Ganapathy kindergarten, Valvai Magalir primary school, Hindu Ladies College, University of Colombo, Sri Lanka, and Victoria University, Melbourne. I also acknowledge all the administration, library, and support staffs of Victoria University who made my journey pleasant. I would like to thank the funding support of the Defense Science Institute (DSI) Collaborative Research Grant (#CR-0030) for their partial support in this research project.

This endeavor would not have been possible without god's grace and the selfless support of my family. I express my utmost gratitude to my loving parents who took care of my sons and were always there whenever I needed them. I'm indebted to my brother

who helped me to settle in Melbourne and complete my Ph.D. My heartfelt thanks to my wonderful husband who always stood by my side, and my sons Ashwaththman and Aadvigan for their unconditional love. I honestly thank my family members for their enduring patience throughout my Ph.D. period that was extended due to Covid pandemic. I also acknowledge my relatives and friends for their moral support and motivation.

List of Publications

Published articles

1. Karthiga K. Anpalagan, Jimsheena V. Karakkat, Adam Truskewycz, Ahmed Al Saedi, Paul Joseph, Vasso Apostolopoulos, Kulmira Nurgali, Ivan Cole, Zibo Cai, and Daniel TH Lai, "Bioimaging of C2C12 Muscle Myoblasts Using Fluorescent Carbon Quantum Dots Synthesized from Bread," *Nanomaterials*, vol. 10, no. 8, p. 1575, 2020.
2. Karthiga K. Anpalagan, Jimsheena V. Karakkat, Daniel TH Lai, Vasso Apostolopoulos, Kulmira Nurgali, Adam Truskewycz, and Ivan Cole. "A pilot study on carbon quantum dots for bioimaging of muscle myoblasts," in 2020 IEEE 20th International Conference on Bioinformatics and Bioengineering (BIBE), 2020, pp. 630-636: IEEE.

Conference presentation

1. Karthiga Anpalagan, Jimsheena Karakkat, Daniel Lai, Kulmira Nurgali, Vasso Apostolopoulos, Adam Truskewycz and Ivan Cole, "Bioimaging of muscle myoblast cells using carbon quantum dots" in IEEE International Conference on BioInformatics and BioEngineering, 2020.

Journal article under review

1. Karthiga Anpalagan, Jimsheena Valiyakath Karakkat, Raz Jelinek, Nila Nandha Kadamannil, Tian Zhang, Ivan Cole, Hong Yin, Kulmira Nurgali, and Daniel T.H. Lai, “A comparison between two green synthesis techniques for carbon quantum dots derived from bread” - submitted to Chemosensors from MDPI

Journal articles under preparation

1. Karthiga Anpalagan, Jimsheena Valiyakath Karakkat, Kulmira Nurgali, and Daniel T.H. Lai, “The impact of carbon quantum dots in C2C12 myotube differentiation” *
2. Karthiga Anpalagan, Jimsheena Valiyakath Karakkat, Hong Yin, Tian Zhang, Ivan Cole, Hong Yin, Kulmira Nurgali, and Daniel T.H. Lai, “The quantum yield enhancement of carbon quantum dots using natural additives” *
3. Karthiga Anpalagan, Jimsheena Valiyakath Karakkat, Tian Zhang, Ivan Cole, Hong Yin, Kulmira Nurgali, and Daniel T.H. Lai, “Near infra-red emissive carbon quantum dots derived from bread for bioimaging application”

*Data collection of these projects were delayed due to Covid pandemic and then paper preparation was postponed in favor of thesis preparation. These articles will be submitted after the completion of thesis.

List of abbreviations

CQDs	Carbon quantum dots
QDs	Quantum dots
QY	Quantum yield
QCE	Quantum confinement effect
PL	Photoluminescence
UV	Ultraviolet
NIR	Near infrared
CT	Computerized tomography
OCT	Optical coherence tomography
MRI	Magnetic resonance imaging
GFP	Green fluorescent protein
LED	Light emitting diode
FWHM	Full width at half maximum
IACR	International Agency for Cancer Research
DNA	Deoxyribonucleic Acid
MHC	Myosin heavy chain
TEM	Transmission electron microscope
SEM	Scanning electron microscope
FTIR	Fourier transforms infrared
XRD	X-ray diffraction
XPS	X-ray photoelectron spectroscopy
NMR	Nuclear magnetic resonance imaging

Table of Contents

Abstract	i
Chapter 1.....	1
Introduction	1
1.1 Research aims	5
1.2 Outline of thesis	7
Chapter 2.....	11
Literature Review.....	11
2.1 Introduction	11
2.2 Quantum dots	11
2.2.1 Photoluminescence of quantum dots.....	12
2.2.2 Cytotoxicity of quantum dots	15
2.3 Carbon quantum dots	16
2.4 Carbon quantum dots from natural and edible precursors	18
2.4.1 Fruits and vegetables as carbon precursor	22
2.4.2 Animal by-products and eggs as carbon precursor	24
2.4.3 Coffee and tea by-products as carbon precursor.....	27
2.5 The cell bioimaging using natural precursors derived CQDs	28
2.5.1 Human cervical cancer (HeLa) cells	28
2.5.2 Adenocarcinoma human alveolar basal epithelial (A549) cells.....	29
2.5.3 Human hepatocellular carcinoma (HepG2) cells.....	30
2.5.4 Human breast cancer cell lines MCF-7	31
2.6 Synthesis techniques of carbon quantum dots	32
2.6.1 Hydrothermal/ Solvothermal method.....	33
2.6.2 Microwave assisted method	35
2.6.3 Thermal decomposition/Thermolysis method.....	37
2.7 Structure and properties of carbon quantum dots.....	38
2.7.2 Photoluminescence and photostability.....	40
2.7.3 Quantum yield	42
2.8 Surface modification of carbon quantum dots.....	44
2.9 Doping of carbon quantum dots.....	46
2.10 Cytotoxicity of carbon quantum dots	49
2.11 Bioimaging of carbon quantum dots.....	50
2.11.1 Requirements for cell bioimaging	56
2.12 Characterization techniques for carbon quantum dots	57
2.12.1 Ultraviolet-Visible (UV-vis) Spectroscopy.....	58

2.12.2 Photoluminescence (PL) Spectroscopy	59
2.12.3 Transmission electron microscopy (TEM)	60
2.12.4 X-ray diffraction (XRD)	61
2.12.5 Nuclear magnetic resonance (NMR)	62
2.12.6 Fourier transform infrared spectroscopy (FTIR)	63
2.12.7 X-ray Photoelectron Spectroscopy (XPS)	64
2.9 Green engineering and sustainability	65
Chapter 3	66
Fabrication of carbon quantum dots from bread and paper for bioimaging	66
3.1 Abstract	66
3.2 Introduction	67
3.3 Materials and methods	69
3.3.1 Fabrication of CQD from bread	69
3.3.2 Fabrication of CQDs from papers	71
3.3.3 Characterization of CQDs derived from bread and paper	72
3.3.4 Cell culture and bioimaging	74
3.4 Results and discussion	75
3.4.1 Characterization of CQDs	75
3.4.2 Internalization of CQDs by C2C12 cell lines	83
3.4.3 Cytotoxicity	86
3.4.4 Uptake of CQDs by Muscle Myotube and Imaging	87
3.5 Conclusion	89
Chapter 4	91
Investigating C2C12 myotube formation in presence of carbon quantum dots from bread	91
4.1 Abstract	91
4.2 Introduction	92
4.3 Materials and methods	95
4.3.1 Fabrication of CQDs using toasting method	95
4.3.2 Characterization of CQDs	95
4.3.3 Cell culture and bioimaging	96
4.3.4 MTT assay	97
4.3.5 Western blotting	98
4.4 Results and discussions	98
4.4.1 Fabrication of CQDs	99
4.4.2 Characterization of CQDs	99

4.4.3 Bioimaging	101
4.4.4 MTT assay.....	102
4.4.5 Western blotting	103
4.5 Conclusion.....	105
Chapter 5.....	107
A comparison of carbon quantum dots fabricated using the hydrothermal technique and toasting method.....	107
5.1 Abstract	107
5.2 Introduction	108
5.3 Materials and methods.....	110
5.3.1 Fabrication of CQDs	110
5.3.2 Characterization of CQD samples	112
5.3.3 Cell culture	114
5.3.4 <i>In vitro</i> cytotoxicity evaluation	115
5.4. Results and discussion.....	115
5.4.1 Fabrication of CQDs	115
5.4.2 Characterization of CQDs	116
5.4.3 Bioimaging Application.....	123
5.4.4 Cytotoxicity of CQDs	128
5.4.5 Internalization of CQD	130
5.5 Conclusions	130
Chapter 6.....	132
Quantum yield enhancement of carbon quantum dots using green edible additives....	132
6.1 Abstract	132
6.2 Introduction	133
6.3 Materials and methods.....	136
6.3.1 Fabrication of carbon quantum dots	136
6.3.2 Characterization of CQDs	139
6.4 Results and discussion.....	141
6.4.1 Fabrication of CQDs	141
6.4.2 Characterization results of the CQDs.....	142
6.5 Conclusion.....	151
Chapter 7.....	153
Conclusion and future work	153
7.1 Thesis summary	153
7.2 General conclusion	154

7.3 Future work	157
References	160
Appendix	186
Human bone osteosarcoma cells (MG63), brain epithelial glioblastoma cells (U87), kidney cell lines (Vero, HEK293, HK2), and Colon carcinoma cell lines (LoVo, Caco-2)	186
Bacteria and other cell lines	188

List of Figures

Figure 2.1: bandgap energy level due to quantum confinement	14
Figure 2.2: (A) Excitation-dependent luminescence spectra of CQDs. (B) Multicolor photoluminescence of CQDs attributed to different surface energy states	41
Figure 2.3: Cellular uptakes of fluorescent CQDs with HeLa cancer cell lines	54
Figure 3.1: Emission spectra of (A) CQD B1- bread sample derived from toasting method and (B) CQD B2 – bread sample derived from muffle furnace method	76
Figure 3.2: Emission spectra of CQD B1 and CQD B2 at 360 nm excitation	77
Figure 3.3: Emission spectra of CQD P1(newspaper), CQD P2 (paper towel), and CQD P3 (A4 printing paper) at 360nm excitation	78
Figure 3.4: Emission spectra of CQD P3 (Ignition method) and CQD MP3 (muffle furnace method) at 360 nm excitation	78
Figure 3.5: (A, C) TEM image and size distribution histogram of CQD B1 (Bread sample-toasting method), respectively; (B, D) TEM image and size distribution histogram of CQD B2 (Bread sample-muffle furnace method), respectively	79
Figure 3.6: FTIR spectra of CQD B1 (bread sample derived from toasting method) and CQD B2 (bread sample derived from muffle furnace method)	80
Figure 3.7: XRD pattern of CQD B1 (bread sample derived from toasting method) and CQD B2 (bread sample derived from muffle furnace method)	81
Figure 3.8: (A) ^1H spectrum of a colloidal solution of the CQD B2 (bread sample derived from muffle furnace method) in D_2O ; (B) the corresponding ^{13}C spectrum	82
Figure 3.9: Fluorescence images of C2C12 cells after 24 h of incubation with CQDs. (A,B) Cells incubated with water as control; (C,D) cells incubated CQD B1; (E,F) cells incubated with CQD B2; (A,C,E) are images from FITC (green) channel; (B,D,F) are images from TRITC (red) channel	85
Figure 3.10: The time course of the internalization of CQD B1 by C2C12 cells tracked for 0–24 hours. The images were recorded using FITC channel	86

Figure 3.11: Comparison of cell viability after incubating C2C12 cells with CQD B1 for 24 hours. The blue bar represents the number of cells counted at 0 hours, and the orange bar represents the cells counted after 24 hours of incubation with either CQD B1 or equal volume water as a control	87
Figure 3.12: Fluorescence image of C2C12 myotubes incubated with CQDs. (A) Control cells; (B) myotubes incubated for 24 h with CQD B1; (C) myotubes incubated for 24 h with CQD B2. The images are from FITC (green) and DAPI (blue) channels overlaid	88
Figure 4.1: TEM Image of CQD T	99
Figure 4.2: Fluorescence emission spectrum of CQD T at 360 nm excitation	100
Figure 4.3: Differentiation of C2C12 control cells (A, B and C) and in the presence of synthesized CQDs (D, E and F) at 0, 24 and 72 hours. Cells are stained using eosin and methyl green	102
Figure 4.4: MTT assay of C2C12 cells with CQD T against control cells showing no significant reduction in cell viability in presence of 0.5-1.5 mg/ml of CQDs	103
Figure 4.5: Western blotting image of C2C12 differentiation in presence of CQDs compared against control cell differentiation. GAPDH is used as a control and expression of Myf-5, Myo-D and myosin heavy chain (MHC) is tested from 0 to 120 hours of differentiation	104
Figure 5.1: TEM images and size distribution histogram of CQD T1 – toasting method (A, C) and CQD H1 – hydrothermal method (B, D), respectively	117
Figure 5.2: Emission spectra of samples. CQD T1 – white bread (T1), CQD T2 – whole meal bread (T2), and CQD T3 – mixed grain bread (T3) are samples from the toasting method, and CQD H1- white bread (H1), CQD H2 – wholemeal bread (H2), and CQD H3 – mixed grain bread (H3) are samples from the hydrothermal method	118
Figure 5.3: FTIR spectra of (A) samples from the toasting method (CQD T1 – white bread, CQD T2 – whole meal bread, CQD T3 – mixed grain bread) and (B) samples from the hydrothermal method (CQD H1 – white bread, CQD H2 – whole meal bread, CQD H3 – mixed grain bread), and (C) Both CQD T1 (white bread from toasting method) and CQD H1 (white bread from hydrothermal method)	121

Figure 5.4: Confocal microscopy images of mouse colon cancer cells (CT-26) incubated with CQDs for 24 hours. All images are obtained through the green channel (excitation peak at 431 nm and an emission peak at 540 nm) at 20x magnification	125
Figure 5.5: Confocal microscopy images of mouse colon cancer cells (CT-26) incubated with CQDs for 24 hours. All images are obtained through the blue channel (excitation peak at 345 nm and an emission peak at 455 nm) at 20x magnification	125
Figure 5.6: Confocal microscopy images of human colon cancer cells (HT-29) incubated with CQDs for 24 hours. All images are obtained through a green (excitation peak at 431 nm and an emission peak at 540 nm) channel at 20x magnification	126
Figure 5.7: Confocal microscopy images of human colon cancer cells (HT-29) incubated with CQDs for 24 hours. All images are obtained through a blue (excitation peak at 345 nm and an emission peak at 455 nm) channel at 20x magnification	126
Figure 5.8: Confocal microscopy image of CT26 cells incubated with CQD H2 for 24 hours, fixed and stained with nuclear counterstain propidium iodide. Imaged at 63x magnification. (A and D) Imaged through the green channel (B and E) Imaged through the propidium iodide (red) channel and (C and F) Overlay of images from the green and red channels	127
Figure 5.9: MTT assay of CQDs. (A) MTT assay of CT-26 cells with CQD T1, CQD T2, CQD T3, CQD H1, CQD H2 and CQD H3. (B) MTT assay of HT-29 cells with CQD T1, CQD T2, CQD T3, CQD H1, CQD H2, and CQD H3. All CQDs were tested at 0.5, 1.0 and 1.5 mg/mL concentrations	129
Figure 6.1: TEM images of (A) CQD W (whole meal bread), (B) CQD WS (whole meal bread + soybean flour), and (C) CQD WSL (whole meal bread + soybean flour + lemon juice)	145
Figure 6.2: X-ray diffraction spectra of CQD W (whole meal bread), CQD WS (whole meal bread + soybean flour), and CQD WSL (whole meal bread + soybean flour + lemon juice)	146
Figure 6.3: FTIR spectra of CQD W (whole meal bread), CQD WS (whole meal bread + soybean flour), and CQD WSL (whole meal bread + soybean flour + lemon juice)	147

Figure 6.4: XPS spectra of (A) CQD W (whole meal bread), (B) CQD WS (whole meal bread + soybean flour), and (C) CQD WSL (whole meal bread + soybean flour + lemon juice) 148

Figure 6.5: C 1s spectra of (A) CQD W (whole meal bread), (B) CQD WS (whole meal bread + soybean flour), and (C) CQD WSL (whole meal bread + soybean flour + lemon juice) 149

Figure 6.6: O 1s spectra of (A) CQD W (whole meal bread), (B) CQD WS (whole meal bread + soybean flour), and (C) CQD WSL (whole meal bread + soybean flour + lemon juice) 150

List of Tables

Table 2.1: Carbon quantum dots from natural and edible precursors for bioimaging	14
Table 5.1: Quantum yield measurements of all six samples	122
Table 6.1: Details of the fabricated samples	137
Table 6.2: Quantum yield measurement of all the samples	143
Table 6.3: Atomic composition of CQD W (whole meal bread), CQD WS (whole meal bread + soybean flour), and CQD WSL (whole meal bread + soybean flour + lemon juice)	148

Chapter 1

Introduction

Diagnosis can be regarded as an identification of an individual's condition that allows medical decisions about treatment and prognosis to be made. Early detection of a disease is useful to optimize treatment, further specify the prognosis or prevent the recurrence of the disease or condition in the future. Among various diagnosing techniques, bioimaging is an advanced non-invasive technique that is relatively new. Bioimaging can be differentiated into four categories namely molecular bioimaging, medical bioimaging, bioimaging in drug discovery, and computational bioimaging [1]. Medical bioimaging is the typical imaging technique and a useful tool in clinical settings for visualizing the interior functioning of the organism and its disorders. The clinical modalities include ultrasound, computerized tomography (CT), optical coherence tomography (OCT), and MRI [2]. Bioimaging has great potential in illustrating the relationship between the physicochemical properties of nanomedicines and their pharmaceutical profiles in living organisms. It provides direct monitoring and quantification of the pharmacokinetic and pharmacodynamic behavior of nanomedicines in a real-time manner [3].

The research sector including this research study mainly focuses on molecular bioimaging at the cellular level using confocal microscopy, fluorescence microscopy, electron microscopy, mass spectrometry imaging, fluorescence tomography, biochemical luminescence, and optoacoustic imaging [4]. Cell bioimaging allows researchers to observe cellular uptake, targeted delivery, and biodistribution of

therapeutics in an isolated, detailed manner using different parts of the electromagnetic spectrum. It can be performed on a living organism *in vivo* or outside of a living organism *in vitro*. Cell bioimaging is useful to detect the abnormalities, monitor the cellular functions, and observe the uptake of essential drugs [5-7]. For example, bioimaging is crucial for the early detection of tumors as well as the identification of metastasis and the resurgence of cancer [8]. Likewise, in regenerative medicine in order to understand the natural organ development process bioimaging is used in stem cells [9].

In cell bioimaging studies, a fluorescent probe is commonly used to highlight certain function and view the image of the cells/specimen species. Numerous organic fluorophores such as fluorescent dyes and fluorescent proteins are commercially available and currently in use. Even though they are very bright, a few challenges are there in the usage of organic fluorophores in bioimaging. They are less photostable and easily move out from the cytoplasm to media, undergo degradation while irradiating with light during the imaging process, no possibility of tuning the optical properties and may change the metabolism of live cells due to toxicity [10, 11]. For example, the green fluorescent protein (GFP) has opened a new area of biomedical research for monitoring protein–protein interactions, protein localization and gene expression in the past few decades. However, the poor photostability and weak fluorescence signal of GFPs make long-term imaging difficult, limiting their widespread applications in biomedical field [12].

Compared to organic fluorophores, metal-based quantum dots such as CdSe show high photostability since they have the core-shell structure capped with ligands. The advantages of semiconductor quantum dots over organic fluorophores are due to their unique property such as tuneable photoluminescence which is a result of quantum

confinement. However, the main issue is biocompatibility. Most of the quantum dots exist with the presence of toxic heavy metals like Cd, Pb and Hg in their composition. Even though they were enfolded with the surface coverage, within the cell during the imaging analysis, there is a chance of release of those toxic metals into the medium that are harmful to the live cells [10]. Their interference with cellular function also needs to be researched as they can affect them.

In order to overcome the abovementioned problems of unfortunate biodegradability and toxicity, novel fluorescent materials with better biocompatibility should be developed for bioimaging of live cells. In this context, carbon quantum dots (CQDs), have emerged as potential candidates for application in real time bioimaging. Compared to the conventional organic fluorophores and recent inorganic semiconductor quantum dots, the new family of carbon quantum dots are superior in terms of resistance to photobleaching, chemical inertness, facile surface functionalization, and sheer size. Interestingly, carbon quantum dots exhibit low cytotoxicity, high aqueous solubility and spontaneous cellular internalization capabilities due to their nanoscale structure that enables them to be easily utilized in the field of biomedical research especially in both *in vivo* and *in vitro* bioimaging. *In vivo* involves bioimaging within the living organism. Clinical trials and animal studies fall in this category. *In vivo* studies are reliable and specific for observing biological effects in the test subject. Yet, it is time consuming process with strict regulations and compliance standards. On the other hand, *in vitro* bioimaging is performed with cells, tissues or other biological components that have been removed from the living organism of interest. It is an essential component of research that provides a way to study the response of human, animal, or microbial cells in culture. *In vitro* is relatively simple and under experimental control, but the variety of cells and available experiments are physiologically limited [13, 14].

CQDs are a new classification of nanoparticles, with carbon cores and associated surface ligands. The discovery of fluorescent carbon nanoparticles was accidental, during the separation and purification of single-walled carbon nanotubes via electrophoresis by Xu in the year of 2004 [15]. Then, Sun and his research group named the small carbon nanoparticles as carbon quantum dots derived from graphite powder using laser ablation technique. These nanoclusters, with an average diameter of 10 nm, exhibit unique optical characteristics. They generally show strong absorption in the ultra-violet region and exhibit excitation-dependent emission in the visible spectrum [16-19]. CQDs are versatile nanomaterials with a wide range of applications, including chemical sensing, bio-sensing, bioimaging, drug delivery, solar technology, photocatalysis, and electro-catalysis [10, 20-24] [25-28]. In comparison with traditional quantum dots and organic fluorophores, the excellent biocompatibility, inexpensiveness, facile synthesis, high surface area, flexible functionalization, nontoxicity, photostability, high water-soluble nature and low toxicity of CQDs make them a promising technology for the biomedical field [29-31].

There are numerous precursors and various synthesis techniques available to produce different sizes of CQDs. Alongside chemical precursors, a huge selection of edible or green raw materials is currently emerging in practice [32-45] such as fruit juices, vegetable and fruit peels, starches, and food waste. However, in most of these fabrication processes, the natural precursors are used with other organic chemicals to obtain quantum dots. Even though these chemicals are washed out or neutralized, a minimal amount would curtail their biocompatibility and interfere with cell functions when used for bioimaging. The alternative, which is the focus area of this thesis, is to seek green precursors and chemical-free fabrication techniques to develop truly biocompatible CQDs.

The current research studies are practicing the fabrication of CQDs through various routes. Green fabrication allows to use fewer resources, reduce pollution and waste, neglect harsh chemicals and develop practices that lessen their impact on the environment [46]. Greening the fabrication process of CQDs has already begun [43, 47, 48], but much more work is needed to optimize the precursors and synthetic routes. Specially to use the CQDs in the biomedical applications performance, nontoxicity and safety should be guaranteed. A particular drawback of using natural precursors is the low quantum yield (photoluminescence brightness). Unlike florescent dyes such as Rhodamine, the photon emission of the CQDs derived from these precursors is mostly deficient. Therefore, various techniques including doping and surface passivation are used to enhance the quantum yield [49-51]. Again, harsh synthetic materials involve and diminish the biocompatibility of CQDs while increasing the emission. Chemical-free additives and green pathways are needed to enhance the emission and grow the application. These processes fall under green engineering which seeks to maximize efficiency and minimize health and environmental risks throughout the fabrication procedures. This green engineering focus aligns with sustainability which necessitates the process of moving away from hazardous and non-renewable resources, and moving toward safer and reusable materials [52]. This study aims to align with this concept and produce biocompatible CQDs for bioimaging.

1.1 Research aims

Bread is selected as the main precursor to fabricate carbon quantum dot in this study. It is a very common food that sold and consumed across the world and approximately 10% of the manufactured bread is wasted globally [53]. In Victoria 125 million bread

loaves are wasted annually. The Water, energy, land, and fuel go into the production of the bread we buy. Hence the wastage is causing a significant drain on Victoria's natural resources, costing almost \$800 million dollars each year [54]. This study aims to synthesis CQDs from bread using green methods to reduce wastage and support sustainability. This project also intends to overcome the cytotoxicity, inadequate photostability, photo bleaching and mainly the poor biocompatibility of organic fluorophores. Biocompatibility is an ability of a material to perform its desired function without causing any local or systemic adverse response in the recipient of the material [55, 56]. Fluorescent dyes like Rhodamine are generally high in quantum yield but low in biocompatibility [57]. For long term live-cell bioimaging processes which enable monitoring the variations in cells and tracking the cellular functions, biocompatible is more essential than the brightness. Therefore, all the steps including synthesis, modification and quantum yield enhancement should be performed without curtailing the biocompatibility of the CQDs.

Therefore, the main aim of this study is to:

- Fabricate CQDs from natural, cheap and easily accessible resource using efficient synthetic routes and enhance their quantum yield to utilize these CQDs in bioimaging.

The secondary aims to support the main goal are:

1. Fabricate biocompatible CQDs from edible precursor for bioimaging, so that the food waste could be used for a valuable cause.
2. Invent a novel, green synthesis method to produce comparable CQDs to the commonly used fabrication methods.

3. Investigate the impact of CQDs on cellular function and their relationship with cytotoxicity.
4. Explore green strategies to enhance the quantum yield of biocompatible CQDs instead of chemical functionalization routes.

1.2 Outline of thesis

This thesis is organized as follows.

- **Chapter 2** – This chapter reviews the literature related to traditional quantum dots, carbon quantum dots, bioimaging and characterization techniques. The fabrication methods, properties and bioimaging of the CQDs are reviewed in detail with emphasis placed on natural/edible precursors and green fabrication routes. This chapter also provides an insight into photoluminescence and the enhancement of quantum yield. The fluorescent probes used in bioimaging and the bioimaging capability of CQDs derived from natural resources is reviewed for comparison. The cytotoxicity of CQDs and its impact on bioimaging is also analyzed. In addition, the techniques that are generally used to characterize CQDs were illustrated clearly.
- **Chapter 3** – The use of chemicals is very common in CQD fabrication. Even a majority of reported work starting with natural precursors end with using chemical additives to fabricate CQDs. This chapter aims to demonstrate that fluorescent CQDs can be produced without the addition of chemicals. Herein, the CQDs were fabricated from two precursors. First was an edible resource, namely bread and the second one was a reusable material, namely paper. Facile thermolysis synthesis

routes such as toasting method, muffle furnace method and carbonization techniques were employed and optimized. The CQDs were characterized, and the samples with better fluorescent emission were selected for bioimaging C2C12 muscle myoblast cell lines. The CQDs derived from bread were almost ten times brighter than the CQDs produced from paper. This chapter demonstrated that the biocompatible CQDs for bioimaging could be fabricated without adding any chemicals.

- **Chapter 4** – As the previous chapter showed the bioimaging capability of the CQDs fabricated without any additives, this chapter investigated their cytotoxicity and their influence in cell function. The CQDs derived from bread using the novel toasting method were added to the C2C12 myotube differentiation process and the effect caused by CQDs during the formation of C2C12 myotube formation was investigated. A delay in myotube formation in the presence of CQDs was witnessed clearly from the images at various time points. The western blotting confirmed the delay in myotube formation as the expression of transcription factors Myf-5, Myo-D and myosin heavy chain (MHC) was altered in presence of CQDs. This investigation of chemical-free CQDs arises the question regarding the biosafety of chemical-derived CQDs. According to MTT assay, cell viability of the bread-derived CQDs was not affected even at a concentration of 1.5 mg/ml and this concentration was nearly 1000 times higher than the concentration required by a fluorescent probe for cell labelling. It was demonstrated that the CQDs from bread derived via a chemical-free synthesis route is safe to be used in bioimaging up to 1 mg/mL concentration.

- **Chapter 5** – This chapter expanded on the fabrication techniques by introducing the hydrothermal technique and widened the selection of breads to whole meal bread and mixed grain bread. It investigated the efficiency of toasting method by comparing it to the standard and common hydrothermal technique. Here, three types of bread and two fabrication technique were employed. The white bread, whole meal bread and mixed grain bread based were also compared based on their optical properties. All the six CQDs were characterized, and it was found that the CQDs derived from whole meal bread using hydrothermal method possess the highest quantum yield of 0.81 %. However, CQDs from both fabrication techniques were fluorescent and well internalized by the colon cancer cell lines, namely CT26 and HT29 cell lines, extracted from mouse and human respectively. These cell lines were used to show that the CQDs can be used to mark and monitor cancer cells. This chapter proved that the facile, time efficient and cost-effective toasting method could produce comparable CQDs for bioimaging cancer cells.
- **Chapter 6** – Even though the CQDs derived from whole meal bread were bright and were able to bioimage the cancer cells, their quantum yield was less than 1 %. The literature shows multiple techniques for quantum yield enhancement, but all those methods include chemical additives for surface modification. This chapter aimed to enhance the quantum yield of the CQDs derived from whole meal bread solely with natural additives. We showed that the soybean flour and lemon juice can be used as alternatives for chemical additives in the process of quantum yield enhancement. The X-ray photoelectron spectroscopy, fourier transform infrared spectroscopy, transmission electron microscopy and X-ray photoelectron spectroscopy were the characterizations used explained the improvement in

emission. The quantum yield was increased by 1.5 % and reached 2.31 %. It was the highest quantum yield obtained for CQDs derived from bread in the absence of additive chemicals. This chapter demonstrated that the enhancement of quantum yield can be reliably achieved by natural additives and a whole green (only natural resources) fabrication process.

- **Chapter 7** – This chapter provided a summary of all the previous chapters and highlights the significance of this research. It clearly discussed the contribution to the knowledge and presented a conclusion of this study. This section also outlined the scope for further work in this area which included looking at new techniques for fabrication of CQDs with near infra red emission, quantum yield enhancements using green routes and further biotoxicity studies on different cell lines. In addition, it described the future work planned in regard to the bioconjugation of CQDs with human proteins and development of a handheld device to detect the inflammation of tissues in clinical settings.

Chapter 2

Literature Review

2.1 Introduction

This chapter reviewed the literature on carbon quantum dots (CQDs) and their related topics. It initiated with the introduction of traditional quantum dots and their properties. Then, it moved towards the CQDs and highlighted their biocompatibility compared to the traditional quantum dots. The natural and edible precursors used for the fabrication of CQDs were tabulated and discussed. Various types of cell lines that were visualized using these natural precursor - bone CQDs were also presented. Alongside these, a few bottom-up fabrication techniques for CQDs were analyzed in detail. The structure and properties of CQDs were analyzed and they were followed by the surface passivation and doping techniques that alter the properties of CQDs. Later, the quantum yield of CQDs and their utilization in bioimaging were reviewed extensively. The common characterization techniques employed to study CQDs were also reviewed in detail. Finally, this chapter concluded with the significance of green engineering and sustainability.

2.2 Quantum dots

During the past few decades, quantum dots (QDs) have become a remarkable topic of research interest in the field of nanotechnology. The QDs are semiconductor particles with a few nanometers in size. They display excellent optical and electronic properties that differ from those of larger particles as a result of the quantum confinement effect.

The change in the electronic and optical properties of a material due to the confinement in at least one dimension. This effect can be observed if the size of the particle is too small compared to the wavelength of an electron [58]. The use of semiconductor quantum dots such as Silicon gallium arsenid (GaAsaAs) inspired technologies from computers and mobile phones to lasers and satellites [59]. The histroy of quantum dots began with their first discovery in glass crystals in 1980 by Russian physicist Ekimov [60]. Traditional QDs are generally composed of elements from groups III–V, II-VI, or IV-VI of the periodic table, such as CdS, CdSe, CdTe, CdS-ZnS, CdSe-ZnS, and CdSeTe-ZnS. QDs possess attractive characteristics such as tunable photoluminescence, high quantum efficiency, broad absorption, and excellent resistance toward photobleaching. These superior properties make them potential candidates in many areas, including light-emitting diodes (LEDs), displays, solar cells, photovoltaic cells, telecommunication, photocatalysis, and gas sensors [61-68].

2.2.1 Photoluminescence of quantum dots

The strong quantum confinement of these quantum dots paves path to advantageous optical properties. Quantum confinement take place when electrons are constrained to a structure comparable with their de Broglie wavelength. This effect is basically due to changes in the atomic structure as a result of the direct influence of ultra-small size (100 – 10nm or less) scale on the energy band structure [69]. Quantum confined structures are classified as two dimensional, one dimensional and zero dimensional (2D, 1D, and 0D) and these include quantum wells, quantum wires, and quantum dots (QDs), respectively. As size of the QD become smaller, quantum confinement increases the effective bandgap, leading to a blue shift of the absorption and emission spectra. The

bandgap increases as the size of the nanoparticle decrease. Nanoscale semiconductors are characterized by the gap amid their two bands called valence and conduction. When a photon consists of excitation energy that exceeds the semiconductor bandgap, it gets absorbed by a quantum dot. As a result, electrons get promoted from the valence band to the conduction band with high energy. The excited electron then relaxes to its ground state by emitting another photon with energy equal to the bandgap [70]. This energy emitted by the electron is released as light in quantum dots and this process is called photoluminescence.

The Color of the emitted light depends on the difference (band gap) between the valence band and conduction band. Usually, larger QDs of 5–6 nm diameter emit orange and red colour in longer wavelengths of visible light. Blue and green colours of shorter wavelength are observed from smaller QDs with diameters between 2 and 3 nm [71]. The optical properties of quantum dots is very exceptional and still under investigation.

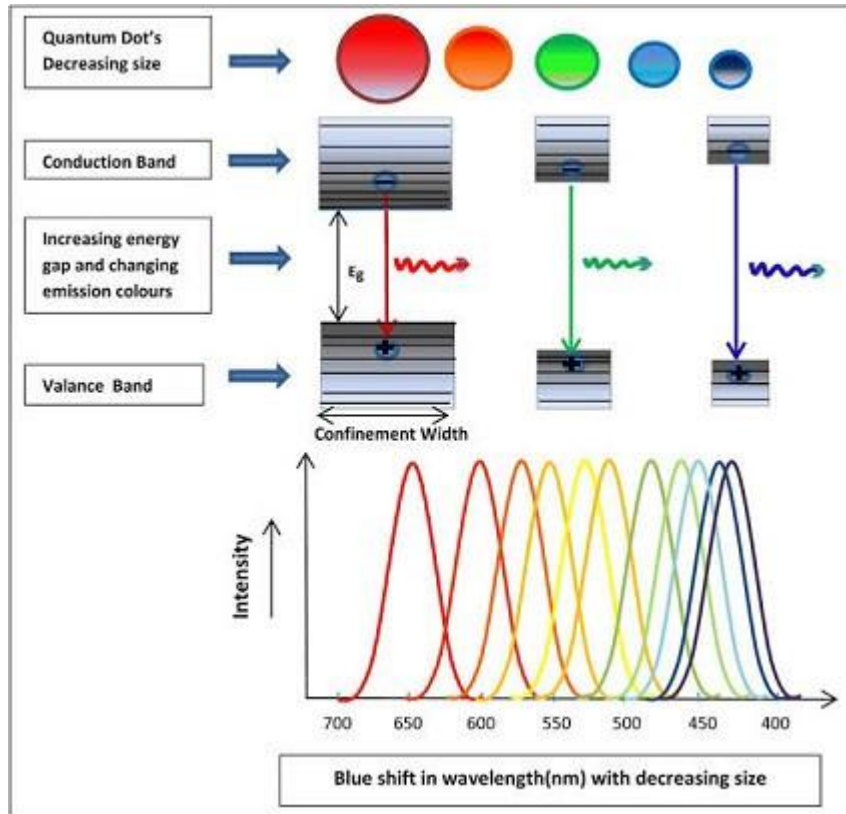


Figure 2.1: Bandgap energy level due to quantum confinement [72]

The Brus equation [73] can be used to describe the emission energy (E) of quantum dot semiconductor nanoparticles. The Brus equation is given below

$$\Delta E(r) = E_{gap} + \frac{h^2}{8r^2} \left(\frac{1}{m_e^*} + \frac{1}{m_h^*} \right) \quad (1)$$

Here, E_{gap} is band gap energy, h is Planck's constant ($6.62607015 \times 10^{-34}$ Js), radius of the quantum dot is r , the effective mass of the excited electron is m_e^* and the effective mass of the excited hole is m_h^* . Here E_{gap} , m_e^* , and m_h^* are unique for each nanocrystal composition.

The radius of the quantum dot affects the luminescence wavelength due to the quantum confinement, and this equation explains the effect of changing the radius of the quantum dot on the wavelength of the emitted light.

Therefore, the emission energy is $\Delta E = \frac{hc}{\lambda}$ (2)

where, λ is the wavelength and c is the speed of light. This is useful for calculating the radius of a quantum dot from experimentally determined parameters.

2.2.2 Cytotoxicity of quantum dots

Most of the metal-based quantum dots pose risks to human health and the environment under various conditions. In Accordance with *In vitro* studies that based on cell cultures suggest that the toxicity of quantum dots may derive from multiple factors including their physicochemical characteristics (size, shape, composition, surface functional groups, and surface charges) and their environment factors. Evaluating their potential toxicity is complex as these factors include properties such as quantum dot' size, charge, concentration, chemical composition, capping ligands, and also it depends on their oxidative, mechanical and photolytic stability [74-76]. Notably, CdX is one of the most researched QD due to its superior optical and electrochemical properties. Cadmium based QDs exhibit quite narrow full width at half maximum (FWHM) (20 ~ 30 nm) and super high luminescent quantum yield (>95%) [77]. However, the toxicity of Cadmium ion has gained more attention than its advantages. Cadmium is considered a extensive environmental and occupational pollutant and poison, which has been classified as a carcinogen in Group 1 by the International Agency for Cancer Research (IARC) (IARC, 2013). It accumulates in the human body to cause inflammation, lung

injury, and potential long term conflicting effects [78]. It has been reported that during exposure to ultraviolet radiation or oxidation by air, CdSe QDs release free cadmium ions causing cell death [79]. Group II–VI QDs also have been demonstrated to induce the formation of reactive oxygen species after exposure to light, which in turn can harm cellular components such as proteins, lipids and DNA [80].

Some studies have also shown that addition of a ZnS shell inhibits the process of reactive oxygen species in CdSe QDs. Another aspect of QD's toxicity is that there are, *in vivo*, size-dependent intracellular pathways that accumulate these particles in cellular organelles that are inaccessible by metal ions, which may result in unique designs of cytotoxicity compared to their constituent metal ions [81]. The reports of QD localization in the cell nucleus [82] display additional modes of toxicity because they may promote DNA mutation, which in turn will spread through future generation of cells, causing various diseases. Nevertheless, a better knowledge of the composition and behavior of a QD will enable the investigation of minimizing and managing their toxicity. The development of strategies to handle the toxicity of QDs is being explored [83]. Even though, the excellent quantum yield and photostability of QDs help them replace fluorescent dyes in bioimaging application, the concern about toxicity, and temperature dependency [84] limited their use in human health. Due to the low biocompatibility and high toxicity of traditional quantum dots, metal-free quantum dots such as silicon quantum dots and carbon quantum dots were emerged.

2.3 Carbon quantum dots

Carbon is the most useful material from nature, and it is generously available. Carbon based nanostructured materials represent a wide-ranging category including nano-

diamonds, carbon nanotubes, fullerenes, sheets of graphene, carbon quantum dots (CQDs) [85]. CQDs are the most explored member of the carbon family in focus of biomedical applications. These CQDs are zero-dimensional fluorescent nanoparticles with a carbon core and related ligands [29, 86]. Most CQDs contain an amorphous to nano-crystalline core, generally composed of sp^2 carbon, along with lattice spacing that is constant with graphitic carbon [87]. Unlike traditional quantum dots, CQDs possess excellent biocompatibility and low toxicity, thus promising candidate for bioimaging application [88]. These nanoclusters were first discovered by Xu et al during the purification of single-walled carbon nanotubes through preparative electrophoresis in 2004 [15], yet, Sun et al. [89] were the first to produce and designate those fluorescent particles as carbon quantum dots.

As a group of newly emerged fluorescent nanomaterials with average size less than 10nm, carbon quantum dots have displayed excellent potential as versatile nanomaterials for a extensive range of applications, including chemical sensing, bio-sensing, bioimaging, drug delivery, photocatalysis, photodynamic therapy and electrocatalysis [25, 26, 28, 90-92]. Compared to conventional semiconductor quantum dots, the unique attributes of CQDs, such as their biocompatibility, low-toxicity, benign chemical composition, tunable fluorescence emissions, facile fabrication and functionalization, extremely small size, large surface area, high solubility, great electrical conductivity and excellent physicochemical and photochemical stability make them very attractive for imaging applications [88, 93-98]. CQDs can be fabricated from both chemical and natural precursors. The natural precursors that are used to derived CQDs and their application in cell bioimaging are presented in the following sections.

2.4 Carbon quantum dots from natural and edible precursors

The most attractive property of carbon quantum dots (CQDs) is, they can be fabricated from cheap, readily available and easily accessible resources. A large selection of low-cost natural resources can be converted into valuable CQDs and utilized in favorable applications. The list of natural precursors includes plants, vegetables, fruits, beverages, juices, bakery products, and wastes. These CQDs are promising materials because they are sustainable, inexpensive, highly renewable, eco-friendly and biocompatible. Even though the CQDs produced from chemical-free natural resources are used in various fields, their application in bioimaging is very promising due to their innate biocompatibility. Yet, their quantum yield needs to be enhanced without curtailing biocompatibility. Moreover, facile, efficient, and cost-effective fabrication techniques are required to scale-up the production and improve applications. Here are some natural and edible precursors that were used to fabricate CQDs for bioimaging application.

Table 2.1: Carbon quantum dots from natural and edible precursors for bioimaging

Category	Precursor	Fabrication method	Quantum yield (%)	Ref
Fruits	Apple	Hydrothermal	4.27	[99]
	Winter melon	Hydrothermal	7.51	[100]
	Pomegranate	Hydrothermal	7.6	[101]
	Orange juice	Hydrothermal	26	[36]
	Lemon juice	Hydrothermal	28	[102]
	Papaya juice	Hydrothermal	7	[103]
	Durian	Hydrothermal	79	[104]
	Prunus avium	Hydrothermal	13	[105]
	Lychee seed	Pyrolysis	10.6	[106]
	Watermelon peel ▲	Pyrolysis	7.1	[45]
	Mango peel ▲	Hydrothermal	8.5	[107]
	Kiwi	Hydrothermal	20	[108]
	Avacado	Hydrothermal	35	[108]
	Pear	Hydrothermal	23	[108]

	Banana peel ▲	Hydrothermal	5	[21]
	Jackfruit seeds	Microwave-assisted	17.9	[109]
Vegetables & Spices	Onion waste ▲	Hydrothermal	28	[110]
	Garlic	Hydrothermal	17.5	[111]
	Ginger	Hydrothermal	13.4	[112]
	Mushrooms	Hydrothermal	5.5	[113]
	Cabbage	Hydrothermal	16.5	[41]
	Sweet potatoes	Hydrothermal	8.64	[42]
	Carrot	Hydrothermal	5.16	[114]
	Beetroot	Hydrothermal	6	[115]
	Cinnamon	Hydrothermal	35.7	[116]
	Red chilies	Hydrothermal	26.8	[116]
	Turmeric	Hydrothermal	38.3	[116]
	Black pepper	Hydrothermal	43.6	[116]
	Potatoes	Hydrothermal	6.1	[37]
Animal products	Cow manure ▲	Chemical oxidation	65	[117]
	Eggs	Pyrolysis	5.96	[118]
	Dried shrimp	Hydrothermal	54	[119]
	Milk	Hydrothermal	7.6	[120]

Other Products	Flaxseeds	Hydrothermal	14.2	[121]
	Oatmeal	Hydrothermal	37.4	[122]
	Starch	Hydrothermal	21.7	[123]
	Corn flour	Hydrothermal	7.7	[124]
	Rice husk ▲	Pyrolysis	15	[125]
	Coffee grounds	Pyrolysis	3.8	[126]
	Sugarcane juice	Hydrothermal	5.67	[37]
	Waste frying oil ▲	Pyrolysis	3.66	[127]
	Peanut shell ▲	Pyrolysis	9.91	[128]
	Date kernel	Hydrothermal	12.5	[129]
	Wheat straw ▲	Hydrothermal	7.5	[130]
	Chickpea peel ▲	Pyrolysis	10	[131]
	Ice-biryani	Carbonization	41	[132]
	Sugarcane molasses	Hydrothermal	5.8	[133]
	Waste green tea ▲	Hydrothermal	12	[134]

▲ - Waste products

The table presented above comprises of various types of biomasses that are transformed into fluorescent CQDs to visualize cells, tissues and organs. The juices, peels and seeds

from most of the fruits could produce CQDs under various fabrication conditions. Many vegetables and their peels also can be used as precursors. Other than this, animal by-products like milk and egg were also produce CQDs for bioimaging. Moreover, beverages like Coffee grounds and green tea, waste products such as rice husk and wheat straw, and many more materials are utilized in CQDs production.

Notably, Hydrothermal method was frequently used to prepare carbon based quantum dots from natural carbon precursors. It was a thermochemical degradation technique which takes place in the presence of water at elevated temperature and pressure. In the hydrothermal method, ratio of water : precursor may range from 5:1 to 75:1 [135]. Fruit and vegetable extracts, and other precursors that disperse in water were suitable for hydrothermal method. The pyrolysis method is mostly used for dry products such as rice husk and wheat straw. Other than these, microwave assisted method and chemical oxidation method also produced CQDs for bioimaging application.

The discussion of each category of precursors are given below in detail

2.4.1 Fruits and vegetables as carbon precursor

Fruits and vegetables contain vitamins, fiber, minerals and many other nutrients. These Plant by-products are a valuable carbon source in the nanomaterial sector for producing CQDs due of their innate biocompatibility and benign nature. Alam et al. hydrothermally fabricated CQDs at 140 °C for 5 h by using cabbage as the carbon source [41]. The resultant CQDs have displayed down and up-conversion photoluminescence properties. The existence of nitrogen and oxygen containing functional groups on CQDs surface contributes to their high luminescence by inducing an upward shift in the Fermi level and increased quantum yield. In addition, oxygen

and nitrogen functional groups help enhance the physicochemical and optical features of CQDs. The engineered CQDs showed considerable promise in bioimaging application. A lot of articles reported that the derivatives of vegetables have the highest quantum yield values compared to animal and industrial waste used for fabricating CQDs. Raji et al [21] used banana peel waste for producing the fluorescent CQDs via hydrothermal method. UV-vis and fluorescence spectroscopy displayed the optical properties. The produced CQDs exhibited intense blue fluorescence under the excitation of UV-light (365 nm) with a good quantum yield of 20%. It was successfully utilized for cell imaging applications. Highly photoluminescent CQDs from orange juice were produced hydrothermally with quantum yield noted to be 26%. As evident from FTIR and XPS analysis, the of functional groups (C = O, C-O-C, C-OH and C-H) found on the surface of CQDs were responsible for their excellent solubility in aqueous media. Moreover, they do not display photobleaching behaviour. They have low size distribution (1.5–4.5 nm) and can be utilized in bioimaging applications due to their excellent photostability and low cyto-toxicity [36]. Wang et al [33] reported the fabrication of water-soluble CQDs and ethanol-soluble CQDs in deionized water and 90% ethanol respectively using papaya as carbon precursor by simple green synthesis method. These two CQDs fabricated in different solvents showed different properties. Even though their quantum yield is almost the same, (18.98% and 18.39%), the size (3.4 nm) of the water soluble CQDs is much smaller than that of the ethanol soluble CQDs (10.8 nm).

Therefore, the internalization and bioimaging performance of CQDs prepared in deionized water is better than that of CQDs prepared in 90% ethanol due to their sheer size. Heteroatom doping can alter the properties of BCDs, such as improve the quantum yield, and narrow the band gap. Some vegetables and fruits contain elements such as

N, S, and P, so these vegetables and fruits can be self-doped in the fabrication process. The quantum yield of CQDs produced from natural peach gum polysaccharide [136] as precursor was 5.31%. This quantum yield was increased using ethylenediamine by nitrogen doping. With the increase in the amount of ethylenediamine included from 50 to 200 mg, the quantum yield of nitrogen doped CQDs gradually enhanced from 13.12% to 28.46%. Durian [104] that is rich in a large amount of sulphide, used as the carbon source to prepare Sulphur doped CQDs by effective hydrothermal technique. The Sulphur doped CQDs are produced by lattice substitution mechanism to manage the doping. As synthesized Sulphur doped CQDs displayed a diameter distribution ranging from 2 to 6 nm and an average diameter of 4 nm. The quantum yield of these CQDs was up to 79%. In addition to the above fruits and vegetable, there are many kinds of other products that are used as carbon sources in the fabrication of CQDs.

2.4.2 Animal by-products and eggs as carbon precursor

Yongming et al. [100] engineered hair waste as a carbon source for fabricating highly fluorescent CQDs by thermal treatment. It exhibited excitation-dependent emission property and excellent photostability. The CQDs produced from animal skin via microwave assisted method by heating the pre-roasted skin at 750 W for 25 min. Later, ultrasonication and filtration were performed and these CQDs harnessed to mark *Escherichia coli* [101]. The waste from seafood that are either discarded in the ocean or landfill is one of the challenging environmental issues. Transforming them into valuable materials can be a better solution for this. One of the studies reported the utilization of industrial waste crab shells for fabricating CQDs with excellent

photoluminescence properties through the sonochemical method. The XPS analysis exhibited the hydroxyl and carboxyl groups responsible for the aqueous solubility of CQDs and their functionalization. The Oxygen and nitrogen functional groups on the surface of CQDs displayed the excellent biocompatible behaviour towards HeLa cells. The confocal microscopy studies demonstrated that these CQDs employed as an efficient fluorescent imaging probe for identifying cancer cells specifically [137]. Hair, silk, and feathers of animals or insects are also considered as appealing candidates for producing heteroatom doped CQDs. As the waste From poultry is a rich source of nitrogen, sulphur, oxygen and carbon, Ruili et al. utilized the goose feather as a precursor for producing highly photoluminescent CQDs by hydrothermal technique. The as-produced CQDs displayed 2D (two dimension) uniform morphology with a diameter of 21.5 nm and quantum efficiency of 17.1% [138]. The CQDs obtained from silkworm chrysalis with excellent solubility and stability in an aqueous medium displayed excitation-dependent photoluminescence. Under an inverted fluorescence microscope, these CQDs display blue green and red colours, which showed their promising potential in bioimaging [139]. The commercial bee pollen, an economical and eco-friendly approach in the reported research, is selected as a carbon source for producing ultra-small size CQDs. Generally, the high reproducibility of CQDs increases the probability of their production on a large scale without affecting the mass conversion ratio. These CQDs showed promising application in bioimaging and light-emitting devices. As produced CQDs at concentration 0.5 mg /mL are considered safe from the cytotoxicity measurements [97]. The carbon based nanoparticles of diameter 2 nm were synthesized from baked lamb and emitted strong blue fluorescence when exposed to ultra violet light as reported by Wang et al [140]. Similarly, several more by-products of animals such as prawn shell [141], pigeon feathers [142], shrimp shells

[143], duck blood [144], duck breast [145], whey [146], and spoiled milk [146] are also exploited for the production of CQDs.

Eggs are one of the important requirements in our day-to-day lives, with abundant proteins, carbohydrates, and fat. A large number of eggshells is utilized in fertilizers, but maximum amount is rejected as waste. Recently, it was found that they can be utilized in the production of CQDs via a simple strategy. A study reported the production of CQDs from egg white that showed favorable fluorescent properties and excellent pH stability demonstrating its immense potential in bioimaging sector [147]. Likewise, Wang and co-workers [148] reported the fabrication of luminescent nitrogen doped CQDs using boiled egg yolk. Emission spectra showed the red shifting of peaks that were excitation dependent. It indicated their potential application in multi-colour imaging. In addition, the existence of oxygen and hydrophilic groups on nitrogen doped CQDs increased their aqueous stability without precipitation for several months and made them available for bioimaging and energy storage applications. Similarly, Mirza Muhammad et al. produced fluorescent CQDs by using inexpensive egg whites via a one-step heating reaction. Like a fluorescent labelling agent, it quantitatively detected the presence of curcumin from the complex samples. Also, its excellent water solubility and high quantum yield allow them to be used in biosensing and imaging applications [149]. Chicken eggshell membrane was used by Srikrishna Pramanik et al. for the fabrication of a highly fluorescent nanoprobe for base-pair selective and sequence-specific DNA identification with a narrow particle size distribution of 1–5 nm [150].

2.4.3 Coffee and tea by-products as carbon precursor

The coffee is a very common beverage that is consumed by many people around the world. Coffee beans are rich in carbohydrates, proteins, antioxidants, amino acids, and other nutritional ingredients. Akhiruddin et al. [151] synthesized CQDs by utilizing coffee grounds as a carbon precursor. Coffee grounds were added to 0.2 M NaOH (250 mL) solution with continuous stirring until sufficiently mixed and was autoclaved at 100° C for 1 hour. Dynamic light scattering (DLS) showed the size of CQDs to be 7.74 nm in diameter. These hydrothermally produced CQDs displayed uniform morphology, hydrophilic nature, and graphitic structure. Liang and his workers [152] investigated coffee driven CQDs as a fluorescent probe for imaging HeLa cells. After injecting the fluorescent probe solution around the nucleus, the cell cytoplasm exhibited enhanced fluorescence, which clearly confirmed that CQDs entered the cell and remained emissive. A few studies reported the fabrication of CQDs from discarded tea waste extract as a carbon precursor [153]. Mostly hydrothermal method is used and green tea leaf residues were preferred over normal tea leaves for the CQD synthesis. The fluorescent CQDs produced from green tea residue via the bottom up method were highly stable towards pH variation, ionic strength, and ultra violet radiation, however they were highly sensitive to the change in temperature [154]. Similarly, oolong tea and black tea also employed in producing CQDs hydrothermally. These CQDs displayed good biocompatibility, high photostability, less cytotoxicity, and high sensitivity [155, 156].

2.5 The cell bioimaging using natural precursors derived CQDs

The CQDs derived from natural precursors inherit biocompatibility and therefore suitable for bioimaging application. A few cell lines that were used in bioimaging with CQDs derived from natural precursors given below.

2.5.1 Human cervical cancer (HeLa) cells

HeLa is an immortalized cell line used in scientific research sector. It is the oldest and most commonly used human cell line [157]. The HeLa cell line was derived from cervical cancer cells obtained on February 8, 1951 [158]. It was named after Henrietta Lacks, a 31-year-old African-American mother of five, who died of cancer on October 4, 1951 [159]. The cell line was found to be unusually durable and prolific, which allows it to be used widely in research study [160, 161]. HeLa cells were the first human cells to be successfully cloned in 1953 by Theodore Puck and Philip I. Marcus at the University of Colorado, Denver [162]. Since that, HeLa cells have continuously been used for research into cancer [163-168], AIDS, polio eradication [169-171], virology [159, 172-178], the effects of radiation and toxic substances, genetics [159], and countless other scientific pursuits including space microbiology [179]. In the 1960s, HeLa cells were sent on the Soviet satellite Sputnik-6 and other human space missions to investigate the long-term effects of space travel on living cells and tissue. Scientists discovered that HeLa cells divided even more rapidly in space at zero gravity [159]. According to author Rebecca Skloot, by 2009, more than 60,000 research articles

had been published about the study done using HeLa cell lines, and that number was increasing steadily at a rate of more than 300 papers each month [180].

There are a lot of studies on bioimaging HeLa cell line using CQDs derived from natural and green precursors. The CQDs with photoluminescence efficiency were obtained using grape peel [181] and *Enteromorpha prolifera* [182] precursors. The precursors, which provide CQDs with approximately two times higher than these precursors, were papaya [33] and grape juice [183]. The bioimaging of these CQDs was performed using HeLa cell-line. Currently, CQDs fabricated using the purple perilla precursor were used in bioimaging the HeLa cell-line and they reported low cytotoxicity, and good biocompatibility [183]. Besides, two CQDs with high quantum yield were produced using the hydrothermal method using lemon juice [184] and pigskin [185] as precursors were successfully used in HeLa cell-line bioimaging.

2.5.2 Adenocarcinoma human alveolar basal epithelial (A549) cells

The A549 cell line is a widely used human lung adenocarcinoma cell line that was derived from a primary lung tumour of a 58 year old Caucasian male [186]. The cells are utilized as models for the study of lung cancer and the improvement of drug therapies against it [187, 188]. A549 cells have also served as models of alveolar Type II pulmonary epithelium, finding utility in research investigating the metabolic processing of lung tissue and possible mean of drug delivery to the tissue [188]. In the process of lung cancer drug development, these cells were used as testing grounds for novel drugs. Single-cell tracking of A549 has allowed the development of pedigree-tree profiles and demonstrated correlations in behavior among sister cells [189]. Such observations of correlations can be utilized as a proxy measurements to recognize

cellular stress and inheritance as a response to drug treatment [190]. A549 has also been used in viral research and associated protein expression variation as a consequence of viral infection [191]. Although A549 is a cancer cell line, it has also been studied for its response to tuberculosis, specifically the production of chemokines as it is induced by the invading bacteria [192].

In studies that confirmed bioimaging application using the A549 cell-line, green-synthesized CQDs with 14% quantum yield and maximum emission peak between 420nm and 470nm were reported. To fabricate these CQDs, bagasse [193], Bombyx mori silk [194], and ginger [112] were used as carbon precursors. Currently, CQDs with 15% quantum yield produced using sweet corn as precursor were used in bioimaging applications using Vero and A549 cell-line and showed more than 90% of cell viability in both cell-lines at 250 mg/mL [154].

2.5.3 Human hepatocellular carcinoma (HepG2) cells

The Hep G2 is an immortal cell line which was obtained in 1975 from the liver tissue of a 15-year-old Caucasian male from Argentina with a well-differentiated hepatocellular carcinoma [195]. These cells are epithelial in morphology, possess a modal chromosome number of 55, and are not tumorigenic in nude mice [196]. The cells contain a variety of major plasma proteins, and the acute-phase proteins fibrinogen, alpha 2-macroglobulin, alpha 1-antitrypsin, transferrin and plasminogen. Hep G2 cells are an appropriate in vitro model system for the study of polarized human hepatocytes. Another well-characterized polarized hepatocyte cell line is the rat hepatoma-derived hybrid cell line WIF-B [197]. With the proper culture conditions and

maintenance, Hep G2 cells show robust morphological and functional differentiation with a controllable formation of apical and basolateral cell surface domains that resemble the bile canalicular (BC) and sinusoidal domains, respectively, *in vivo*. Due to their high degree of morphological and functional differentiation *in vitro*, Hep G2 cells are a better choice to study the intracellular trafficking and dynamics of bile canalicular, sinusoidal membrane proteins, and lipids in human hepatocytes *in vitro* [198]. These cells and their derivatives are also used as a model system for studies of liver metabolism and toxicity of xenobiotics [199], the detection of environmental and dietary cytotoxic and genotoxic [200].

In a recent study, Irmania et al. fabricated manganese-doped CQDs using a waste green tea precursor to induce magnetic resonance properties, and these CQDs with 12% quantum yield were utilized to screen HeLa, HepG2, and B16F10 cancer cells [200]. Likewise, folic acid and chlorin e6 conjugated Mn-CQDs displayed no significant toxicity up to 500 ppm. Nitrogen and sulfur dual-doped CQDs were developed with better quantum yield using fungus fibers and utilized for imaging in the HepG2 cell line [201]. The CQDs used in the HepG2, HeLa, and 293 T cell-lines, was synthesized by hydrothermal processing of cocoon silk [202]. Moreover, various other precursors such as sweet potato [42], honey [203], watermelon juice [204], and glucose were used as carbon sources to fabricate CQDs and bioimage HepG2 cell line.

2.5.4 Human breast cancer cell lines MCF-7

MCF-7 is a breast cancer cell line isolated in 1970 from a 69-year-old white woman and it is one of the most studied human breast cancer cell line in the world. The results from this cell line have had a fundamental effect upon breast cancer research and patient

outcomes. Notably, nearly 25000 scientific publications used this cell line [205], MCF-7 is the acronym of Michigan Cancer Foundation-7, which is now known as the Barbara Ann Karmanos cancer institute. This cell line was established in 1973 by Herbert Soule and co-workers at this institute [206]. MCF – 7 is a valuable cell line in cancer research, as this mammary cell line was capable of living longer than a few months [207].

In a recent study, Tadesse et al. developed Nitrogen doped CQDs using citrus lemon precursor and used it for bioimaging in MCF-7 cell-line [208]. In a study where CQDs with an average diameter of 12 nm were fabricated using walnut oil as a precursor, PC3, MCF-7, and HT-29 human carcinoma cell lines were used for bioimaging [209]. In this study, the initiation of apoptosis by CQDs was accompanied by an enhancement in the activation of Caspase-3 was also reported. CQDs produced from citric acid have been used for imaging in MCF-7 and HeLa cell lines after functionalization with folic acid. It was stated that they were bright and their biocompatibility was 97% [209]. Moreover, there were also MCF-7 imaging studies of CQDs produced from garlic and dried shrimp as precursors [111, 119].

2.6 Synthesis techniques of carbon quantum dots

CQDs have attracted the increasing attention of many researchers worldwide due to their facile fabrication techniques without expensive raw materials and sophisticated equipment. To date, two categories of techniques are commonly used in the fabrication of CQDs; they are “top-down” and “bottom-up” techniques. The former involves breaking down carbonaceous materials through chemical or physical routes which includes arc discharge [15], laser ablation [89, 210], chemical oxidation [211, 212], and electrochemical synthesis [98, 213]. The latter involves the carbonization of small

organic molecules or step-by-step chemical fusion of small aromatic molecules [98, 214, 215] such as hydrothermal/solvothermal treatment [216, 217], carbonization [218, 219], microwave - assisted synthesis [94, 220], thermal decomposition/ pyrolysis/ thermolysis [221, 222]. Nowadays, there has been much interest in exploring and improving bottom-up approaches due to the ease of techniques, precise control of precursor molecules, low cost, and environmental friendliness [223, 224] compared to the top-down techniques. A few bottom-up approaches are reviewed in detail here.

2.6.1 Hydrothermal/ Solvothermal method

Hydrothermal process is the most commonly used bottom-up method to produce carbon nanomaterials from diverse range of precursors. The list of precursors used in hydrothermal method includes organic materials [225-227], saccharides [228, 229], juice and peel from fruits [21], and vegetables [229] and animal products [230]. Hydrothermal method is popular and widely accepted due to its low-cost and environment friendliness compared to other bottom-up techniques. The hydrothermal/solvothermal method fabricate nanomaterials using experimental settings that employ high vapor pressures with a good production yield. Both the morphology and composition of nanostructure can be controlled by the manipulation of the vapor pressure and temperature of the reaction. Hydrothermal synthesis can generate nanoparticles which are not stable at high temperatures. Nanocrystals with high vapor pressures can be fabricated by the hydrothermal method with minimum loss of

materials. The compositions of nanoparticle to be synthesized can be well controlled in hydrothermal synthesis via liquid phase or multiphase chemical reactions [231].

The standard approach of this technic is either dissolving or dispersing the precursors in ultra-pure water/ Milli-Q water and transfer them to a Teflon-lined stainless steel autoclave reactor. This hydrothermal reactor is specifically made for hydrothermal reactions that take place under high temperature and pressure. It mainly made up of two parts: the outer high-quality stainless steel jacket and the inner Teflon liner or Teflon chamber. Inside the Teflon-lined autoclave, usually the reaction is carried out at maximum 240-degree Celsius (428 Fahrenheit), while the safe temperature is 200-degree Celsius (392 Fahrenheit). This reactor is a special requirement for hydrothermal process. The precursors in the reactor are fused together at relatively high temperature and pressure for several hours to form carbon cores that eventually grow into CQDs with a particle diameter generally less than 10 nm. An oven or muffle furnace is generally used to heat the precursors in the reactor and the duration of heating vary between 4 hours and 12 hours. After the reaction, the solution is allowed to cool down to room temperature naturally. It is followed by various filtration and purification processes depends on the precursors and planned applications. Long duration and high energy consumption are the concerning factor of this fabrication method.

There are CQDs engineered via hydrothermal method with better characteristics and utilized in cellular bioimaging. In 2019, Xue et al. synthesized lignin hybridized CQDs (L-CQDs) via a facile one-pot hydrothermal technique using alkali lignin in the presence of different molar ratios of citric acid and ethalenediamine. They demonstrated that L-CQDs synthesized with equal molar ratio of citric acid and ethalenediamine exhibited the highest fluorescence emission [232]. The L-CQDs showed good water dispersibility and a near spherical morphology inferior to 10 nm in

diameter, arranged mainly in interunit linkages and aromatic ring structures. As for the optical characteristics, the L-CQDs manifested an excitation dependent emission attitude, with emission maximum varying from 454 to 535 nm under excitation at 375 to 460 nm. As a results of the increase in excitation wavelengths, a red-shift is caused in the maximum emission wavelengths of the L-CQDs with a decrease in fluorescence intensity. The L-CQDs possess good cellular internalization and displayed low cytotoxicity to HeLa cells. Fabrication of CQDs, utilizing aconitic acid (AA) as the carbon precursor and ethylenediamine as the co-doping reagent through a hydrothermal reaction, was carried out by Qian et al. [233]. As produced CQDs were water soluble and displayed an excitation independent emission behaviour as the L-CQDs mentioned above. They exhibited a bright blue fluorescence and an absolute quantum yield of 56.5% in aqueous solution.

2.6.2 Microwave assisted method

The microwave is one of the electromagnetic waves that has wide spectra of wavelengths ranging from 1 to 1,000 mm that produce strong energy to break down the chemical bonds present in a substrate. It has been extensively utilized in the fabrication of carbon-based nanomaterials. The usage of microwave radiation provides an uniform heating and fast heating rates that interact firmly with carbon nanomaterials. Also, there is another advantageous feature that encourages the use of microwave-assisted methods is the control of internal and volumetric heating of the precursors [234]. Microwave-assisted techniques depends on providing heating at the molecular-level due to the alternating electric and magnetic fields that interfere with the dipole moment of polar molecules exists in a solvent. The heat that is produced through this interaction is

termed dielectric heating and is absorbed by the carbon-based precursors. In opposition to conventional heating processes such as pyrolysis, microwave radiation infiltrates the target materials and generates thermal energy at atomic/molecular levels, which in turn promotes steady and consistent volumetric heating [235]. Due to the ability of producing carbon-based nanomaterials in short-reaction times, low energy consumption, and accurate control of the reaction temperature, microwave assisted techniques have been widely employed in green synthesis approaches [94]. In this technique, various amounts of reaction medium and carbon precursor are mixed with distilled water. Then, the resultant transparent solution is heated in a microwave oven, generally of 500 W for 2 to 10 min. Within a minute, color changes can be observed. Mostly colorless liquid turn into to pale yellow, and further, it increases to dark brown indicating the formation of carbon quantum dots. After cooled to room temperature naturally, the resultant product undergoes separation and purification processes to obtain fluorescent carbon quantum dots. However, despite the numerous advantages that can be detailed for the use of microwave radiation in CQDs production, this technique still presents some limitations. For example, the use of bulk metallic materials is restricted, because it causes interferences with the electromagnetic field. However, this limitation can be easily cleared by the usage of smaller metal particles. The technique can be processed if the particle size is small enough to avoid the reflection [235]. Also, the emission of harmful microwave radiation, which is to be handled with precautions.

CQDs for biomedical imaging applications are produced from microwave-assisted method. Lu and team [236] produced N-doped CQDs in 2019, using citric acid, garlic acid, and ethylenediamine by a microwave assisted method. As synthesized CQDs fluorescence intensity was constant at different ion concentrations, but the continuous

exposure to ultraviolet light decreases the intensity of fluorescence. The CQDs maintained their fluorescence in the pH ranging between 5 and 9, and the maximum fluorescence intensity was observed when pH was equal to 5. A 25% of quantum yield is determined for the generated CQDs. After the assessment for antitumor activity by MTT assays and *in vivo* antitumor experiments were carried out, it was confirmed that CQDs hold the antitumor activity of their carbon precursor namely gallic acid. The CQDs displayed an excellent antitumor activity towards HeLa cells in a dose dependent manner. Liu and co-workers produced highly luminescent CQDs by using citric acid and several amine molecules through microwave assisted method [237]. The primary amine molecules played a double role as N-doping and surface passivating agents for preparing CQDs that helped in tuning the photoluminescence intensity. The quantum yield values increased for the CQDs up to 30.2% with the increment of the nitrogen content. The results depicted the high biocompatibility of CQDs that have great potential in the biomedical field.

2.6.3 Thermal decomposition/Thermolysis method

Thermal decomposition is a facile and fast technique to produce carbon nanoparticles. In this method, external heat is provided to dehydrate and carbonize precursors to form CQDs. This process is inexpensive, does not necessarily require solvent, and is easy to operate in a scalable operation [238, 239]. Moreover, no specific equipment or trained personals are required for this thermolysis technique. However, temperature cannot be controlled in most of the thermolysis process, and it is the main challenge. As the complete carbonization won't produce fluorescent CQDs, the carbonization should be

managed using the duration of heating. Hence, optimizing the duration for each and every precursor is very important for this method.

The fabrication of CQDs using thermolysis method is not extensively used. In 2021, Nallayagari et al. produced CQDs by heating citric acid in a heating mantle at 200 °C for 10 min. The pyrolysis of citric acid leads to CQDs rich of carboxylic moieties, very versatile groups that can be easily converted into amide groups by reaction with amines [240]. At another instant, fluorescent CQDs were simply fabricated by heating ascorbic acid in aqueous media at low temperature [241]. The results showed that CQDs had favorable biocompatibility, excellent aqueous dispersibility, fluorescence emission that depends on pH, excitation and polarity, and up-conversion fluorescence properties. These simply synthesized CQDs can be a future candidate for fluorescence probes, biosensors, and bioimaging devices.

The structure and properties of the fabricated CQDs plays an important role in their application. Those features are discussed below.

2.7 Structure and properties of carbon quantum dots

CQDs possess most remarkable and unique properties such as a wide spectrum of light emitting from ultraviolet (UV) to near infrared (NIR), tuneable fluorescence, efficient multiphoton up conversion and down-conversion. All the characteristics of CQD can be effectively modified through changing the size and shape, surface functionalization, and surface doping on the basis of quantum confinement effect (QCE), surface effect, and edge effect [242].

2.7.1 Morphology, structure and surface chemistry

The CQDs are usually quasi-spherical in shape and consist of either amorphous or crystalline carbon. Their principal constituents are sp^2 graphitic carbon sheets combined with fluorescence-inducing sp^3 chemically modified carbon sheets. It is worth noting that many researches have validated the presence of crystalline sp^2 carbon. According to the surface morphology of CQDs, most of the carbon-based nanomaterials are 2 to 8 nm in diameter, but slightly bigger particles also observed [243]. The surface functional groups of CQDs have been the matter of much research during the last few decades. Mainly because these functional groups are responsible for their photoluminescence. According to Liu et al., soot from burning candles can be treated with oxidative acid to form luminous CQDs with OH and COOH functional groups on their surfaces [244]. CQDs demonstrated $n \rightarrow \pi^*$ and $\pi \rightarrow \pi^*$ transitions in the majority of cases owing to their simply available transition energies. The aromatic sp^2 -hybridized carbons in the core of CQDs are responsible for their π -states [245]. According to Lee et al., the gap between π -states and aromatic rings decreases steadily with an increase in aromatic rings, just as it does for π -conjugation in organic molecules [246]. CQDs are caused by lone pair-containing functional groups such as amine, carboxyl, amide, and thiol. When functional groups with electron lone pairs are attached to the aromatic sp^2 -hybridized carbons, electron transitions from their n states to the π^* -states of the aromatic rings ($n \rightarrow \pi^*$) can occur [247].

2.7.2 Photoluminescence and photostability

One of the most promising features of CQD is their tunable photoluminescence which allows their application in bioimaging, cell labeling, biosensing, and optical diagnostics. The exact fluorescence mechanism of the CQDs is not completely explored yet and has been a controversial issue among scientists. Though there are many proposed mechanisms for the origin of the photoluminescence, and they are not sufficiently confirmed by experimental analysis of theoretical models. The fluorescence emission can originate mainly from two sources: one from bandgap transitions of conjugated π -domains and the other from surface defects [248, 249]. CQDs usually exhibit absorption of light from the ultra-violet region (260–320 nm) to the visible range (400–700 nm). CQDs are photon-harvesting agents, that is the reason the absorption is maximum in short wavelength. The highest absorption peak is typically around 230 nm which is attributed to the π - π^* transition of sp^2 conjugated carbon, whereas a shoulder peak around 300 nm is attributed to n - π^* conversion of hybridization with heteroatoms (for example, N, S, Mg, P, O) [250]. The absorption property of CQDs can indeed be tuned by the surface passivation or modification technique [51]. Jiang and co-workers successfully fabricated red, green, and blue luminescent CQDs via the hydrothermal method by employing three isomers of phenylenediamines [251]. The gradual, red-shifted absorption spectrum was observed in these three types of CQDs. Furthermore, heteroatom doping is also an effective technique to modify the absorption of CQD. Qu and his co-workers reported that the doping of CQDs with S, N heteroatoms moved the absorption band into the visible region 550–595 nm [252].

The CQDs that show strong absorption in the ultra-violet region, typically display excitation-dependent emission mostly in the visible spectrum [253]. Tuneable

photoluminescence is the most attractive property of CQDs giving them a wide emission range and high-intensity emission peaks ranging from visible to the near-infrared region. So, the colorful emission of CQDs is tuneable according to the given excitation wavelength using the quantum confinement effect (QCE) and the diameter of nanoparticles [254]. Figure 2.2 (A) given below presents the excitation-dependent emission spectra of a CQD sample and their corresponding colours [255]. The photoluminescence property of CQDs initiates from the energy states correlated with surface defects upon the surface passivation of CQDs for high quantum yield. Several studies have demonstrated the experiments which support the luminescence model shown in Figure 2.2. (B) given below. This explains that the surface state of CQDs is directly connected to luminescence [256].

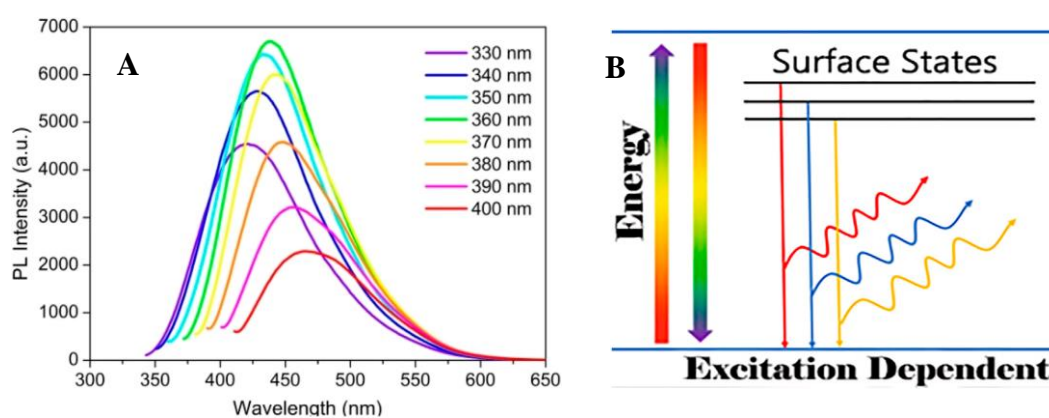


Figure 2.2: (A) Excitation-dependent luminescence spectra of CQDs. (B) Multicolor photoluminescence of CQDs ascribed to various surface energy states [255] [256]

Moreover, there is another important property of CQDs that holds is their non-blinking photoluminescence and excellent photostability when compared with those of organic fluorophores. The non-blinking photoluminescence characteristic allows monitoring of

a single molecule, whereas photostability enables long-term bioimaging in real time. The intensity of photoluminescence of CQDs synthesized by the laser ablation method is decreased by only 4.5 % after 4 hours as compared to that of organic fluorophores that photobleached within 0.5 hours [19].

2.7.3 Quantum yield

Fluorescence quantum yield is a characteristic property of carbon quantum dots and is defined as the ratio of the number of photons emitted through fluorescence, to the number of photons absorbed by the fluorophore . The magnitude of quantum yield is directly connected to the intensity of the observed fluorescence [257]. Higher the quantum yield, brighter the CQD. It is a tool to estimate the brightness and make a comparison with other fluorophores. Fluorescence quantum yield can be measured using two different methods. One is the absolute method and the other one is the relative method. Relative quantum yield measurements are carried out using the comparative method. Here, the quantum yield of a sample is estimated by comparing its fluorescence intensity to another sample of known quantum yield – it is termed the reference. Unlike absolute quantum yield measurements, which require an integrating sphere, the relative method uses conventional fluorescence spectrometers with a standard single cell holder [258]. The relative method does, however, require knowledge of the absorbance wavelengths of both the reference and the sample. The absolute method is applicable to both solid and liquid samples. Here, the quantum yield of the sample can be determined in a single measurement without the requirement of a reference standard or absorbance data. It is especially helpful for samples that absorb and emit in wavelength regions for which there are no reliable quantum yield standards available. This

approach, however, requires an integrating sphere which allows the instrument to collect and calculate all of the photons emitted from the sample. By simply comparing the total number of emitted photons with the total number of absorbed photons, the absolute quantum yield of the sample can be evaluated [259, 260]. Generally, CQDs fabricated from chemical resources such as m-phenylenediamine, L cysteine, aconitic acid, ethylenediamine (EDA), sodium citrate, urea exhibits high quantum yield [233, 261, 262]. For example Perylene, Nitric acid and Sodium hydroxide were combined in a solvothermal method and produced CQDs with 80 % quantum yield [263]. Another hydrothermal synthesis generated CQDs with 72 % quantum yield using Resorcinol and Ethanol [264]. But, the quantum yield of CQDs derived from natural resources is quite low. For instance, the quantum yield of CQDs obtained from carbohydrate based food caramels namely, jaggery, sugar caramel and bread displayed quantum yield of 0.55 %, 0.63%, and 1.2% respectively [265] , Banana peel waste derived CQDs via hydrothermal technique exhibited 5 % of quantum yield [21],. To enhance their yield, various chemical based modification technics are used. For example. The quantum yield of CQDs derived from fresh tomatoes was 1.77%, and when it is modified with EDA and urea the quantum yield increased to 7.9% and 8.5% respectively [266]. Similarly, the rice residue with EDA produced CQDs with quantum yield of 23.48% [267] and the CQDs from potato starch showed 10% of quantum yield after acid oxidation [268].

The properties of CQDs, for example their photoluminescence, can be modified using surface modification and doping. These techniques are presented with examples.

2.8 Surface modification of carbon quantum dots

Modifying the surface of carbon quantum dots plays an important role in absorption and photoluminescence properties [269]. It also alter their ability to interact with other organic molecules, ions, cells, drugs and living organisms, and affects their functional properties such as bio imaging and bio-sensing [270, 271]. This modification can be performed by either surface passivation or functionalization. The surface passivation of CQDs is one of the most important options to consider with respect to their biological applications such as internalization, cell localization, cytotoxicity studies [272, 273]. The surface passivation reduces the adverse effect of surface contamination which impact the optical properties and fluorescent intensity of CQDs. This can be carried out by forming of a thin insulating layer of coating materials such as oligomers (polyethylene glycol), thionyl chloride, thiols and spiropyrans on the surface of CQDs. The process of surface passivation increases the quantum yield which can be achieved by the soft shell of passivation agents that covers the hard fluorescent core of the CQDs [10] [51]. The surface functionalization introduces functional groups like, carbonyl, carboxyl, hydroxyl, and amines which can enforce various surface defects on CQDs. These defects can serve as surface energy traps and lead to the changes in fluorescence emission property of CQDs. Surface functionalization can be performed by surface chemistry or interactions such as coordination, π - π interactions and covalent bonding [274-277]. Since the CQDs are oxygenous in nature, they are appropriate for covalent bonding with functionalizing materials. Compared to bare CQDs, functionalized ones are superior in photo reversibility, high stability, good biocompatibility and low toxicity [95]. Sometimes, carbon nanoparticles may utilize both passivating and functionalizing

agent in which there will be no need of additional modification process during the post-fabrication treatments [276].

Various kinds of neutral and charged (positive and negative) macromolecules are used for surface passivation. Polyethylene glycol (PEG) is one of the neutral macromolecules that is biocompatible, biodegradable and prevents the non-specific binding of proteins to avoid an immune response [278-280]. Cationic macromolecules such as polyethyleneimine (PEI) gives a positive charge to CQDs, which supports them to bind negatively charged proteins in cell membranes. Hence, positively charged CQDs impact cell membrane integrity, which aids in the transection of cells [281, 282]. Further, positively charged functional groups such as PEI are beneficial in the binding of DNA and RNA to CQDs [283, 284]. Also, PEI-coated CQDs possess thermo and pH regulating properties that are beneficial in developing stimuli-based drug release [277]. The functionalization procedures causing an overall neutral or negative charge on the surfaces of the CQDs are useful for therapeutic applications. This is because neutral groups can get away from immune system clearance, while negatively charged surface groups can prevent adsorption on proteins due to electrostatic repulsion, which will ensure their widespread circulation in blood [285-287]. But, the overall quantities of neutral or negative charges on CQD surfaces also impact their internalization ability in cancerous cells. This was witnessed as a subsequent decrease in their therapeutic activity [288, 289]. In contrast, the positive surface charge assists the progress of cellular internalization due to its electrostatic interactions with the negative charge of cell membrane [290, 291]. Positively charged CQDs can also get away from endosomal degradation inside the cell via a “proton sponge” effect [292-296]. Therefore, the surface modification procedure plays an essential role in the fate of CQDs in biomedical

applications. Except surface passivation and functionalization, the doping with heteroatoms and nitrogen also can be used to enhance the characteristics of CQDs.

2.9 Doping of carbon quantum dots

Doped CQDs are generally produced via doping of the hetero atoms. For example boron (B), fluorine (F), nitrogen (N), sulphur (S), and phosphorous (P) are commonly doped into the general composition (i.e., C, H and O) of the CQDs [297, 298]. Further, co-doping of these (B, F, N, P, and/or S) heteroatoms into the CQDs is also developed [299, 300]. Doping and/or co-doping of CQDs are mainly carried out to adjust the photoluminescence phenomenon and improve their fluorescence efficacy, which is calculated in terms of quantum yield (QY%) [301-303]. In 2012, Liu et al. fabricated nitrogen doped (N-doped) CQDs with blue emission, through hydrothermal technique of a natural resource, namely grass. They observed a size-dependent quantum yield variation, where the quantum yield increases from 2.5% to 6.2% when the size decreases from 22 to 2 nm [304]. Later in 2013, Dey et al. developed blue-light emitting CQDs with enhanced nitrogen doping content of 18–22% through the reactions between glucose and urea under both hydrothermal and microwave conditions. But their quantum yields were 0.7 and 1%, respectively [305].

In another research, Wang et al. have synthesized nitrogen doped CQDs with blue emission using an aqueous phase method, namely hydrothermal treatment from folic acid as precursor, where these CQDs have shown better photoluminescence and a quantum yield of 23% [306]. Besides, Niu et al. have used glutamic acid as the primary precursor to develop N-doped CQDs with blue emission and enhanced quantum yield of 28% using pyrolysis method at 200 °C, where nitrogen and carbon atoms might have

decomposed together from glutamic acid to form these CQDs [307]. N and S doped CQDs were produced using L-cysteine and citric acid as fundamental precursors [308]. As obtained CQDs displayed a high quantum yield and favorable fluorescence properties. One step synthesis method has been performed for nitrogen doped CQDs (N-CQDs) using various nitrogen and carbon rich chemical precursors. The doping of nitrogen during fabrication evidently enhanced the fluorescence intensity as well as quantum yield of the produced N-CQDs. Another facile one step hydrothermal synthesis method was developed for N-CQDs, which were used for live cell imaging in light of their low toxicity and high quantum yield (22% in ethanol) [309]. Further, N-CQDs were superior bio-imaging agents over CQDs due to their high resistance to photo bleaching, enhanced emission efficiency, and photostable properties [310]. Currently, N and S doped CQD were synthesized from organic precursors such as caffeine and urea via solid state synthesis to provide high quantum yield and better fluorescence properties [270].

Shan et al. initially produced the B-doped CQDs with blue emission and quantum yield of 14.8% using solvothermal method from boron tribromide as B dopant, and hydroquinone as carbon precursor [311]. Then, Bourlinos and co-workers have fabricated olive-green colored B-doped CQDs by microwave heating method of an aqueous solution of citric acid, boric acid and urea, where boric acid was the B dopant. The excitation of these CQDs at 350 nm has given an emission band at 450 nm corresponding to blue photoluminescence with quantum yield of 10–15% [312]. Zuo et al. produced F-doped CQDs via solvothermal technique by using citric acid as the carbon source, and 4,5-difluorobenzene-1,2-diamine as the fluorine source, and compared them with un-doped CQDs fabricated by using o-phenylenediamine as the carbon sources, [313]. F-doped CQDs have exhibited yellow light emission under the

excitation wavelength of 480 nm, and higher quantum yields of 31% and 14% at the corresponding emission wavelengths of 550 nm and 600 nm, in comparison to the quantum yields of 28% and 11% for un-doped CQDs at emission wavelengths of 500 and 550 nm, respectively. In another research, the same authors have prepared F-doped cationic CQDs via solvothermal process by using tetrafluoro terephthalic acid as fluorine source. F-CQDs have displayed a nuclear/polymer nanostructure by combining a carbonaceous nuclear core, and a fluorine-bearing cationic polymer film surface [314].

Zhou and co-workers have suggested that phosphorous, operating as an n-type donor, can create substitutional defects in CQDs, and thereby can alter their luminescence properties [315]. Based on this suggestion, they have developed P-doped CQDs through solvent-thermal reaction between phosphorous tribromide (as P source) and hydroquinone. Herein, P doping in CQDs have shown strong blue emission in comparison to un-doped or pure CQDs . But Sarkar et al. have fabricated P-doped CQDs with green emission via thermal coupling between citric acid and Na-salt of glycine, L-valine, and L-isolucine in the presence of sodium dihydrogen phosphate (as P source) [316]. These P-doped CQDs using glycine, L-valine, and L-isolucine displayed higher quantum yield of 15.2%, 11.0% and 19.7% respectively compared to their un-doped CQDs which shown quantum yield of 8%, 8.9% and 3.7% respectively.

As fabricated and functionalized CQDs are examined for their cytotoxicity attributes and then utilized in bioimaging. The following sections discusses these topics.

2.10 Cytotoxicity of carbon quantum dots

The low cytotoxicity is one of the major advantages of CQDs over conventional quantum dots. It has been broadly researched in many types of cell lines across various concentration levels [317-319]. Generally, the CQD penetrates better into cells and maintains low or no toxicity so that bioimaging can be performed safely. As the carbon core is non-toxic, its cytotoxicity depends on the functional group attached to it [320]. The cytotoxicity assessments were performed on both functionalized CQDs and pure CQDs. Positively and negatively charged functional groups displayed cytotoxicity at high concentrations ($\leq 50 \mu\text{g}$), but the neutral functional groups are the least toxic [321, 322]. There were no toxic effects of PEGylated CQDs *in vivo* on mice at a dose of 8–40 mg CQD/kg mass of the mouse supplied intravenously (up to 28 days) [323]. In another study on cytotoxicity, electrochemically produced luminescent CQDs were examined by employing human kidney cell line, in which the CQDs exhibited no significant influence on cell viability [324]. Ray et al. introduced an advanced soot-based method for the fabrication of CQDs in which the obtained CQDs, with diameters of 26 nm, had no cytotoxicity at required concentrations for bioimaging [319]. In terms of cytotoxicity evaluation, the CQDs modified with functional molecules, such as PAA (poly acrylic acid) [325], BPEI (branched poly ethylenimine) [326], PEI [320] and PEG [327] were assessed. The CQDs which were coated with PEG in all available sizes were non-toxic and biocompatible even in much higher concentrations than required for cell bioimaging and related applications [323, 328].

Furthermore PEG1500N–modified CQDs were injected into mice and the results showed no considerable toxic effects *in vivo* up to 28 days [323]. Likewise, CQDs functionalized with PPEI-EI (propionyl ethyleneimine-co-ethyleneimine), were

substantially nontoxic to the cells under a comparatively high CQD concentrations [329]. Based on MTT assay of pure PEI, it displayed no toxic effect to HT-29 cells even at high concentrations. Yet CQDs modified with PEI were more toxic than PPEI-EI-modified CQDs obviously because of higher ethylenimine (EI) units in the PEI. Moreover, experimental results explained that both free PAA and PAA-functionalized CQDs were damaging to cells even at low concentrations (50mg/mL) and with low exposure time of 24 hours. High cytotoxic functional groups like BPEI under special circumstances such as low concentrations and short incubation time, still can be applied to functionalize CQDs [320, 330]. Sun et al. [89] performed in vitro and in vivo cytotoxicity studies of CQDs. Viability, proliferation, and cell mortality of MCF-7 cells (human breast cells) and HT-29 cells (human colorectal adenocarcinoma) were evaluated by conducting trypan blue and methyl thiazole tetrazolium assays after exposing them to CQDs.

2.11 Bioimaging of carbon quantum dots

Bioimaging is a relatively new technique for direct visualization of biological processes in real time. Cell bioimaging is emerging as a useful tool for the illustration of biological mechanisms and it is an instrumental aid in unfolding the dynamics and functions of many cellular processes. Bioimaging expands the observation of subcellular structures using light, fluorescence, electrons, ultrasound, X-ray, magnetic resonance and positrons as sources for imaging. This technique can be used to follow cellular processes, quantify ion or metabolite levels and measure interactions of molecules live [10]. Fluorescence based bioimaging has been attracting interest due to its capacity for full-colour imaging and exceptional sensitivity.

A large number of organic fluorophores are commercially available which exhibits high-emission quantum yield. For example, the Rhodamine 6G, which shows the quantum yield value of 80 % is one of the commonly used fluorescent dyes. There are few challenges in the usage of organic fluorophores in bioimaging. They are prone to photobleaching, show less photostability and high cytotoxicity, and high-priced [10]. Compared to the conventional fluorescent dyes and fluorescent proteins which are expensive and toxic, CQDs have the exceptional features of bio-compatibility, non-toxicity, tunable photoluminescence, excellent photostability, physicochemical stability, water solubility, non-blinking characteristics and good resistance to metabolic degradation [323] thus are potentially superior candidates for cell and tissue imaging [331-333]. Their small size (order of magnitude of biological molecules, 1–10 nm) makes these CQDs suitable candidates for the identification and tracking of biomolecules and organelles inside the cell and especially in the nucleus, unlike up conversion nanoparticles, which are larger with 20–50 nm diameter and cannot reach the nucleus [334]. Depending on the encapsulation/functionalization, CQDs are either localized in the cell membrane or cytoplasm. Distribution of CQDs throughout the cytoplasm is also necessary for the high resolution of the image. Several reports have already successfully demonstrated the applicability of CQDs synthesized through different techniques to image HeLa cells, A549, L02 cells, NIH-3T3 fibroblast cells, Ehrlich ascites carcinoma cells, HepG2 cells, Escherichia coli, and macrophage cells [308, 335-338].

In 2019, Zheng et al. [339] synthesized CQDs via a one-pot synthesis using ammonium citrate dibasic mixed with either 3-aminophenylboronic acid, vancomycin hydrochloride, or polymyxin B sulphate to produce BA-CQDs, Van-CQDs, and PM-CQDs. The as-synthesized CQDs were then utilized in the imaging and identification

of six bacteria species: *Escherichia coli* (*E. coli.*), *Desulfovibrio desulfuricans* (*D. desulfuricans*), *Staphylococcus sciuri* (*S. sciuri*), *Listeria monocytogenes* (*L. monocytogenes*), *Staphylococcus aureus* (*S. aureus*), and *Pseudomonas aeruginosa* (*P. aeruginosa*). Yang et al. [340] prepared CQDs through hydrothermal method from quercetin and ethylenediamine. These CQDs exhibited pH-sensitive fluorescence effect under acidic and alkaline conditions and were, therefore, applied as a fluorescent sensor to monitor intracellular pH. The “OFF–ON–OFF” detection of pH values was based on the quenching of CQDs native fluorescence triggered by pH-induced aggregation. In 2020, Zhong et al. [341] produced blood compatible N,S-CQDs through hydrothermal synthesis from *m*-phenylenediamine and tobas acid. Characterization studies revealed a quantum yield of 37.2 % for these CQDs. In vitro studies were later carried out to establish N,S-CQDs cytotoxicity towards human umbilical vein endothelial cells (HUVECs). Both confocal microscopy and flow analysis confirmed that N,S-CDs were efficiently taken up by HUVECs and were afterward localized in the cytoplasm, without considerable cytotoxicity. Additionally, hemolysis rates were found to be inferior to 0.5% after exposure to different N, S-CQDs, suggesting blood compatibility. Shi et al. [342] reported the fabrication of red emissive CQDs from *p*-phenylenediamine by hydrothermal synthesis. The as-prepared CQDs were employed as fluorescent nanoprobes for real-time sensing polarity in living cells based on the red shift of fluorescence emission wavelength confirmed in the presence of increasing polarity.

Reports showed that fluorescent CQDs provide a good potentiality in bioimaging and identifying cancer cell. Wang et al. produced dual-element CQDs with nitrogen and chloride. These CQDs exhibited strong pH-sensitive fluorescent emission for sensing intracellular pH and cytochrome c by multicolour imaging in HeLa cells [343]. The Liang and team [344] developed natural biomass carbon dots for near-infrared

fluorescence imaging-guided PDT of cancer cells and mouse tumours. Also, Ramanan and co-workers synthesized photoluminescent CQDs from eutrophic algal blooms, which served as a potential biomarker in the imaging of MCF-7 cells [345]. The Abdollah Salimi and colleagues [346] developed an ultrasensitive antibody-ssDNA aptamer sandwich type fluorometric immunosensor for sensing the specific CA125 biomarker, in which a CQD–antibody hybrid was employed as the probe for selective imaging of the cancer cells over the OVCAR-3-line cells in ovarian cancer diagnosis. Gao et al. produced silicon and nitrogen co-doped multifunctional carbon dots and utilized their mixed solution with Fe^{3+} to successfully differentiate cancerous cells (A549 and Hep G2) from normal ones because of the different content of GSH by cell imaging [347]. Even though many researched are performed in bioimaging cancer cells, specific marking of cancer cells with CQDs remains as the important challenge. Because identifying elements and ligands on cancer cell surfaces are not found in only one kind of cancer cell. For example, folic acid conjugated CQDs were used for imaging of cancer cells, but the folate receptor appears not only in hepatoma cells or breast cancer cells. Thus, improving the specificity and targeting capability of fluorescent CQDs is much more important for tracking cancer cells [348]. The cellular uptakes of fluorescent CQDs with HeLa cancer cell lines is shown in the figure 2.3

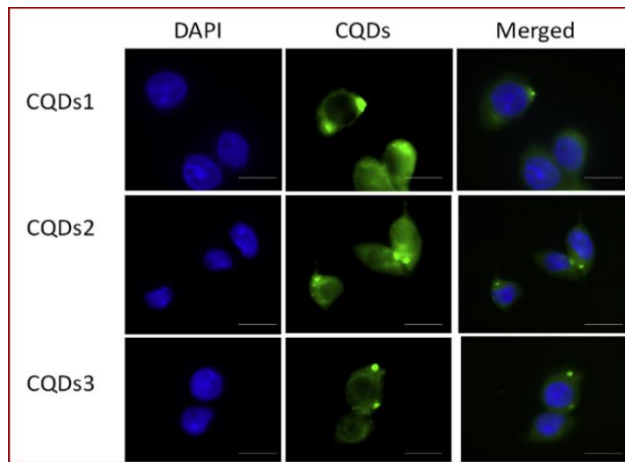


Figure 2.3 Cellular uptakes of fluorescent CQDs with HeLa cancer cell lines [349].

Other than cancer cells, CQDs are utilized in bioimaging stem cells which contributes towards skin repair, bone repair and neuro repair [350-352]. Due to their tiny size and excellent biocompatibility, CQDs can easily penetrate stem cells for imaging via the endocytosis mechanism in a concentration- and time-dependent manner [353]. Zhang and team fabricated yellow-emission CQDs to mark three different kinds of stem cells without any apparent impact on their proliferation or differentiation ability during long-term imaging [354]. Recently, the Yang team employed citric acid-based CQDs and their derivatives for identifying and tracking of rat bone marrow mesenchymal stem cells (rBMSCs) [355]. Afterwards, Chen et al. showed the promoting effects of multifunctional photoluminescent CQDs for neuronal differentiation of EMSCs via a non-viral gene delivery mode, because the as-prepared CQDs possessed attractive properties to condense macromolecules of the plasmid DNA [356].

On basis of in vitro studies, CQDs are highly promising for in vivo biomedical applications. Yang et al., for the first time, reported the in vivo imaging of CQDs by adopting three injection avenues in mice [327]. Following that many studies were

performed to explore the *in vivo* bioimaging of CQDs by animal models. According to the study of Huang et al., the CQDs could be quickly excreted from the body after three different injection routes in mice, and its clearance rate was ranked as intravenous (tail vein) > intramuscular (muscle of left leg) > subcutaneous (under the skin of left leg) [357]. Recently, Nadia et al. Experimented the biodistribution and uptake of CQDs in rats and tumour mice through radio element labelling and dynamic experiments of positron emission tomography, which displayed a rapid renal clearance of CQDs from the *in vivo* systems [358].

Presenting fluorescent probes to brain tumours and normal nerve terminals are one of the most challenging issues in neuroscience operations due to the blocking effect of the blood brain barrier (BBB). The BBB penetration of CQDs heavily depends on their small nanoparticle sizes and hydrophilic surface properties, that extend the circulation time and support passive targeting through enhancing the permeability and retention effect [359, 360]. It has been reported that CQDs with diameter less than 45 nm exhibited great BBB crossing capabilities and showed strong preference to accumulate in the brain over other organs, thus providing a new prospect in the treatment of malignant glioma. Further, the CQDs could target a human glioma xenografted in mice brain [361], and fluorescence imaging indicated that they exhibited a maximum uptake in the brain just 5 minutes after the tail vein injection, and then the CQDs were quickly cleared by mice from the tumour site.

Afterwards, Zheng et al. Fabricated novel tuneable full-colour emitting CQDs with better biocompatibility by using glucose and aspartic acid for aiming toward glioma in a mouse model, which is the very common primary tumour in the central nervous system [362]. *In vivo* imaging displayed that high-contrast biodistribution fluorescent signals of the aspartic acid - functional CQDs were detected in the glioma mass 20

minutes after tail vein injection, confirming the ability of these CQDs to freely penetrate the BBB and precisely target the glioma site rather than normal brain tissues. Also, the biocompatible nitrogen-doped CQDs (N-CDs) could cross the BBB in a concentration-dependent manner as presented in the real-time live-cell imaging and in vitro BBB model in Lu's study [363]. Based on the advantage that CQDs display great BBB crossing capabilities and a tendency to accumulate in the brain, the possibility of using transferrin-conjugated CQDs to transport drugs across the BBB to target cells has been extensively explored. Borisova et al. investigated the neuroactive effects of fluorescent CQDs on the key characteristics of both GABA (glutamate and g-aminobutyric acid) and glutamatergic neurotransmission in isolated rat brain nerve terminals [364]. The combination of the fluorescent and neuromodulator properties of CQDs enables their potential usage in fluorescent probing and visualization of key functions in nerve terminals and related neurological processes in therapeutics.

2.11.1 Requirements for cell bioimaging

Imaging the appearance and biological processes of cells are highly dependent on the conditions provided and maintained. In focus of avoiding the cellular stress, the environmental conditions must be nearly close to natural cellular ambiances. Depending on the category of cell, the medium has to be used and changed. Generally, Dulbecco's modification of MEM (DMEM) and Roswell Park Memorial Institute (RPMI) are used as medium in which serum is included to provide all the important nutrients for cell growth. Most of the mammalian cells develop between the pH 7.2–7.4. Considering the cellular toxicity, compared to RPMI, DMEM is more prone to changes in pH. So, in order to minimize the pH changes, buffering agents are generally

used in cellular bioimaging. It is also important to maintain a suitable physiological temperature to prevent the cellular detachment or alteration in morphology during the continuous exposure of cells. Typically, 37°C is maintained by temperature regulatory system such as an incubator to avoid the rapid evaporation of the medium while culturing the cells. The temperature should not vary much even during the live-cell imaging process. Phototoxicity and photobleaching are the two main challenges of live cell imaging. The toxicity experienced by the cells due the light sources is termed phototoxicity.

For instance, variation in membrane structure, cell death, and vacuolation are the possible effect of high-energy light radiation such as laser or ultraviolet light as a light source. When the light radiation interacts with the cells, it increases the temperature and stimulates the formation of free radicals which may attack cellular membrane and lipids. Loss or degradation of fluorescent signals during the live cell imaging process is called photobleaching. Photosensitivity of fluorescent probes, the expression level of fluorescent probes and size of imaging objects are the factors influencing the photobleaching process. Live cell imaging of small fluorescent vesicles is more prone to photobleaching compared to the imaging of larger fluorescent organelles like nucleus [10].

2.12 Characterization techniques for carbon quantum dots

The characterization techniques play a significant role in investigating the properties of carbon quantum dots (CQDs). Several microscopic and spectroscopic methods are in practice for standard characterization, and they provide a large amount of useful

information about CQDs' properties. As a nanomaterial, a better understanding of CQDs' features such as structure, morphology, chemical nature, functional groups and physical characteristics are essential.

2.12.1 Ultraviolet-Visible (UV-vis) Spectroscopy

UV-Vis spectroscopy refers to absorption spectroscopy or reflectance spectroscopy which occupies a part of the ultraviolet and the full visible regions of the electromagnetic spectrum. Being relatively cheap and can be easily implemented, this methodology is widely used in optical characterization of CQDs. The only requirement is that the sample needs to absorb in the ultraviolet and visible region. The absorption spectroscopy is complementary to fluorescence spectroscopy. Strong absorption in ultraviolet (UV) region is usually shown by CQDs prepared using various precursors and fabrication techniques, but still the positions of absorption peaks in the ultraviolet region are completely different for each precursor and fabrication route used for the production of CQDs. UV-Vis spectroscopy of CQDs can be used to aid in the identification of CQDs' bonds in surface functional groups, by evaluating the interactions between these groups, particularly conjugation. For example, an absorption peak at 275 nm corresponds to $n \rightarrow \pi^*$ transition was related to C = O bond, and a peak at 225 nm is caused by the $\pi \rightarrow \pi^*$ transition associated with aromatic sp^2 domains [365].

Li and colleagues [366] included active carbon into 70 mL of hydrogen peroxide to make a solution and sonicated it for 2 hours at room temperature. After filtration, fluorescent and water-soluble CQDs were obtained with a diameter range of 5-10 nm. Typical absorption of these CQDs was represented by the common UV-visible

absorption band peak at 250-300 nm. Wang et al. [367] immediately included 0.5 g citrus extract anhydrous into N-(β -aminoethyl)- γ -aminopropyl methyl dimethoxy silane solution with vigorous stirring at 240 °C and maintained the same temperature for 1 minute. Amorphous CQDs of diameter 0.9 nm were added. After natural cooling and purification steps, they were very luminescent (QY=47%). The CQDs thus produced showed a strong UV-visible absorption peak at 360 nm. Dong and co-workers [368] used carbonation of citrus acid to form fluorescent CQDs at 200 °C. Their CQDs were nanosheets of 0.5-2.0-nm thickness and ~15 nm in width, exhibiting absorption in ultraviolet region at 362 nm. The CQDs were consistent in diameter, and this was evident by the narrow peak width. The maximum emission wavelength stayed unaltered at a point when excited at various excitation wavelengths.

Tang et al.[369] performed pyrolysis of a glucose solution assisted by microwave for the preparation of CQDs and the diameter of the produced CQDs was 1.65 nm with a fluorescence QY of 7-10%. Two sharp UV absorption peaks at 228 and 282 nm were shown by the aqueous solution of these CQDs. The intensity of both UV absorption peaks was increased by increasing the microwave heating time, whereas the peak positions remained unchanged and displayed no connection with CQDs' size.

2.12.2 Photoluminescence (PL) Spectroscopy

As another class of nanomaterials, photoluminescence is the most attractive and useful characterization of CQDs. CQDs inherit certain optical properties that may reflect impacts from particles of different sizes in the sample. In addition to this, different emissive sites are distributed on each CQDs. However, research on the optical properties of small-sized CQDs are doubtful because the precise mechanism of PL is

still unclear. The vibrant PL of CQDs can be attributed to the presence of a surface energy trap established by surface passivation. The emission spectra of CQDs not only allow the assessment of the uniformity of CQDs' chemical properties, as a wide bandwidth emission is often connected to mixed populations of CQDs, but also decides if the fluorescence emission is excitation wavelength dependent or not. This characterization is very crucial as it allows for a better understanding of the possible origin of fluorescence, as the interference of surface states seems to create excitation dependent emission behaviour, and an independent behaviour appears to be compared with passivated surface states [370, 371]. Additionally, the combination of data collected through UV-vis and photoluminescence spectroscopy can be used to evaluate the quantum yield value of CQDs [127].

By utilizing surfactant-modified silica spheres as carriers and resoles as carbon precursors, CQDs of 1.5~2.5 nm were fabricated followed by surface passivation with PEG1500N. The resulting quantum yield of modified CQDs was measured as 14.7%. A suspension of passivated CQDs displayed strong blue luminescence when excited at 365 nm. These CQDs show broad emission spectra, extending from 430 to 580 nm, and they showed excitation wavelength dependent PL emission [372].

2.12.3 Transmission electron microscopy (TEM)

TEM can be used to study and analyze the nanostructure of CQDs because it possesses angstrom resolution. TEM technique has very high demand in pharmaceuticals, material science, nano electronics, and nano research sectors. The morphology of a nanomaterial, which cannot be visualized by naked eye, can be analyzed by this technique. This TEM technique is used to study the information regarding the size, shape and dispersion of a nanoparticle. TEM is extensively used as a primary part of

the characterization of CQDs. To observe and study the fine structure of CQDs, that are less than 5nm in diameter, high-resolution TEM (HRTEM) can also be used. TEM uses the incidence of a highly energetic electron beam upon a very thin layer of the CQD sample to image and study the morphological structure of nanomaterials with a nano scale resolution. Electromagnetic lenses are used to focus the electrons, and the image is captured either on a fluorescent screen or recorded on film or digital camera. TEM is one the most used techniques in the characterization of carbon nanomaterials, as it confirms the existence of nanoparticles in the sample. TEM and SEM (scanning electron microscopy) share several features, and both can determine particle agglomeration to check if adequate particle dispersion was accomplished. However, TEM is chosen in situations where the particle size exceeds the resolution of SEM, because TEM possesses' higher resolution power.

The crystalline feature of CQDs can be divided into two types of lattice fringes, named as interlayer spacing and in-plane lattice spacing, respectively. Interlayer spacing generally is focused at around 0.34 nm, whereas in-plane lattice spacing is focused at 0.24 nm [373]. Zhang et al. [354] performed acid oxidation of graphite in order to fabricate CQDs and their lattice spacing was typically less than 0.3 nm, showing that the large part of CQDs were actually separate graphene. Shinde and Pillai [374] synthesized CQDs from multi-walled carbon nanotube dots by means of an electrochemical technique, and at the same time, two kinds of lattice fringes were visualized in the high-resolution TEM image [373].

2.12.4 X-ray diffraction (XRD)

XRD is competently used to characterize CQDs and to obtain information of particle phase purity, dimension and crystal structure [48]. XRD clearly shows the crystalline

phases of CQDs [375]. Its working principle is that the interference between X-rays and crystalline materials produce constructive interference that allows the determination of the materials based on their diffraction patterns. From the values of peak positions, FWHM (full width at half maximum), and area of the peak, it is possible to calculate CQDs percentage crystallinity [376]. Liu and co-workers [377] developed CQDs by using hexa-peri hexabenzocoronene as the primary precursor. CQDs with a size of ~60 nm in width and 2-3 nm thickness were produced in this process, after pyrolysis at high temperature, surface modification, reduction treatment, and oxidative peeling. As produced CQDs exhibited a fluorescence quantum yield of 3.8%.

Mao et al. [378] fabricated photoluminescent CQDs with glycerol via a one-stage pyrolysis of poly acrylic acid. The different structures and optical features of the as obtained CQDs were altogether investigated. The XRD design showed a wide peak near $2\theta = 24^\circ$, further confirming the graphite structure of the fluorescent CQD. Bourlinos and team [379] produced CQDs via the calcination of ammonium citrate salt at 300 °C; the relating XRD design exhibited two reflections that were superimposed, which confirmed the presence of unique carbon alkyl groups that were surface modified.

2.12.5 Nuclear magnetic resonance (NMR)

An NMR characterization is commonly used to obtain structural information of CQDs. In this characterization technique, the sample is kept in a magnetic field and the NMR signal is created by the excitation of the nuclei sample with radio waves into nuclear magnetic resonance, which is received by sensitive radio receivers. The intramolecular magnetic field around an atom in a carbon molecule varies the resonance frequency, thus giving access to the information of the electronic structure of a CQD and its

attached functional groups. As the fields are unique or highly characteristic to individual compounds, in the modern organic chemistry studies, NMR spectroscopy is the accurate method to identify monomolecular organic compounds. The most used nuclei are ^1H and ^{13}C , although isotopes of many other elements, such as ^{19}F , can be analyzed by high-field NMR spectroscopy as well. In order connect with the magnetic field in the spectrometer, the nucleus need to have an intrinsic nuclear magnetic moment and angular momentum. This takes place when an isotope has a nonzero nuclear spin, meaning an odd number of protons and/or neutrons. Nuclides with even numbers of protons and neutrons have a total spin of zero and are therefore NMR-inactive [380].

Tian and team [211] utilized natural gas burning sediment as a carbon source and performed the refluxing with nitric acid, which resulted in the synthesis of CQDs. Aromatic (sp^2) carbons showed resonance in the region extending from 90-180 ppm, whereas aliphatic (sp^3) carbons display resonance in the region ranging from 8-80 ppm. The structural insights of CQDs is found with the help of NMR analysis by differentiating sp^3 carbons from those of sp^2 [381].

2.12.6 Fourier transform infrared spectroscopy (FTIR)

FTIR is one of the gold-standard techniques in the determination of the functional groups of CQDs, as it allows their differentiation based on the vibration of interatomic bonds. CQDs are mostly consist of carbon, oxygen, and hydrogen. Due to the synthesis of CQDs by the partial oxidation of a carbon precursor, carboxyl or carboxylic acid groups, hydroxyl groups, and ether/epoxy are abundant on the surface of CQDs. For the investigation of these groups containing oxygen, FTIR is a valuable technique.

Thus, absorption around the 3210–3640 cm^{-1} region can be attributed to O-H, primary amines show absorption around the 1580–1660 cm^{-1} region, and peaks at 1690–1760 cm^{-1} that are associated with absorption at 1080–1300 cm^{-1} , the existence of carboxylic acid functional groups [382]. As carboxyl, hydroxyl, and amine functional groups tend to occupy different proportions on the CQDs surface, the utilization of FTIR is beneficial in their characterization.

Peng and team [383] produced CQDs of size 1–4 nm via the compound oxidation of carbon strands of one micron and the as-produced particles were soluble in water. The infrared spectroscopy results of these were recorded. Peaks of characteristic absorption at 1724 cm^{-1} and 3307 cm^{-1} confirmed carboxyl groups' appearance on their surface; the presence of a double bond was displayed by the peak of absorption at 1579 cm^{-1} , and the existence of ether linkage was shown by an absorption peak at 1097 cm^{-1} [384].

2.12.7 X-ray Photoelectron Spectroscopy (XPS)

XPS is a surface-sensitive, quantitative spectroscopic technique based on the photoelectric effect that can identify the elements that exist within a material (elemental composition) or on the material, covering its surface. It identifies their overall electronic structure, chemical state, and density of the electronic states in the material. XPS is an excellent measurement technique because it not only shows what elements are present, but also what other elements bonded to them as a molecule. XPS is generally used to characterize CQDs and study their structure in the research sector. It relies on the elimination of photoelectrons of inner shells and the evaluation of their kinetic energy, which is caused by the irradiation of the sample with X-ray photons. It

is capable of identifying all elements except for hydrogen, and often does not show enough spatial resolution to study every CQDs [385].

2.9 Green engineering and sustainability

Green engineering and engineering for sustainability use the same ethics of brilliance, innovation, and creativity, which are the legacy of the engineering disciplines. This new application of engineering excellence to sustainability is one of the most complex and critical challenges faced by science and technology. While amazing benefit has been obtained from the vision and value statements on the requirement for sustainability, scientists and engineers believe that change will only occur when sustainable technologies are implemented in industry and spreaded throughout society. The importance of sustainability has been made clear over the past decade through research, analysis, and political summits. But the scientific and technological solutions to address this importance are only in their initial stages. The vital and significant work done in green and sustainable engineering to date is a fraction of what is yet needed and realizable [386].

The worldwide need for a greener and sustainable production has had an influence on various industries, including nanotechnology and nanomaterials. Green synthesis of nanomaterials has become as a new topic of reserach in order to create nanomaterials that are reliable, sustainable, and environmentally benign. Green engineering and nanotechnology are likely to go beyond the restrictions of conventional methods by focusing on a more sustainable approach, which can help to build a more sustainable and safer future [387].

Chapter 3

Fabrication of carbon quantum dots from bread and paper for bioimaging

3.1 Abstract

In the previous chapter, an extensive literature review was done and various carbon-based precursors for carbon quantum dot (CQD) synthesis were explored. So far, many organic, natural, and reusable precursors have been reported. Generally, the addition of inorganic chemicals during the fabrication process is common irrespective of the precursor, in order to improve the properties of the CQDs. The fabrication of CQDs from solely natural precursors using chemical-free fabrication routes has seldom been reported in the literature. This chapter intends to investigate if the CQDs can be fabricated completely chemical-free and if they can still be adequately used in the bioimaging of cells. For this study, an edible carbohydrate resource, namely bread, and a recyclable material, namely paper, were used as carbon precursors. Bread occupies a major part of global food waste and in Victoria 125 million loaves are wasted annually. Paper is commonly recycled; however, 6 million tons of paper go to wastage every year in Victoria. This study intended to convert these waste products into valuable materials. The fabrication techniques included the ignition method, toasting method, and muffle furnace method. The toasting method is proposed for the first time in this study to fabricate CQDs. The muffle furnace method produced brighter samples from bread (CQD B2) and paper (CQD MP1 – MP3), compared to the other synthesis techniques. The CQDs synthesized from bread (CQD B1 – toasting method and CQD B2 – muffle furnace method) were 10 times more fluorescent than the CQDs obtained from paper.

The CQDs derived from bread were applied for the first time to bioimage C2C12 muscle myoblasts cells. Even though the muffle furnace method produced better CQDs, the toasting method was facile, faster, and more efficient. The results indicated that bread was a better potential precursor than paper, warranting further investigation on optimizing fabrication techniques and enhancing quantum yield.

3.2 Introduction

Carbon quantum dots (CQDs) have attracted the increasing attention of many researchers worldwide due to facile fabrication techniques without the need for expensive raw materials and sophisticated lab equipment. Recently, research has focused on the use of edible hydrocarbon resources that constitute food. A large selection of edible resources such as strawberry juice [32], papaya [33], peach [34], pear juice [35], orange juice [36], sugarcane juice [37], lemon juice [38], carrot [39] [40], cabbage [41], sweet potato [42], chocolate [388], rice [267], rice flour [389], cherry tomato [390], and bread [391] [265] have been reported as suitable hydrocarbon precursors for the fabrication of CQDs. Likewise, recyclable materials and waste products are also being utilized in CQD fabrication. lemon peel [43], taro peel [44], watermelon peel [45], facial tissue [392], paper [393], and orange peel [394] are some examples of them. However, most of the currently practiced fabrication techniques that employ natural resources also require the additional use of harsh acids, bases, or solvents with synthetic chemical precursors.

When these edible resources are combined with chemicals, the applications of the quantum dots to the biological field become limited. Particularly, the biomedical field necessitates biocompatible CQDs with non-toxic elements or elements with minimal

biological impact for safe application. Although most of the fabrication methods claim that the neutralization and dialysis are used to remove the excess unreacted chemicals, it is much better to guarantee this by seeking a greener route and eliminating the use of pure chemicals entirely. If chemical-free synthesis routes can produce similar or better CQDs in a cost-effective and time efficient fashion, this will be a more desirable for future biomedical applications such as in vivo cell bioimaging.

Bread is a cheap, widely available, and an emerging carbohydrate precursor for CQD fabrication. It is consumed by many people across the world in different forms and approximately 10% of the manufactured bread is wasted globally [53]. As bread is a carbohydrate, it contains the natural precursor for carbon quantum dots. Previously, when CQDs were fabricated from bread, concentrated phosphoric acid (14.6 M), sulfuric acid (2 M) and nitric acid were often used for passivation [395], and oxidation [391]. Even though, it was claimed that the chemicals were neutralized using purification techniques; a minimal amount would cause cell death. This chapter investigates the use of bread as a primary precursor for CQD fabrication without any chemical additive. We explore more novel and environmentally benign routes to fabricate CQDs from bread.

Likewise, in the search of another easily accessible, cheap carbon resource, a recyclable material, namely paper, is considered. Papers are one of the substantial products that are extensively used globally. Paper production has grown over the past few decades as well as the number of discarded papers also increased. Even though it is believed that most of the discarded papers are recycled as new papers through the conventional paper recycling, in reality, only 60% of the discarded papers are recycled and the rest 40% are wasted [396]. Reusing the paper as a precursor is potentially a green solution. As the main constituent of paper is cellulose, it can serve as a carbon source for CQD

fabrication. Hence, in this chapter different types of papers also used as precursors for CQD fabrication.

This work presented the facile fabrication techniques, to produce CQDs from bread and different types of papers without adding any chemicals. Particularly, the domestic bread toaster is used for the first time to fabricate CQDs for bioimaging application. Section 3.3 details the fabrication and characterization of CQDs. It also illustrates the cell culture and bioimaging procedures. Section 3.4 presents and discusses the results of various characterization and cellular bioimaging. The efficacy of the derived CQDs in bioimaging without any further modification or passivation was explored and reported., while section 3.5 concludes the chapter.

3.3 Materials and methods

3.3.1 Fabrication of CQD from bread

In the present study, white bread (sourced from a local supermarket) was used for CQD fabrication by using two different methods. In the first method, a domestic bread toaster (TARSST19B, Target Corporation, Williams Landing, Australia, operating at 220–240 V, 50 Hz, 780–830 W) was used to toast two slices of bread ($56.57 \text{ g} \pm 0.1 \text{ mg}$) over different time intervals starting from 2 minutes to 6 minutes with one minute increment. The heating temperature increased from room temperature and the final temperature depended on the duration of toasting. After analyzing the resulted products using their emission spectra as the key performance indicator (KPI), the fabrication conditions were optimized. The appropriate time duration and temperature for toasting method were identified as 5 minutes and 240 °C, respectively. The carbon residues from the

charred part of the bread slice were carefully scrubbed out, and ground using mortar and pestle until a fine powder of 3.64 g (± 0.1 mg) was obtained. About 0.5 g (± 0.1 mg) of fine carbon powder was dispersed in 50 mL of Milli-Q water by bath sonication (Soniclean, LABOUIP Technologies, Bayswater, Australia) for 5 min where ultrasonic energy is supplied, and the mixture was then centrifuged (MSE centrifuge, Thomas Scientific, New Jersey, USA) for 5 min at 3000 rpm. The centrifugation speed was optimized based on the fluorescence. The resulting supernatant was filtered using a number 1 (90 mm) filter paper (Whatman, GE Healthcare UK limited, Amersham, UK). A sterile syringe filter unit (Minisart, Sartorius, Gottingen, Germany) of 0.2 μm was used to purify the sample solutions and prevent bacterial growth. This sample was labelled CQD B1.

In the second method, the two similar bread slices of 56.52 g (± 0.1 mg) were cut into smaller pieces and transferred into a ceramic crucible to heat in a muffle furnace (SurTec, SUNVIC, Hamilton, UK). The temperature of the muffle furnace increased from the room temperature to the chosen temperature. The bread pieces were heated at different temperatures, starting from 180 °C to 260 °C with the 20⁰C increment, and for several time intervals starting from 20 minutes to 50 minutes in 10 minutes increments. The photoemission spectra of the resulted products were used as the KPI to optimize the muffle furnace procedure. The bread pieces that were carbonized for 30 minutes and removed from the furnace at 220 °C were very promising. The dark brown colored charred bread products were ground using mortar and pestle until a fine powder of 8.21 g (± 0.1 mg) was obtained. Another sample was prepared from 0.5g of this fine carbon powder dispersed in Milli-Q water. The same purification procedure used for CQD B1 (toasting method) was used here, and this sample was labelled CQD B2 (muffle furnace method).

3.3.2 Fabrication of CQDs from papers

In this fabrication process, different sources of papers from newspapers (sourced from the household), paper towels (Viva, local supermarket)), and A4 printing paper (Reflex, office works) were used, and two fabrication methods were employed. As the initial method, 5g (± 0.1 mg) of each paper sample were carbonized by ignition inside the fume hood. After complete carbonization, 0.5 g of charred product from each type of paper was separately dispersed in 50 ml of Milli-Q water by sonication (Soniclean, LABOUIP Technologies) for 5 minutes and the mixture was then centrifuged (MSE centrifuge, Thomas scientific company Pty. Ltd) for 5 minutes at 3000 rpm. The resulting supernatant was filtered using a number 1 (90 mm) filter paper (Whatman, GE Healthcare UK limited). The samples were labelled as CQD P1 (newspaper), CQD P2 (paper towel), and CQD P3 (A4 printing paper).

In the next method, 5 g of each paper samples were collected in a crucible and kept inside the muffle furnace (SurTec, SUNVIC UK) one by one for complete carbonization. At the completion of the carbonization process, which took 45 minutes with the temperature settings of 280°C, each sample was charred and black in colour. The charred products were obtained, and the samples were prepared using the same procedure described above. The samples were labelled as CQD MP1 (newspaper), CQD MP2 (paper towel), and CQD MP3 (A4 printing paper).

3.3.3 Characterization of CQDs derived from bread and paper

Initially all the samples were optically characterized and then two samples (CQD B1 and CQD B2) were selected for further characterizations.

Fluorescence Measurements

Fluorescence measurements were carried out on a CLARIOstar® (BMG LABTECH, Ortenberg, Germany) 96-welled plate reader with a Costar® 96-Well Black Polystyrene Plate (Ortenberg, Germany). Maximum excitation and emissions were determined by scanning aqueous samples (150 µL) from 320 to 520 nm in 20 nm increments. Emissions spectra were recorded between 20 nm above the excitation value to 700 nm.

Transmission Electron Microscopy (TEM)

The lyophilized samples were prepared by resuspending them in ultrapure water (18 MΩ) and filtering through a 0.2 µm filter. The filtrate was dropped onto a holey-carbon grid and allowed to dry. Morphological characteristics of the particles were observed using a JEOL 1010 TEM (JEOL Ltd, Tokyo, Japan) operated at an accelerating voltage of 100 kV.

Fourier Transform Infrared Spectroscopy (FTIR)

FTIR spectra of the lyophilized samples were determined by Fourier transform infrared spectroscopy (Perkin Elmer, Waltham, MA, USA). An average of 16 scans with a resolution of 4 cm⁻¹ was performed within the range of 4000–400 cm⁻¹.

Nuclear Magnetic Resonance Spectroscopy (NMR)

With a view to obtaining the chemical natures of the CQD materials, we employed a Bruker 600 MHz NMR instrument (Billerica, MA, USA) and the ^1H and ^{13}C spectra were ran in deuterated water (D_2O) at ambient probe conditions. In the case of the proton spectrum, an in-built spectral editing technique was used to “suppress” the undesirable and otherwise prominent residual proton signal from water. The collected spectra were then processed by proprietary software from Bruker (TopSpin, version 4.0.8; Software for Processing the Acquired NMR Data; Bruker plc, Melbourne, Australia, 2016).

X-Ray Diffraction (XRD)

The extent of crystallinity of the lyophilized samples was determined by a diffractometer, XRD (Bruker AXS D8 DISCOVER, Billerica, MA, USA), equipped with a Cu $K\alpha$ radiation source ($\lambda = 1.5418 \text{ \AA}$) operating at 40 kV and 35 mA. Spectral data were attained in the μ -2 θ locked-couple mode over a 2θ interval of 5–90°.

Zeta Potential

Particle surface charges were measured in ultrapure water (18 M Ω) using a Malvern 2000 Zetasizer, Malvern, UK following appropriate dilution and sonication within a DTS 1060C cuvette (Malvern, UK).

3.3.4 Cell culture and bioimaging

The synthesized CQDs were tested on C2C12 mouse muscle myoblasts (ATCC[®] CRL-1772[™] via Sigma, Australia) to evaluate their potential in bio-imaging of cells. C2C12 cells were routinely maintained in DMEM media containing 10% FBS (fetal bovine serum) and 1x Antibiotic-Antimycotic (Gibco[®] Catalog number: 15240062) and kept at 37 °C in a humidified, 5% CO₂ atmosphere. The cells were seeded on to coverslips pretreated with poly-L-lysine and after 24 hours, CQDs (185 µg/mL) were added to the media at a 1:2 (CQDs: media (volume/volume)) ratio and incubated for the specified amount of time along with the control group cells. The control group cells were treated with an equal volume of sterile water, no CQDs were added. Cytotoxicity of CQDs was tested by seeding equal number of cells in 6-well plates and treating them with CQDs, or water. After 24 hours of incubation, the cells were lifted by treating them with 1× TrypLE[™] Select enzyme for 5–10 minutes and diluted with the complete media. The cells (0.1 mL) were treated with an equal volume of trypan blue solution (0.4%) and viable cells were counted using hemocytometer and calculated. Cells from four individual wells were counted in duplicates for each sample set for representation.

Differentiation was initiated by washing 90–95% of the confluent cultures with phosphate buffered saline (PBS) and incubation in differentiation media (DM: DMEM with 2% horse serum and 1% PS), for 3–5 days with media change every 24 hours. The differentiated myotubes were treated with CQDs as described above for 24 hours.

For imaging, all coverslips with cells were fixed with 4% formalin for 15 minutes, washed with PBS, and mounted on slides with or without DAPI. The cells were visualized with a fluorescent microscope (Nikon-Tish-A1R-MP, Melville, USA) at 20×

setting. All images were converted to the tagged information file format and processed with the Adobe Photoshop program (Photoshop CC 2015, Adobe, San Jose, CA, USA).

3.4 Results and discussion

This section discusses the results obtained from various characterization and bioimaging.

3.4.1 Characterization of CQDs

Fluorescence measurements

The emission spectrum at different excitation wavelengths was recorded to analyze the photoluminescence property of all the samples. As shown in Figure 3.1, five excitation wavelengths between 340 nm and 420 nm were used and it was observed that both bread samples (CQD B1 and CQD B2) had similar emission trends with maximum intensity at 360 nm excitation wavelength. Any further increase in the excitation wavelength resulted in the reduction of emission intensity and slight shifting in peak wavelength. The emission spectra also exhibited a redshift and displayed an excitation tunable emission. The red-shift of emission under various wavelengths can be explained by radiative recombination of the excited electrons from the $n-\pi^*$ transition of C=O in multiple surface emissive trap states [397]. The excitation dependent emission property of the fabricated CQDs is in agreement with several previous studies reported in the literature [265, 398, 399]. Figure 3.2 showed a comparison of both CQD B1 and CQD B2 at 360 nm excitation. The fluorescence intensity of CQD B2 (muffle furnace

method), was 50% higher than CQD B1 (toasting method). The toasting method is a facile technique that heated the bread slices to a high temperature (240°C) rapidly within five minutes. On the contrary, muffle furnace method used 30 minutes to gradually increase the temperature to 220°C. The difference in heating process resulted CQDs with different photoluminescence property. The gradual heating profile of muffle furnace method with the heating rate of 7.33°C/minute was found to produce CQDs with better emission compared to the toasting method.

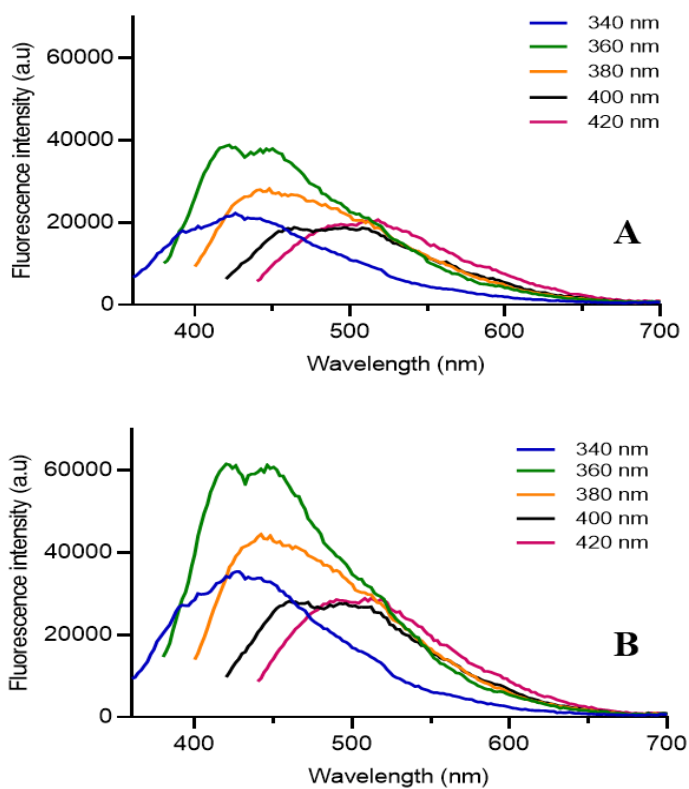


Figure 3.1: Emission spectra of (A) CQD B1- bread sample derived from toasting method and (B) CQD B2 – bread sample derived from muffle furnace method

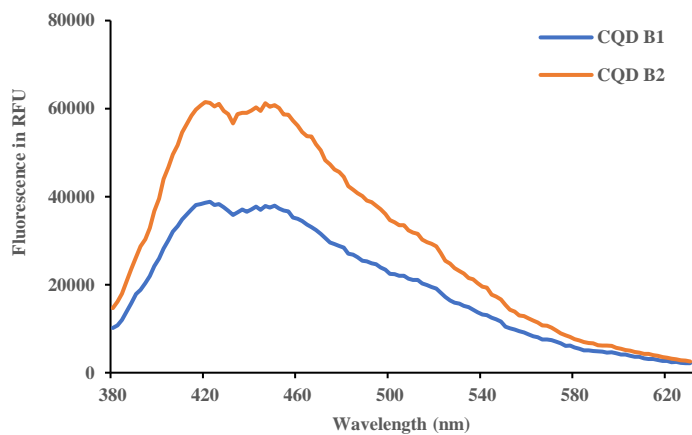


Figure 3.2: Emission spectra of CQD B1 (bread sample derived from toasting method) and CQD B2 (bread sample derived from muffle furnace method) at 360 nm excitation

The emission spectra of the samples fabricated using different types of paper were also obtained, as shown in Figure 3.3. All the samples were luminescent at 360 nm excitation, with the emission peaks between 405 and 415 nm. The fluorescent intensity of CQD P2, which is derived from a paper towel, was less than the other two samples. The CQDs obtained from A4 printing paper using two different carbonization methods and named CQD P3 and CQD MP3 were compared (Figure 3.4). The sample obtained from muffle furnace methods (CQD MP3) showed enhanced photoluminescence compared to the ignition method (CQD P3).

However, the fluorescent intensity of these samples from papers was insufficient. On the other hand, the emission intensity of bread samples (CQD B1 and CQD B2) was approximately ten times greater than the samples from different types of papers. Hence, only the CQDs obtained from bread were further characterized and applied in bioimaging of cells in the following sections.

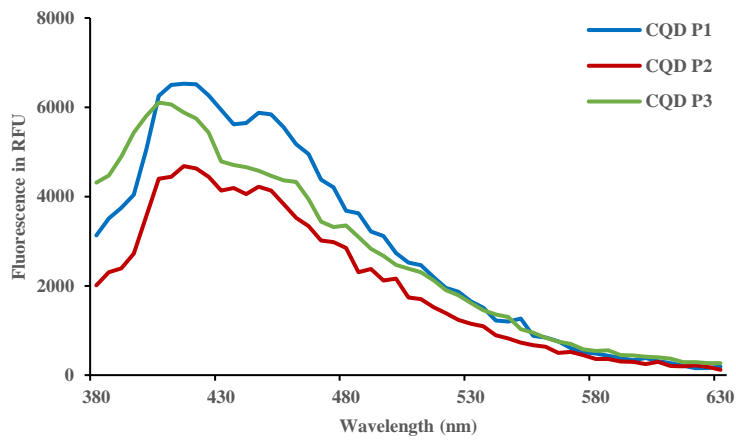


Figure 3.3: Emission spectra of CQD P1(newspaper), CQD P2 (paper towel), and CQD P3 (A4 printing paper) at 360nm excitation

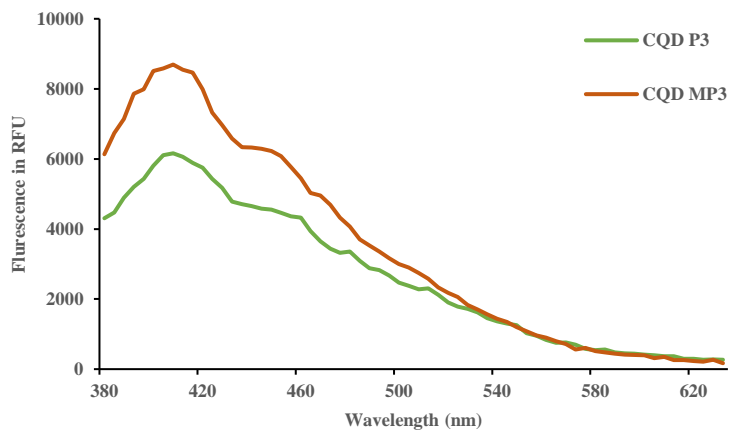


Figure 3.4: Emission spectra of CQD P3 (Ignition method) and CQD MP3 (muffle furnace method) at 360 nm excitation.

Transmission electron microscopy (TEM)

Transmission electron microscopy (TEM) was performed to determine the morphological characterization. Figure 3.5 shows the TEM images and the size distribution histogram of the lyophilized samples for both CQD B1 (toasting method) and CQD B2 (muffle furnace method). The presence of spherical quantum dots was clearly visible in both samples. The particle size distribution histograms depicted that most of the nanoparticles were less than 10 nm in diameter. It was observed that CQD B2 consistently consisted of smaller particles than CQD B1.

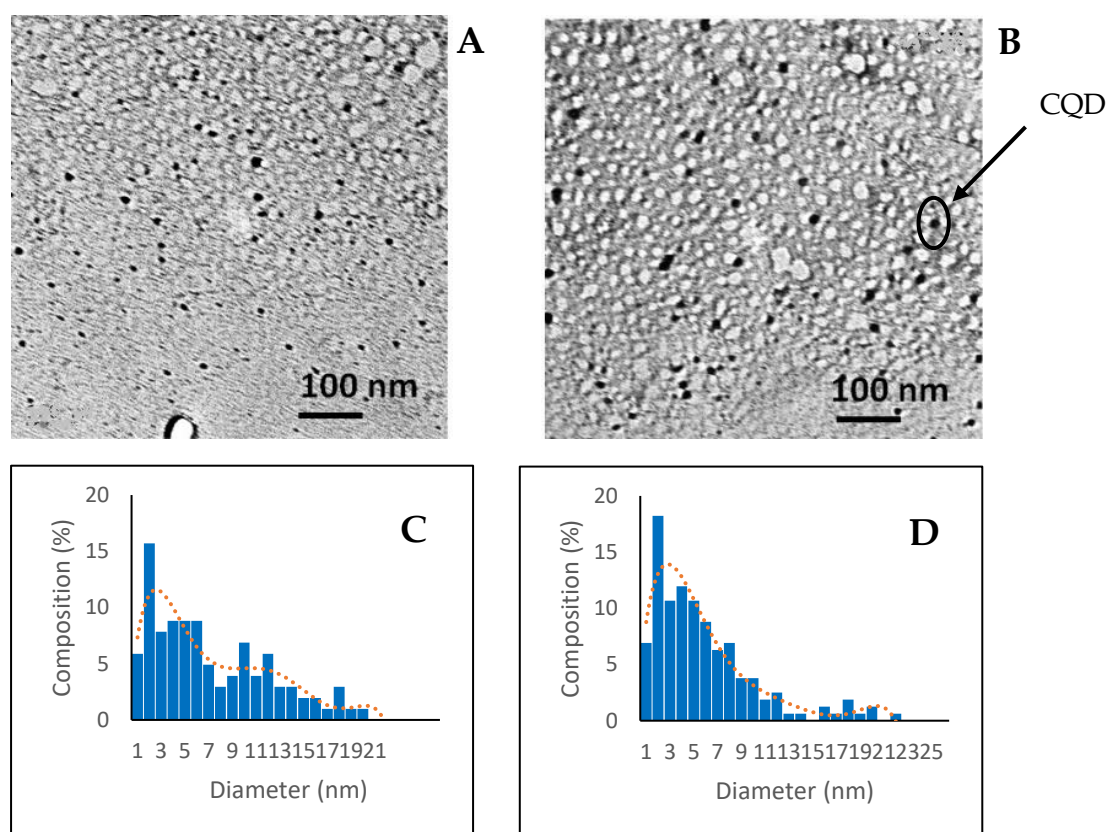


Figure 3.5: (A, C) TEM image and size distribution histogram of CQD B1 (Bread sample-toasting method), respectively; (B, D) TEM image and size distribution histogram of CQD B2 (Bread sample-muffle furnace method), respectively

The particle size of CQDs derived from muffle furnace (CQD B2) method are primarily between 2nm and 8nm. The toasted bread sample (CQD B1) has more particle with 10nm in diameter and higher compared to the muffle furnace sample (CQD B2). This variation is due to the different heat rates of two methods.

Fourier Transform Infrared Spectroscopy (FTIR)

FTIR analysis showed that the overall vibrational spectral patterns of both CQDs (CQD B1 and CQD B2) very closely resembled that of the parent carbohydrate (i.e., starch molecule). The broad peak at between 3200 and 3500 cm^{-1} could be attributed to the hydroxyl group (-OH), either from the unburnt starch matrix or from terminal hydroxyls attached to the graphitic carbons. The presence of the carboxyl (-COOH) group was clearly visible through C=O bond stretching (around 1700 cm^{-1}). The peaks at 1200 cm^{-1} and at 1100 cm^{-1} depicted the C – O bonds.

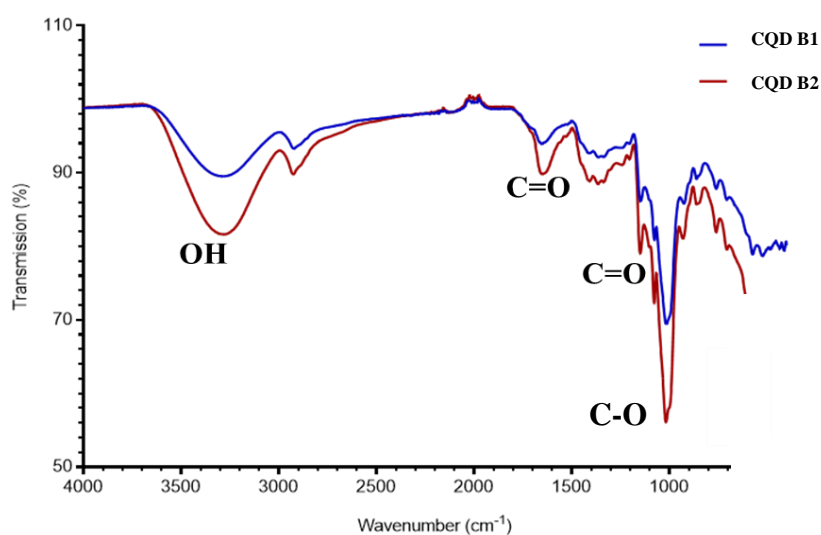


Figure 3.6: FTIR spectra of CQD B1 (bread sample derived from toasting method) and CQD B2 (bread sample derived from muffle furnace method)

X-Ray Diffraction (XRD)

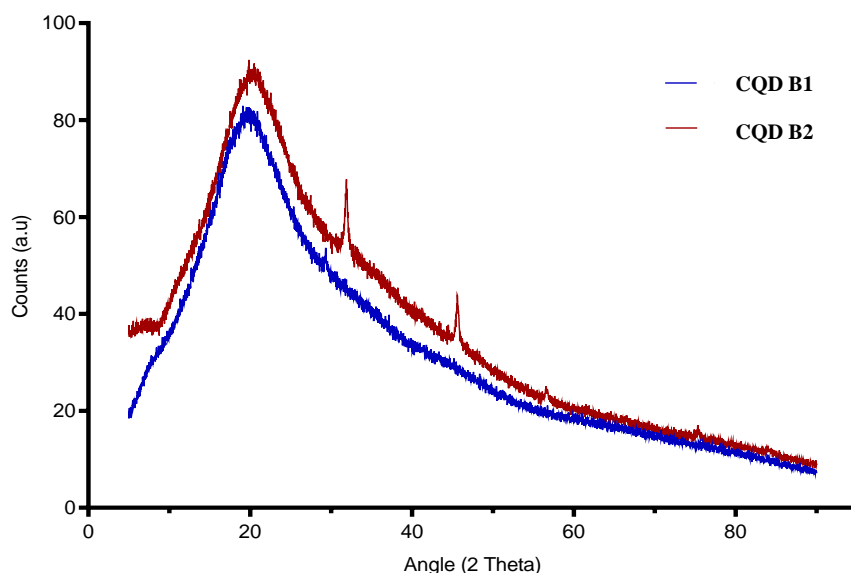


Figure 3.7: XRD pattern of CQD B1 (bread sample derived from toasting method) and CQD B2 (bread sample derived from muffle furnace method)

The structural and morphological features of the synthesized samples were primarily elucidated through X-ray diffraction studies. The XRD spectra of the two samples showed negligible well-defined peaks indicating that the conditions generated during pyrolysis did not favor the production of crystalline carbon dots. Even though both samples confirmed their identical nature, CQD B1 (Toasting) is more amorphous (80.2%) than the CQD B2 (muffle furnace) (74%). The broad diffraction peaks were seen at 21 degree for both samples. This was comparable with previous reports and the spectra was in alignment with pure graphite (JCPDS 41-1487) [400].

Nuclear Magnetic Resonance (NMR)

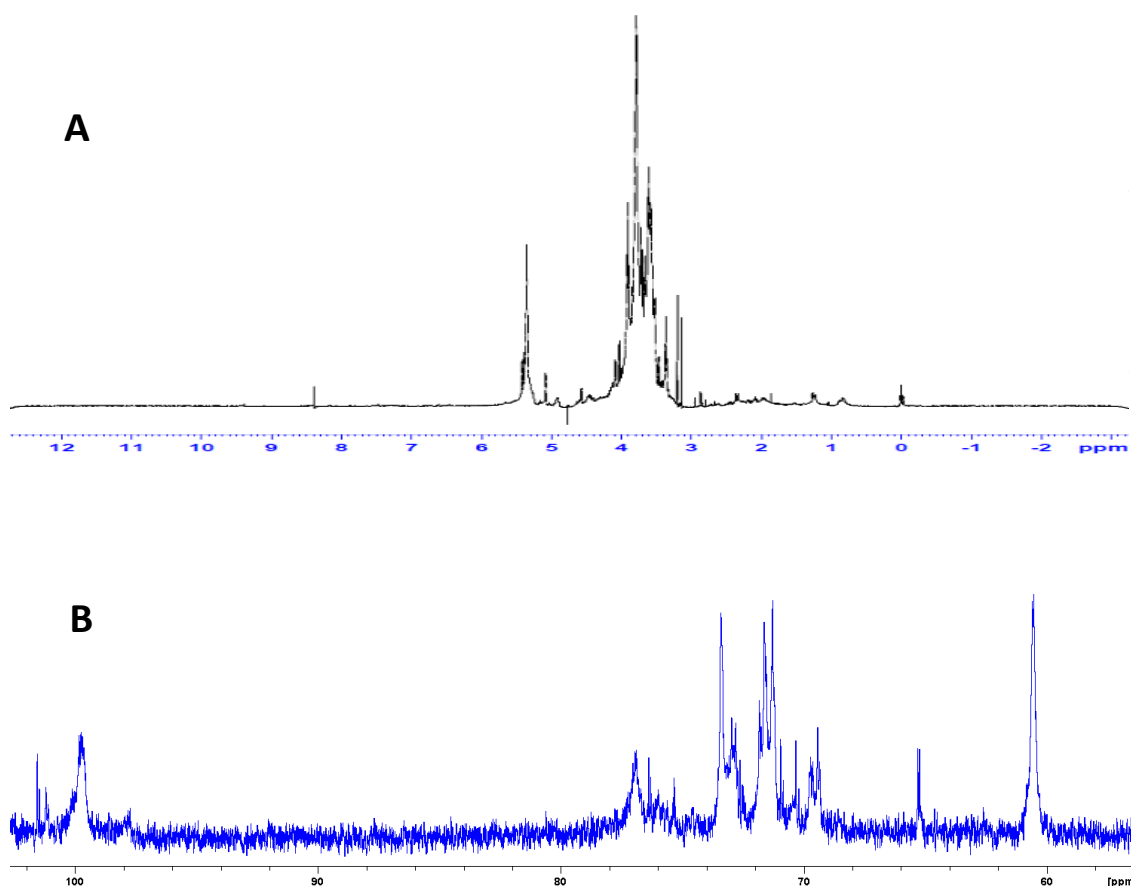


Figure 3.8: (A) ^1H spectrum of a colloidal solution of the CQD B2 (bread sample derived from muffle furnace method) in D_2O ; (B) the corresponding ^{13}C spectrum.

In the NMR spectra, there was evidence regarding the chemical environments of protons, as well as the chemical nature/hybridization states of the carbon atoms to which the protons were attached [130, 401]. These broadly agree with the complementary information obtained through the FTIR spectra. The signals in the ^1H spectra (Figure 3.8 A) can be assigned as follows: 1–3 ppm (H attached to sp^3 carbons); 3–6 ppm (for the protons attached to oxygenated, such as hydroxyl and ether, and carbonyl groups; 8–10 ppm (aldehydic protons). In the corresponding ^{13}C NMR

spectrum (Figure 3B), at least three corresponding signals/regions can be unambiguously identified: 20–80 ppm (sp^3 carbons and carbons bonded hydroxyl groups); 80–100 ppm (for carbons attached to ether functions); 100–120 ppm (aromatic, or sp^2 carbons).

Zeta potential

Zeta potential, which is indicative of particle surface charge, is widely used to characterize nanometer-sized particles in the dispersion [402] and analyze particle colloidal stability. The particle surface charge of samples CQD B1 and CQD B2 was -10.42 mV and -7.24 mV, respectively. The stability of the colloidal dispersions generally increases with the magnitude of the zeta potential [403]. The zeta potential of the cells should be greatly negative (membrane potential of -50.5 ± 0.8 mV) and the particles showed only very weak stability.

3.4.2 Internalization of CQDs by C2C12 cell lines

In bio-medical research, staining is a reliable tool to visualize and enhance features inside cells, tissues, and animal models [404]. Several colored and/or fluorescent stains and dyes like, hematoxylin-eosin, DAPI, fluorescein isothiocyanate, and rhodamine are widely used to achieve this. However, one of the main disadvantages of many of the inherently fluorescent particles is their sheer size, and hence the inability to cross live cell membranes. Most fluorescent dyes are also toxic to live cells, and this necessitates fixing the cells prior to staining. Since the size of synthesized CQDs is less than 10 nm

and that they are derived from natural sources with a green route of synthesis, their capacity to cross live cell membranes was tested.

C2C12 or mouse muscle myoblast cell lines, were selected as they are capable of differentiating into myotubes and are widely used to study muscle formation in vitro. Thus, imaging the myoblasts and myotubes are crucial in this specific research scenario as an application example of real time bioimaging. This can be further applied to other 2D or 3D cell culture model systems, which have the ability to differentiate to several different cell/tissue types across biological systems.

The C2C12 cells were incubated with the prepared carbon quantum dots, CQD B1 and CQD B2. The cells were grown on coverslips pre-treated with poly-L-lysine. The CQDs with the concentration of 185 ug/mL were additionally filtered through 0.2 μm filters (to prevent bacterial growth) and added to the media containing cells. Since the CQDs were dissolved in water, the corresponding volume of water was added to the control cells. As the doubling time of C2C12 is 15 h [405], the initial incubations were set at 24 h, which is estimated to be ample time for testing the internalization. After 24 h, the wells containing coverslips were fixed using formalin and after washing with PBS, the coverslips were inverted and mounted onto the slides. The fluorescence imaging was carried out using filters for fluorescein isothiocyanate (FITC) for green and tetramethyl rhodamine (TRITC) for red, depicting the excitation filter wavelengths of 475–490 nm and 545–565 nm respectively. The results showed a clear internalization of CQDs by C2C12 cells as compared to control cells, both in green and red filters. Since CQD B1 yielded better fluorescent intensity when compared to CQD B2, CQD B1 was chosen for further experiments. Significant cell death was not observed during this experiment suggesting that these CQDs could potentially be safe candidates for bio-imaging.

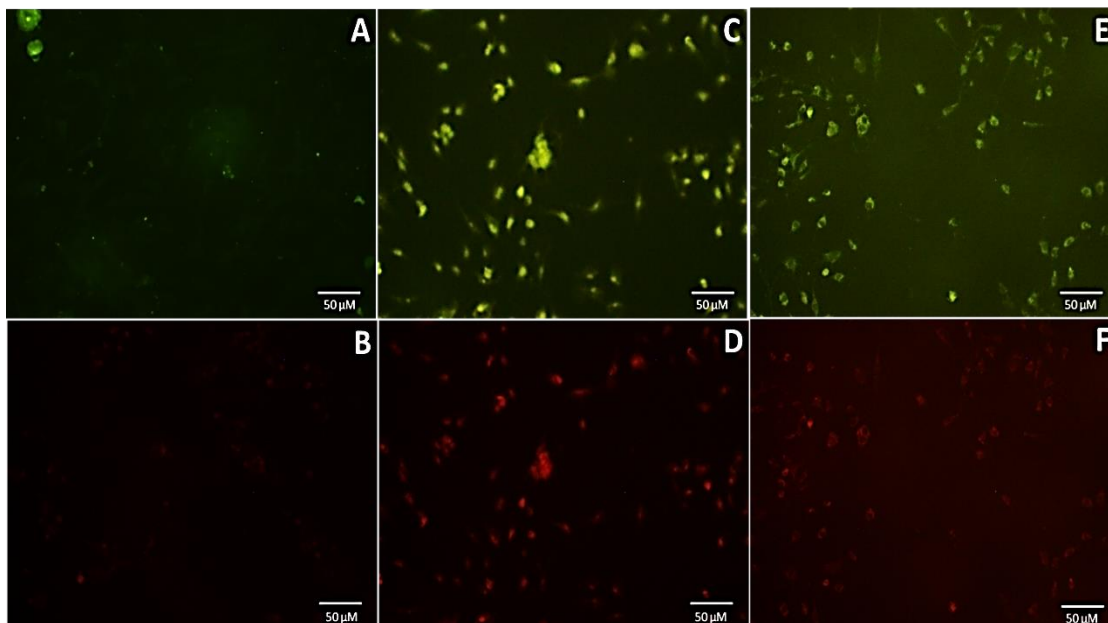


Figure 3.9: Fluorescence images of C2C12 cells after 24 hours of incubation with CQDs. (A,B) Cells incubated with water as control; (C,D) cells incubated CQD B1; (E,F) cells incubated with CQD B2; (A,C,E) are images from FITC (green) channel; (B,D,F) are images from TRITC (red) channel.

Having observed the successful internalization of CQDs by C2C12 cells, the time period taken for this was followed by incubating C2C12 cells with CQD B1 for different time intervals (0, 6, 12, 16, 20, and 24 hours). The data (Figure 3.10) showed that at the end of 16 hours, the cells exhibited a remarkable change in fluorescence intensity compared to the control group. This also gives us an estimate of incubation time required for quantum dots with live cells for the purpose of bio-imaging. From the data, 16 hours or overnight of incubation is deemed sufficient, thus making them potentially good candidates for applications in bio-imaging.

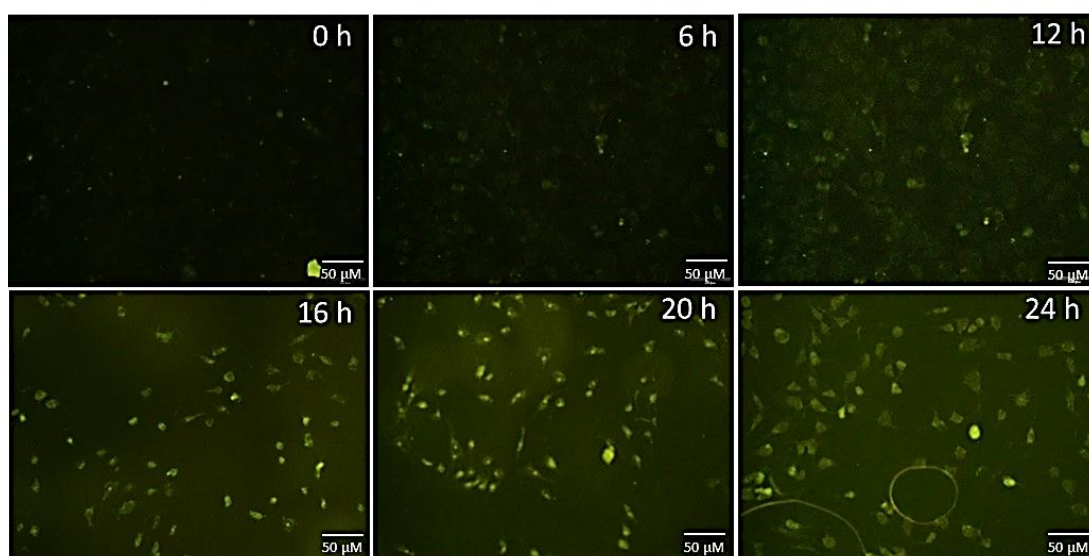


Figure 3.10: The time course of the internalization of CQD B1 by C2C12 cells tracked for 0–24 hours. The images were recorded using FITC channel

3.4.3 Cytotoxicity

Since low cytotoxicity and resultant minimal cell death is one of the crucial advantages when imaging cells using CQDs, we further estimated cell death after incubating C2C12 cells with CQD B1. For this, 15,000 cells were seeded to each of the cell culture wells. After 24 hours of incubation, CQD B1 was added. The cells were counted before and 24 hours after the addition of CQDs. The results (Figure 3.11) showed that the CQD B1 exhibited very low cytotoxicity. More than 96% of the cells were alive after incubation of 24 hours. This is in agreement with several studies published earlier using CQDs derived from natural sources [16, 17, 406]. Considering that the doubling time of C2C12 cells is 15 hours [405], an incubation period of 24 hours with CQDS was found to be ample for the purpose. Furthermore, the minimal extent of cell death through cyto-toxicological effect, as exhibited by C2C12 cells in the presence of CQD

B1, is negligible. This further confirms that the synthesized CQDs can be used safely for long – term imaging of cell culture systems, and for other biological applications.

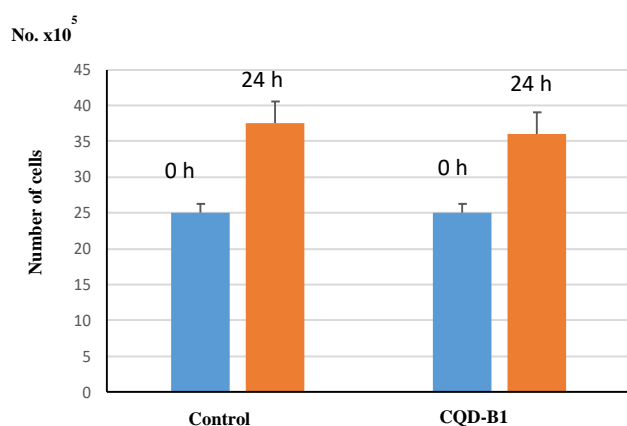


Figure 3.11: Comparison of cell viability after incubating C2C12 cells with CQD B1 for 24 hours. The blue bar represents the number of cells counted at 0 hours, and the orange bar represents the cells counted after 24 hours of incubation with either CQD B1 or equal volume water as a control

3.4.4 Uptake of CQDs by Muscle Myotube and Imaging

Two-dimensional and three-dimensional cell culture model systems, apart from helping to elucidate basic biochemical mechanisms, have tremendous potential in *in vitro* disease models, tissue engineering, regenerative medicine, cell therapy, as well as for pharmaceutical applications, especially, in drug discovery and development [407]. A simple, low cost, effective, and rapid staining method, therefore, is crucial in different stages of these studies. Evidently, C2C12 cells are one such model system used to study muscle myotube formation from myoblasts. Hence, staining different stages of myotube formation becomes vital in these studies and, if successful, can be studied and applied

to other *in vitro* cell culture model systems and can also be further extended to animal models.

In order to test the ability of CQDs to stain myotubes, C2C12 cell myoblasts were cultured in differentiation media to form myotubes. Several myoblasts fuse to form mature myotubes, thus giving the appearance of multinucleated tubes. After the formation of myotubes in differentiation media, CQD B1 and CQD B2 were added to the media containing myotubes and incubated for 24 hours. The cells were counterstained with nuclear specific stain DAPI to visualize the multinucleated structure. The Figure 3.12 shows that the CQDs were able to cross the membrane of myotubes and depict a clear image of myotubes without any additional staining methods to visualize them.

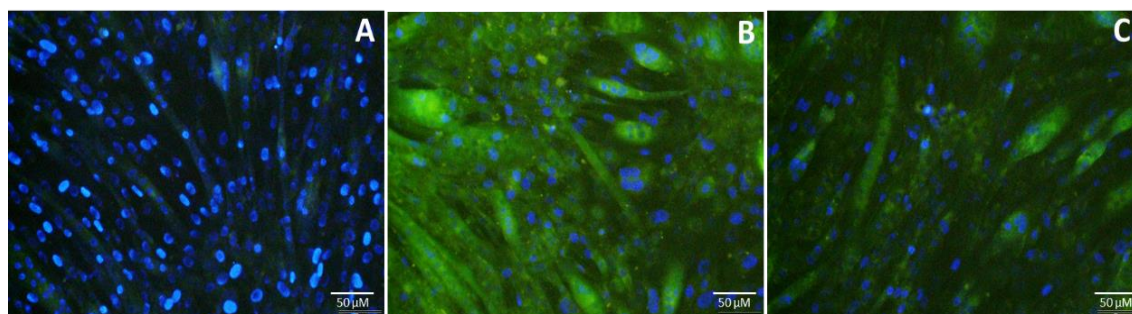


Figure 3.12: Fluorescence image of C2C12 myotubes incubated with CQDs. (A) Control cells; (B) myotubes incubated for 24 hours with CQD B1; (C) myotubes incubated for 24 hours with CQD B2. The images are from FITC (green) and DAPI (blue) channels overlaid.

These experiments reveal the fluorescence characteristics of the CQDs and that they are easily internalized, by both myoblasts and myotubes, illustrating their use in biological imaging. They are also made from inexpensive sources, have very low cytotoxicity to live cells and human beings, and require incubation time of only 24 hours, making them cheaper and safer alternatives to the commercial fluorescent dyes used in biological imaging.

3.5 Conclusion

Food waste is a global problem, that causes significant environmental harm and resulting in substantial economic losses globally. Bread is the commonly wasted food item in the developed world mainly in restaurants and cafes. Besides, paper is one of the major causes of municipal waste, that increased the disposal cost over the years. Recycling these easily accessible products into a highly applicable nanomaterial would be a valuable contribution towards sustainable manufacturing. In this study, carbon quantum dots were fabricated from bread and papers using facile processes and in the absence of any undesirable chemicals for the first time. These CQDs exhibited excellent fluorescence and other favorable physical and chemical properties. The intrinsic fluorescent property of the CQDs was successfully made used for imaging C2C12 muscle myoblast cells and myotubes. The cytotoxicity of these biocompatible CQDs was found to be comparatively low. Hence this study showed that the CQDs derived without the use of any additional chemical are capable of bioimaging. Given that the fabrication process employed in the present work does not resort to conventional wet-chemistry procedures, the results open a new perspective that warrants further investigations for optimizing the production of CQDs from bread. As bread exhibited

favorable photoluminescence and promising applicability in bioimaging, it will be our choice precursor in CQD fabrication in the remainder of this thesis. As the CQD derived from toasting method was unique, it is further investigated. The cytotoxicity is an important property that needs comprehensive exploration given that the CQD is used in biomedical application. The following chapter will further investigate the cytotoxicity of the CQDs derived from toasted method at various concentrations and report their impact on C2C12 myotube formation.

Chapter 4

Investigating C2C12 myotube formation in presence of carbon quantum dots from bread

4.1 Abstract

The previous chapter demonstrated the fabrication of carbon quantum dots from various facile techniques and their application in bioimaging. With other CQDs, a significant sample that derived from the toasting method was also studied. This toasting method was used for the first time to synthesize CQDs and these bread derived CQDs were used in bioimaging C2C12 cells and differentiated myotubes. The time course of internalization of these CQDs by C2C12 cells was also tracked for up to 24 hours. This chapter intended to investigate if these CQDs, derived from the unique and chemical-free synthesis route, impact C2C12 myotube differentiation and analyze their safety in long-term bioimaging. For this study, the C2C12 myotubes were allowed to differentiate in the presence of 1 mg/mL CQDs and they were followed at different time points. In the presence of these CQDs, myotube formation is obviously delayed and it was clearly confirmed with images at various time points. In addition, western blotting was carried out with these CQDs and it further confirmed the delay in myotube formation as the expression of transcription factors Myf-5, Myo-D and myosin heavy chain (MHC) was altered in presence of CQDs. The cytotoxicity of the CQDs was studied for concentrations from 0.5 mg/ml to 1.5 mg/ml. The MTT assay reflected that cell proliferation and cell viability were not affected even at a concentration of 1.5 mg/ml. This concentration is nearly 1000 times higher than the concentration needed for cell labeling. Thus, unlike other CQDs that were derived from chemical-related

methods, and displayed their non-toxicity in low concentrations, our bread-derived CQDs were safe up to very high concentrations. Therefore, these CQDs can be used for long-term bioimaging up to 1mg/mL concentration and their influence in cell function above this concentration require further investigation.

4.2 Introduction

The suitable physicochemical and optical properties of CQDs make them excellent candidates for biomedical applications. CQDs can be applied in various applications in the biomedical field such as gene delivery, electrochemical biosensing, pharmaceutical formulations, photodynamic and photothermal therapy, and treatment of bacterial infections and inflammations due to the excellent properties of CQDs such as low toxicity, aqueous solubility, chemically inert, non-blinking, and excitation- and size-dependent photoluminescence emission. Their small size and cellular compatibility allow them to be extensively used in cellular bioimaging. CQDs mainly enter cells via endocytosis and highly concentrate in the cytoplasm, although low amounts of CQDs in the nucleus have also been reported [408]. Although CQDs have been used *in vitro* imaging of cell transfection [409, 410], cytotoxicity remains a major barrier against major clinical translation. The carbon cores of the CQDs are non-toxic, however, the functional groups attached to them, or surface passivation performed on them cause cytotoxicity. Neutral functional groups have shown to be the least toxic [321, 322], and negatively charged functional groups are reported to cause cell cycle arrest, stimulated proliferation, and can induce oxidative stress. In contrast, positively charged functional groups are reported to cause cell cycle arrest at the graphite phase [321]. Furthermore,

surface functionalization can increase the cytotoxicity and reduce the cell viability by 60% for CQDs [317].

The current toxicity assessments for CQDs were designed and carried out based on chemical toxicity while ignoring the side effects of CQDs such as size-dependent toxicity, and phototoxicity [411, 412]. The size, surface groups, concentration and dose, and preparation methods of CQDs are the determinants of their biological activity that may lead to potential inflammation, oxidative stress, metabolic pressure, and even chronic toxicity just as other carbon nanomaterials, [413-415] which are not researched sufficiently. Generally low concentration of CQDs were used to investigate the cytotoxicity towards the cell lines. For example Yung et al. produced CQDs, employing arc-discharge of graphite rods, these unmodified CQDs were not toxic to cells up to 0.4mg/ml [327], In another study on cytotoxicity, a series of CQDs were synthesized by changing the mass ratio of diammonium citrate and spermidine, and evaluated the effects of different surface charges on the cytotoxicity, cellular uptake, stability in human umbilical cord derived mesenchymal stem cells. The cytotoxicity evaluation of CQDs was carried out for the concentration of 50 $\mu\text{g}/\text{mL}$. Their results demonstrated that, positively charged CQDs are more cytotoxic compared to negatively charged CQDs [416].

The standardized methodologies and guidelines are absent, making it difficult to compare the safety/toxicity assessments from different research teams [417]. Therefore, studies about the cytotoxicity of CQDs, their real interactions with biological systems and their potential ecological risks should be assessed systematically over a longer period of time [418, 419]. The impact of CQDs on cell functions needs to be investigated by analyzing the cells, that display formation changes or differentiation, in the presence of CQDs.

To assess the cytotoxicity of CQDs and their impact on cell functions, C2C12 cell lines were selected. The C2C12 cell line is a subclone of myoblasts that were originally collected by Yaffe and Saxel at the Weizmann Institute of Science in Israel in 1977 [420]. These cells are capable of rapid proliferation under high serum conditions and differentiation into myotubes under low serum conditions. Mononucleated myoblasts can later fuse to form multinucleated myotubes under low serum conditions or starvation, leading to the precursors of contractile skeletal muscle cells in the process of myogenesis. As C2C12 cell lines display variation in their structure and forms into myotubes, this myotube formation can be tracked and imaged using fluorescent microscopes in the presence of CQDs. Hence it is a suitable cell line to investigate the effect of CQDs on cell functions.

In this chapter, section 4.3 presents the details on materials and methods. It describes the fabrication of CQDs from bread using toasting method, TEM and optical characterization of the produced CQDs, cell culture of C2C12 cell lines, MTT assay procedure, bioimaging of C2C12 myotube formation, and western blotting process. The following section 4.4 analyses the formation of myotubes that was followed at different time points until 120 hours, discusses the cytotoxicity studies and presents the results of western blotting that was used to determine the presence of transcription factors and formation of myosin heavy chain. Finally, section 4.5 concludes the chapter.

4.3 Materials and methods

4.3.1 Fabrication of CQDs using toasting method

The toasting method is a form of thermolysis technique to produce CQDs. It is a very fast and efficient route. As in Chapter 3, a domestic bread toaster (TARSST19B, Target Corporation, Williams Landing, Australia, operating at 220–240 V, 50 Hz, 780–830 W) was used to toast two slices of white bread ($57.24 \text{ g} \pm 0.1 \text{ mg}$) sourced from a local supermarket. In accordance with the optimization carried out in the previous study, the bread slices were toasted for 5 minutes at $240 \text{ }^\circ\text{C}$. The dark brown carbon residues from the charred part of the bread slice were carefully scrubbed out, and ground using mortar and pestle until a fine powder of $3.96 \text{ g} (\pm 0.1 \text{ mg})$ was obtained. About $2 \text{ g} (\pm 0.1 \text{ mg})$ of fine carbon powder was dispersed in 30 mL of Milli-Q water by sonication (Soniclean, LABOUIP Technologies, Bayswater, Australia) for 5 minutes, and the mixture was then centrifuged (MSE centrifuge, Thomas Scientific, New Jersey, USA) for 10 minutes at 3000 rpm. The resulting supernatant was filtered using a number 1 (90 mm) filter paper (Whatman, GE Healthcare UK limited, Amersham, UK). A sterile syringe filter unit (Minisart, Sartorius, Gottingen, Germany) of $0.2 \text{ }\mu\text{m}$ was used to purify the sample solutions and prevent bacterial growth. This sample was lyophilized and labelled CQD T.

4.3.2 Characterization of CQDs

Transmission electron microscopy

The lyophilized samples were prepared by resuspending them in ultrapure water ($18 \text{ M}\Omega$) and filtering through a $0.2 \text{ }\mu\text{m}$ filter. The filtrate was dropped onto a holey-carbon

grid and allowed to dry. Morphological characteristics of the particles were observed using a JEOL 1010 TEM (JEOL Ltd, Tokyo, Japan) operated at an accelerating voltage of 100 kV.

Florescence measurement

Fluorescence measurements were carried out on a Spectro fluorophotometer RF – 5301PC (Shimadzu Europe, Duisburg, Germany) with a 1 mm PMMA cuvette (Shimadzu, Duisburg, Germany). The emission spectra were recorded at an excitation wavelength of 360 nm.

4.3.3 Cell culture and bioimaging

The C2C12 cells were routinely maintained in DMEM media containing 10% FBS (fetal bovine serum) and 1x Antibiotic-Antimycotic (Gibco® Catalog number: 15240062) and kept at 37 °C in a humidified, 5% CO₂ atmosphere. The cells were seeded on to coverslips pretreated with poly-L-lysine and after 24 hours, CQDs (1 mg/mL in phosphate buffer saline (PBS)) were added to the media and incubated for 24 hours along with the control cells. The control cells were treated with an equal volume of PBS.

Differentiation was initiated by washing 90–95% confluent cultures with phosphate buffered saline (PBS) and incubation in differentiation media (DM: DMEM with 2% horse serum and 1% PS) containing 1mg/ml CQDs. Control cells were maintained in differentiation media with equal volume of PBS. The differentiation media was

changed every 2-3 days. Cells were collected at 0, 24, 48, 72, 96 and 120 hours for staining and western blotting.

For imaging, all coverslips with cells were fixed with 4% formalin for 15 minutes, washed three times with PBS and an acidic dye, eosin was used to stain cytoplasm in orange-red-pink color and a basic dye, methyl green was used to stain the nucleus light green. After washes in water, the stained cells were mounted with fluoromount (F4680-25ML, *Sigma-aldrich*: St. Louis, MO), an aqueous mounting medium.

The cells were visualized with an Olympus 1X83 microscope. All images were converted to the tagged information file format and processed with the Adobe Photoshop program (Photoshop CC 2015, Adobe, San Jose, CA, USA).

4.3.4 MTT assay

Cytotoxicity of the CQDs was evaluated by MTT assay. Briefly, 5000 cells were seeded in each well of 96 well plate in four replicates for each concentration tested. After 24 hours, varying concentrations (0 -1.5 mg/mL) of CQD were added and incubated for 24 hours. The CQDs used were dissolved in PBS and hence an equal volume of PBS was used in control cells. The cells were washed with PBS, and 10 μ L of freshly prepared MTT (0.5 mg/mL) solution was added to each well. After 4 hours, 100 μ L of DMSO was added to dissolve the formazan crystals formed. The plate was read at 565 nm using a microplate reader, and data were recorded.

4.3.5 Western blotting

Total protein from C2C12 cells maintained in differentiation media at various time points (0, 24, 48, 72, 96 and 120 hrs) was extracted using the RIPA lysis buffer (1× PBS, 50 mM NaF, 0.5% Na deoxycholate (w/v), 0.1% SDS, 1% IGEPAL, 1.5 mM Na₃VO₄, 1 mM PMSF and 1× Halt® protease and phosphatase inhibitor cocktail, (Thermofisher Scientific) at 4 °C. The supernatant was collected and quantitated with Pierce™ BCA Protein Assay Kit (Cat No. 23225, Thermofisher Scientific) using BSA as standard. A total of 20 ug total protein was boiled to a final concentration of 1x Laemmli Sample Buffer (Cat No. 1610747, Biorad) supplemented with 2-mercaptoethanol and ran on Criterion TGX Stain-Free Precast Gels (Cat No. 5678084, Biorad). The following antibodies were used for western blotting. GAPDH (Cat No. 2118; Cell Signaling Technology), Myf-5 (Cat No. 125301, Abcam), MyoD (Cat No. 133627, Abcam) and myosin heavy chain (MHC) (Cat No. MA5-32555, Thermofisher Scientific).

4.4 Results and discussions

With the focus of investigating the influence of CQDs in C2C12 myotube fusion and their cytotoxicity at high concentration, CQDs were synthesized from bread using toasting method and characterized. The results obtained from bioimaging at various time points, MTT assay and western blotting were analyzed in the sections following below.

4.4.1 Fabrication of CQDs

The CQDs for this experiment was fabricated from the toasting method. This method was employed for the first time in the previous chapter and produced florescent CQDs that were utilized in bioimaging. As this new synthesis route was already optimized, appropriate temperature and heating duration was used here. The concentration of samples prepared for this study is higher than the sample used in the previous study. The CQD sample was lyophilized and resuspended in various concentration according to the requirements of the procedure.

4.4.2 Characterization of CQDs

The sample CQD T was characterized using transmission electron microscopy and fluorescence spectrophotometry to confirm the presence of fluorescent nanoparticle.

Transmission electron microscopy

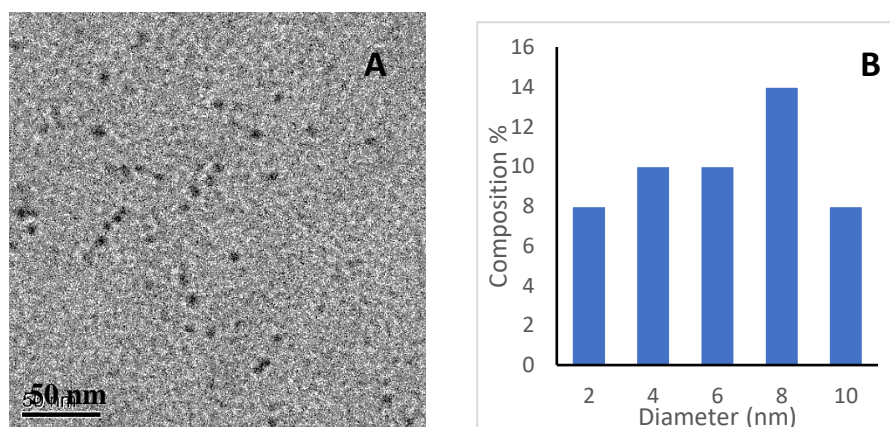


Figure 4.1: (A) TEM Image and (B) size distribution histogram of CQD T. The distribution histogram is produced from counting 50 particles

The transmission electron microscopy was performed to analyze the morphology of the CQD T. The figure 4.1 vividly displays the presence of spherical quantum dots mostly less than 10 nm in diameter. It is consistency with the previously fabricated sample from bread using toasting method.

Fluorescence measurements

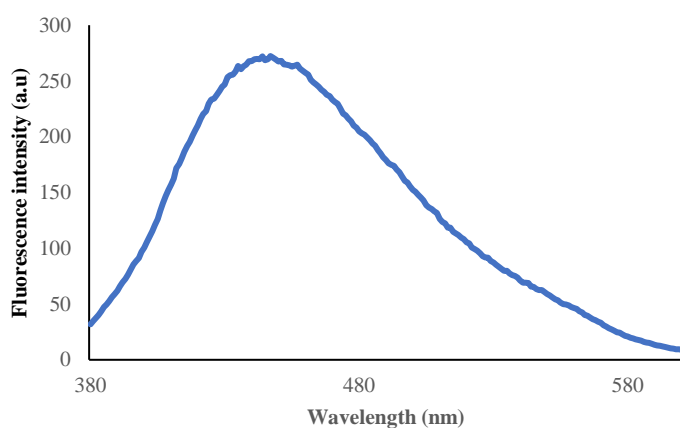


Figure 4.2: Fluorescence emission spectrum of CQD T at 360 nm excitation

The photoluminescence of CQD T was investigated prior using it for bioimaging. The emission spectrum was recorded at 360 nm excitation. As 360 nm excitation was found to be giving highest emission in the previous chapter, the same wavelength was used to check the fluorescence here. According to the characterization results obtained, CQD T displayed an emission around 450 nm. was a fluorescent carbon quantum dot, and it can be utilized in bioimaging.

4.4.3 Bioimaging

Several studies in the past including our own study have shown that carbon quantum dots are safe for biological applications [130, 421]. However, monitoring the cellular functions in the presence of CQDs are under explored. It is not clear what is the maximum concentration of CQDs that could impact cell functions. Indeed, it relies on the attributes of the CQDs. This study investigates the attributes of the CQDs derived from bread using toasting method. For this study, the C2C12 cell lines utilized for bio-imaging applications in previous chapters was used. They are mouse muscle satellite cell line which can differentiate into form myotubes. We attempted to differentiate C2C12 myocytes to myotubes in the presence of CQDs and monitored the influence of The CQDs to confirm their safety in biological imaging applications. Cells were seeded in proliferation media and shifted to differentiation media at 90-95% confluence and incubated up to 120 hours. CQDs were added at a concentration of 1.0 mg/ml both in proliferation and differentiation media along with appropriate controls.

Figure 4.3 shows images from representative times points (0, 24 and 72 hours) for control cells and C2C12 cells in the presence of CQDs. The images show a clear hindrance in the rate of differentiation at various time points indicating the myotube formation is severely delayed in presence of CQDs. The difference in the rate of differentiation is apparent at a time as low as 24 hours indicating how CQDs interfere with the process of myocytes fusing together to form myotubes. If CQDs derived from an edible resource and fabricated through a chemical-free synthesis route impact the cell function such as myotube formation at the concentration of 1 mg/mL, here arises questions regarding the biosafety of CQDs derived from pure chemicals.

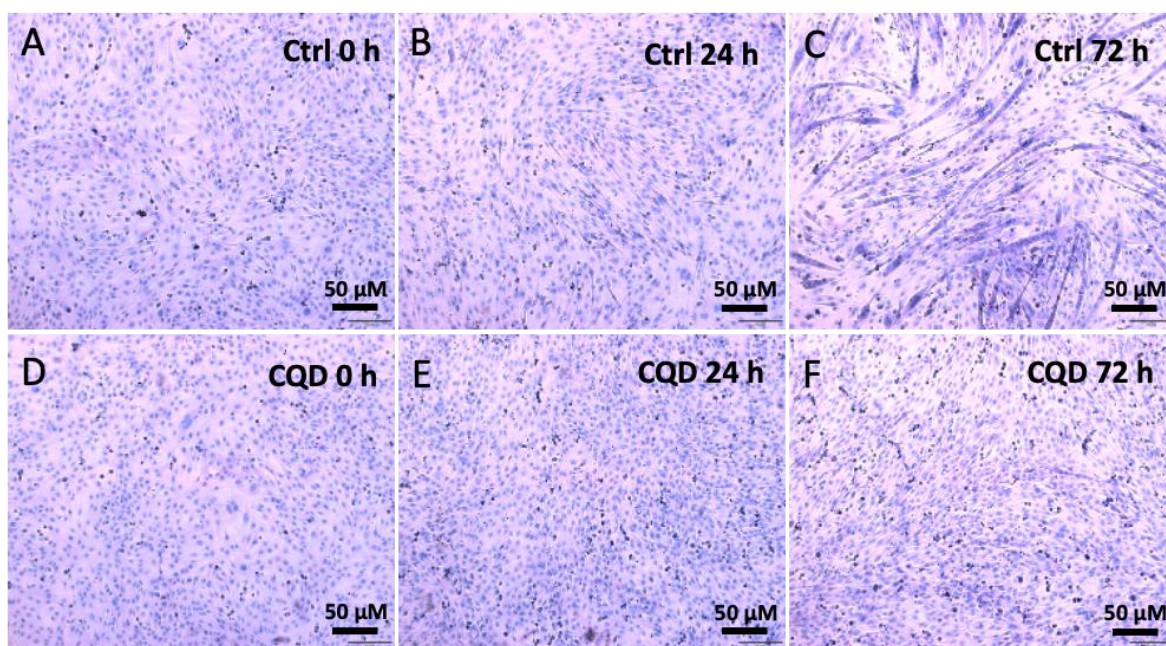


Figure 4.3: Differentiation of C2C12 control cells (A, B and C) and in the presence of synthesized CQDs (D, E and F) at 0, 24 and 72 hours. Cells are stained using eosin and methyl green.

4.4.4 MTT assay

To confirm the cell proliferation, affect by the presence of CQDs in cells, we performed MTT assay. MTT assay is a Colorimetry (Chemical method) for assessing cell metabolic activity [422]. Almost all the CQDs undergo cytotoxicity assessment prior to bioimaging. For MTT assay, generally low concentration of CQDs in the range of fifty to few hundreds of micrograms per milli liter were considered. However low concentration of CQDs are insufficient to show their biocompatibility.

In this study, the cytotoxicity of the CQDs derived from toasting method was evaluated using a standard 3-(4,5-dimethylthiazol-2-yl)-2,5-diphenyltetrazolium bromide (MTT) cell viability assay. C2C12 cells were incubated with as-synthesized CQDs for 24 hours

at a concentration of 0, 0.5, 1.0 and 1.5 mg/ml as described in materials and methods. An equal volume of PBS was used in control cells. More than 95% of cells survived even at 1.5 mg/mL of CQD concentration with cells. This concentration of CQDs exposed to cells were about 100 to 1000 times higher than it required for bioimaging application [319]. These results confirmed that the carbon quantum dots used in this study do not impart any effect of cell viability and cell proliferation which is also in agreement with the results obtained earlier measuring C2C12 cell proliferation in presence of CQDs by cell counting [421].

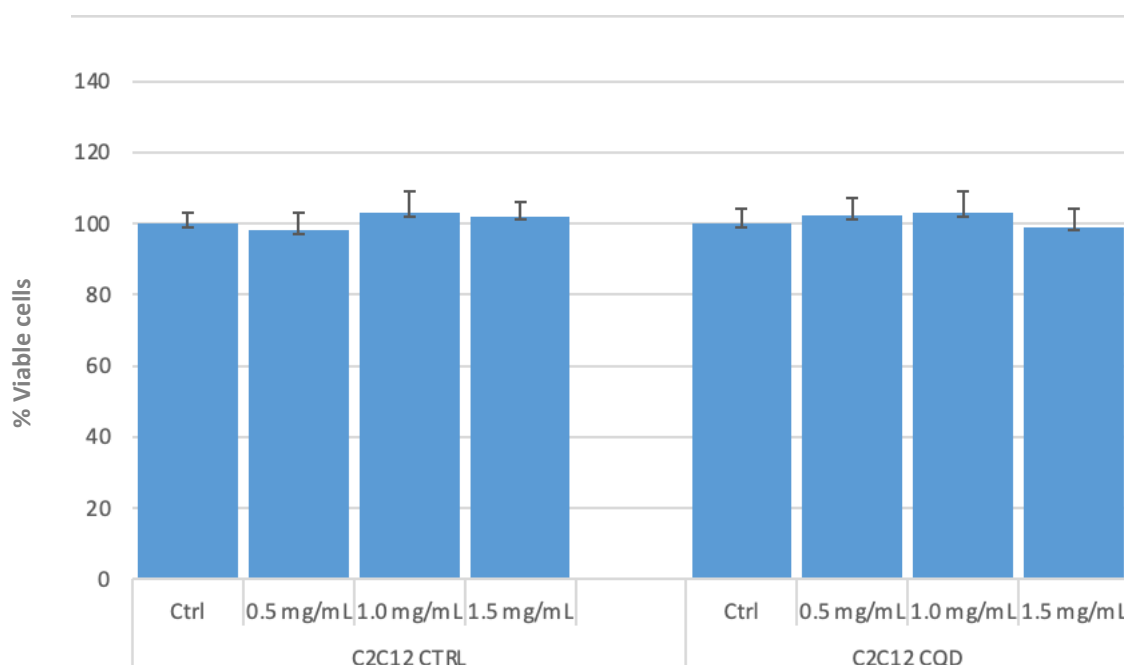


Figure 4.4: MTT assay of C2C12 cells with CQD T against control cells showing no significant reduction in cell viability in presence of 0.5-1.5 mg/ml of CQDs.

4.4.5 Western blotting

As described earlier, C2C12 myocyte differentiation to myotubes was followed through 0, 24, 48, 72, 96 and 120 hours. Total protein was collected at each time point from the

control cells and the cells incubated with CQDs, and western blotting was performed as described in materials and methods section.

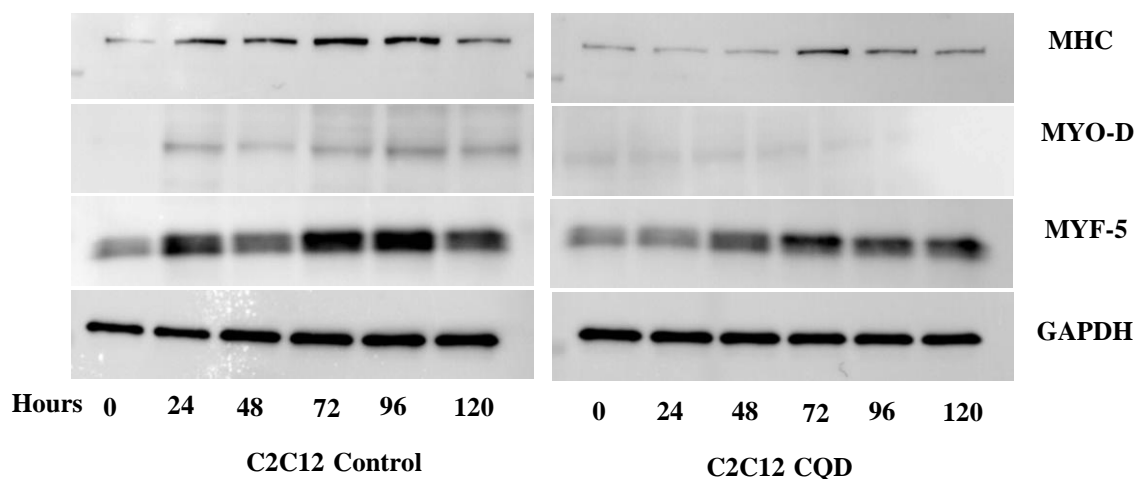


Figure 4.5: Western blotting image of C2C12 differentiation in presence of CQDs compared against control cell differentiation. GAPDH is used as a control and expression of Myf-5, Myo-D and myosin heavy chain (MHC) is tested from 0 to 120 hours of differentiation.

Muscle myoblasts fuse to form muscle myotubes and muscle fibers under the control of muscle specific transcription factors, myogenic differentiation (MyoD), myogenic factor 5 (Myf5) and myosin heavy chain (MHC) [423]. The expression levels of these factors were tested via western blotting in cells differentiated in presence of CQDs against the differentiation of control cells. Glyceraldehyde-3-phosphate dehydrogenase (GAPDH) is one of the housekeeping proteins that is present in almost all tissues in high amounts [424]. Hence GAPDH is used a marker/control to estimate the difference in expression of myogenic transcription factors Myf-5, Myo-D and MHC. These

transcription factors must be optimally present for normal differentiation of myotubes to occur. As observed in Figure 4.5, C2C12 cells differentiated in presence of CQDs exhibited a lower expression of these transcription factors which further confirms the malformation of myotubes in presence of CQDs. Myosin heavy chain (MHC) a component of myotubes also showed a decreased expression when compared to control cell differentiation (Figure 4.5) which is in agreement with the results observed in Figure 4.3 that showed the delay in myotube formation.

4.5 Conclusion

CQDs are well known for their biocompatibility, and they are generally safe for biological application. However, their influence in cellular functions and their cytotoxicity at high concentrations are the two topics that were not explored sufficiently. The effect of CQDs on cell functions could be positive or negative based on the cell line and the function studied. This study investigated the impact caused by CQDs in myotube differentiation and the cytotoxicity of CQDs at various concentrations. The CQDs were fabricated from bread via the facile toasting technique in the absence of any synthetic chemicals. These chemical-free CQDs at a concentration of 1 mg/mL delayed the process of myocytes fusing together to form myotubes in C2C12. The expression level of muscle specific transcription factors that controls the myotube formation were tested via western blotting and they exhibited lower expression in the presence of CQDs. That means that the delay was caused by CQDs. According to the cytotoxicity assessment, more than 95% of cells survived even at 1.5 mg/mL of CQD concentration with C2C12 cells and proved that the CQDs do not impart any effect of cell viability and cell proliferation, Hence, the CQDs derived from

bread in the absence of chemicals are safe to be used in bioimaging up to a high concentration (1mg/mL). If these edible resource-derived CQD could cause a delay in cell function, CQDs derived from chemical-based precursors or CQDs doped/functionalized using chemicals could interrupt cell functions more deeply. Hence, MTT assay alone is not sufficient to assess their cytotoxicity or confirm their biosafety. Obviously further investigations are required in this field of study to standardize the cytotoxicity assessment and promote the CQDs towards clinical trials. As this facile toasting method produced CQDs with low cytotoxicity and better bioimaging capability, effectiveness of this method needs to be confirmed by comparing it with another accepted method.

Chapter 5

A comparison of carbon quantum dots fabricated using the hydrothermal technique and toasting method

5.1 Abstract

The past chapters demonstrated the facile fabrication of CQDs from bread and their characteristics. The toasting method was introduced and employed for chemical-free CQD fabrication in the previous chapters. As produced CQDs were well utilized in bioimaging C2C12 cell lines and their differentiation into myotubes. It was also found that the CQDs could impact cellular functions and concentrations of CQDs higher than 1mg/mL were not advisable for bioimaging C2C12 cell lines as it resulted in delaying myotube formation. In this study, we aim to compare the toasting method with a commonly accepted hydrothermal technique and evaluate its efficiency. Other bottom-up synthesis routes like solvothermal method and microwave assisted method were not used here. Because solvothermal method requires a solvent instead of water which is not preferred, and an expensive microwave reactor is an essential requirement for the microwave assisted method. This research is expanded, and two more types of bread were included in the list of precursors, so that the category with better quantum yield can be determined. These three types of bread were used to derive CQDs through the hydrothermal technique and toasting method. The CQDs from both methods exhibited fluorescence without any additives or surface modification. Among the three types of bread, whole meal bread produced brighter CQDs from both fabrication techniques. The highest quantum yield obtained from the hydrothermal method was 0.81% and the

toasting method was 0.2%. However, it was found that both CQDs could be used to bioimage two different types of colon cancer cell lines, namely CT-26 and HT-29, derived from mice and humans, respectively. It was clearly demonstrated that these CQDs derived from bread can be utilized in cancer cell bioimaging and they are potential candidates for monitoring the mutation of cancer cells.

5.2 Introduction

The variety of fabrication techniques and an enormous number of precursors that evolve CQDs is one of the appealing elements of CQDs. In the earlier studies, with the ignition method and muffle furnace method, a new thermolysis method called the toasting method was tried for the first time. This facile method successfully produced fluorescent CQDs from bread for bioimaging C2C12 cell lines and differentiated myotubes. These CQDs were biocompatible and showed 95% cell viability even at 1.5 mg/mL concentration. Exploring new fabrication routes and comparing them with existing routes will lead to optimizing CQD synthesis processes. Typically, two basic types of techniques are commonly used in the fabrication of CQDs; “top-down” and “bottom-up” methods. The top-down method involves breaking down carbonaceous materials through chemical or physical approaches. The bottom-up method requires the carbonization of small organic molecules or step-by-step chemical fusion of small aromatic molecules [98, 214, 215]. Nowadays, there has been much interest in exploring and improving bottom-up approaches due to the ease of techniques, precise control of precursor molecules, low cost, and environmental friendliness [223, 224]. Among all the bottom-up routes, two major techniques namely

hydrothermal/solvothermal and pyrolysis are widely used for fabricating carbon quantum dots.

The hydrothermal method is a popular fabrication route that adds value to carbohydrates through an environment-friendly method [425]. The synthesis technique is widely in use for CQD fabrication using natural precursors, food waste, and synthetic chemicals. Hydrothermal technique is a well-accepted method that is visibly producing better CQDs [21, 426]. This technique is typically performed at 180 to 260 °C for 4 to 12 hours under water-saturation pressure [427]. In these conditions, water is more reactive and behaves as a non-polar solvent because of the high ionic product and low dielectric constant [428]. The autoclave reactor with PTFE-lined vessel Teflon chambers is required to perform this fabrication under specific pressure and high temperature. The precursors are dispersed in Milli-Q water and transferred into this chamber to be heated using an autoclave or oven.

On the other hand, thermal decomposition/thermolysis is a technique that carbonizes carbohydrates using excess heat in atmospheric conditions. This process takes place above 200 degrees Celsius for a few minutes. The carbonization degree plays a major part in this method because incomplete carbonization will produce luminescent carbon-based quantum dots and complete carbonization will result in carbon residues with weak emission [368]. The toasting method that was tried for the first time in the former chapters sits under thermolysis category. Fluorescent CQDs were successfully engineered from this method and used for cell bioimaging. These CQDs displayed biocompatibility and well internalized by the cell lines.

This chapter aimed to compare toasting method with hydrothermal technique using the same precursors. The efficiency of the newly introduced toasting method can be

determined using this comparison. With the white bread, which was employed previously, two new types of bread, namely whole meal bread and mixed grain bread were included as precursors in this study. Hence the type of bread that can produce better CQDs can be identified. All the three precursors were used to fabricate CQDs via two synthesis routes. Like previous studies, no chemicals additives were added during the fabrication processors. All the six CQD samples were characterized and studied for their ability in bioimaging cancer cells. So that these biocompatible CQDs can be utilized as biomarkers in cancer diagnosis.

The section 5.3 explains the process of two fabrication methods, characterization techniques, cell culture of cancer cells and bioimaging. In the section 5.4, the characterization results were analyzed in terms of structure, composition and photoluminescence. The internalization of CQDs, cytotoxicity and bioimaging capabilities also discussed. Finally, section 5.5 addressed the conclusion of the study.

5.3 Materials and methods

5.3.1 Fabrication of CQDs

Two different synthesis routes were investigated on three types of bread, namely white bread, whole meal bread, and mixed grain bread, giving six different samples. To obtain these six optimized samples the fabrication techniques were repeated many times and around hundred samples were fabricated.

The packs of sliced bread were purchased from the local supermarket. The first method used to fabricate the CQDs from three types of bread was the hydrothermal synthesis

method. 5 g (\pm 0.1 mg) of each type of bread was separately dispersed in 30 mL of Milli-Q water by sonication (Soniclean, LABOUIP Technologies, Bayswater, Australia) for 5 minutes and transferred into three different 50 mL autoclave chambers (Robotdigg equip makers, HK, China) and heated using an oven (RHTOV2HP, Russell Hobbs, Spectrum brands, Victoria, Australia). The heating temperature was experimented from 120 °C to 200 °C with an increment of 20 °C and the duration was tried from 2 hours to 8 hours with the 2 hour increment. The emission of the derived CQDs were analyzed using a florescent spectrophotometer and the optimal conditions were identified as 180 °C temperature and 4 hours duration. Although the hydrothermal process takes place in a range of temperatures and duration of heating with various precursors, this was the most efficient and optimal condition that produced luminescent CQDs from bread. After the heating, the solutions were allowed to reach room temperature naturally. The mixtures were then centrifuged (MSE centrifuge, Thomas Scientific, New Jersey, USA) for 5 minutes at 3000 rpm. The resulting supernatants were filtered using a number 1 (90 mm) filter paper (Whatman, GE Healthcare UK Limited, Amersham, UK). A sterile syringe filter unit (Minisart, Sartorius, Gottingen, Germany) of 0.2 μ m was used to purify the sample solutions and prevent bacterial growth [429]. The sample from white bread was labelled CQD H1, whole meal bread was labelled CQD H2, and mixed grain bread was labelled CQD H3. These samples were also freeze-dried and stored at -20 °C in the freezer for further analysis.

The toasting method was the second method used to synthesize three samples of CQDs. Briefly, two slices of each type of bread were separately toasted at the maximum heat setting for 5 minutes. The heating temperature was increased from room temperature to 240 °C during this toasting period. The temperature was measured using an infrared temperature probe (Sovarcate, Guangdong, China). The heating temperature and

duration for toasting method were optimized in an earlier chapter using the fluorescence emission as the key performance indicator and these optimized conditions were used for this study as well. After the bread slices were mostly charred and turned into dark brown colour, the carbon residues from the bread slices were carefully scrubbed out and ground using mortar and pestle. A 5 g (± 0.1 mg) of the grounded fine powder from each type of bread was dispersed in 30 mL of Milli-Q water separately by sonication (Soniclean, LABOUIP Technologies, Bayswater, Australia) for 5 minutes. The mixtures were then centrifuged, filtered, and purified as the previous samples. The sample from white bread was labelled CQD T1, whole meal bread was labelled CQD T2, and mixed grain bread was labelled CQD T3. All samples were freeze-dried and stored at -20 °C in the freezer for further analysis.

5.3.2 Characterization of CQD samples

All the six samples were characterized using transmission electron microscopy, fluorescence spectrometry, Fourier transform infrared spectroscopy, and quantum yield analysis.

Transmission electron microscopy (TEM)

4 μ L from a 0.01 wt.% solution of samples were placed on a carbon-coated copper grid (Carbon Type B, 400 mesh, with Formvar (Ted Pella, Inc.)). The solutions were allowed to evaporate under ambient conditions. The images were collected at varied magnifications using a Tecnai T12 G2 TWIN microscope operating at 120 kV.

Fluorescence measurements

Fluorescence measurements were carried out on a Spectro fluorophotometer RF – 5301PC (Shimadzu Europe, Duisburg, Germany) with a 1 mm PMMA cuvette (Shimadzu, Duisburg, Germany). The emission spectra were recorded for excitation wavelengths from 360 nm to 440 nm in 20 nm increments.

Fourier transform infrared spectroscopy (FTIR) analysis

FTIR spectra of the lyophilized samples were determined by Fourier transform infrared spectroscopy (Perkin Elmer, Waltham, MA, USA). An average of 16 scans with a resolution of 4 cm^{-1} was performed within the range of $4000\text{--}400\text{ cm}^{-1}$.

Quantum yield measurement

Fluorescence quantum yield is obtained from a Pico Quant FT300 spectrophotometer using an integrated sphere. The quartz cuvette (1cm x 1cm x 5cm) containing the sample solution is positioned in 'IN mode' with 20-degree tiling, where the 423 nm excitation laser directly transmits through the cuvette. For the measurement of low quantum yield values, an emission attenuator (attenuation level at 100) is applied for less than 445 nm, which is used in the quantum yield calculation.

5.3.3 Cell culture

The synthesized CQDs were tested on the human colon adenocarcinoma cell line, HT29, and mouse colon carcinoma cell line, CT-26. Briefly, the cells were maintained in a DMEM medium supplemented with 10% of heat-inactivated fetal bovine serum and penicillin/streptomycin (100 units/mL of penicillin and 100 µg/mL of streptomycin) in a humidified incubator with 5% CO₂ atmosphere at 37 °C. The culture medium is changed every 2 to 3 days, and cells are harvested for experiments at the logarithmic phase using TrypLE™ Select (Gibco™) and diluted with the complete media.

Square glass coverslips (22 mm × 22 mm) were coated with poly-L-Lysine, placed in 6-well tissue culture plates, and 5×10^5 cells were seeded to each well in complete media. After 24 hours of incubation, CQDs dissolved in phosphate buffer saline (PBS) and filtered through 0.2 µM filters are added to the wells at a final concentration of 1 mg/mL. Sterile PBS at an equal volume was used in control wells. After 24 hours of incubation with CQDs, the coverslips were fixed with 10% formalin for 15 minutes, followed by washes in PBS. The washed coverslips were flipped and mounted onto glass slides using ProLong™ Gold Antifade Mountant with or without the nuclear counterstain 4,6-diamidino-2-phenylindole (DAPI) (Invitrogen P10144, P36931) to a final concentration of 300 nM. The cells were visualized with a Leica Stellaris 5 confocal microscope at a 20x or 63x magnification setting. All images were converted to the tagged information file format and processed with Microsoft PowerPoint.

5.3.4 *In vitro* cytotoxicity evaluation

Cytotoxicity of the CQDs was evaluated by MTT assay. Briefly, 5000 cells were seeded in each well of 96 well plate. After 24 hours, varying concentrations (0-1.5 mg/mL) of each CQD were added and incubated for 24 hours. The cells were washed with PBS, and 10 μ L of freshly prepared MTT (0.5 mg/mL) solution was added to each well. After 4 hours, 100 μ L of DMSO was added to dissolve the formazan crystals formed. The plate was read at 565 nm using a microplate reader, and data were recorded.

5.4. Results and discussion

All the results obtained from characterization and bioimaging are presented in the following sections and discussed.

5.4.1 Fabrication of CQDs

The two fabrication methods employed in this study falls under the category of bottom-up techniques. As the main aim of this study is to execute chemical - free fabrication, both methods were compatible with that. As the precursor is bread, Milli-Q water was used to disperse the solid particles during hydrothermal method and toasting method doesn't require any solvent. So, other than the precursor, nothing was included as solvent or additives in both methods. Although solvothermal method is mostly similar to hydrothermal method, it requires a solvent and it is not preferred in this study. The microwave assisted method is another bottom—up method that demands a sophisticated and expensive equipment, called microwave reactor and also the safety of microwaves is still under investigation. Hence, the hydrothermal technique was selected and

compared with the toasting method. A large amount of CQDs are being successfully fabricated via hydrothermal technique using many different types of precursors. The CQDs fabricated via this technique is widely used in bioimaging and it is worth analyzing [21, 232, 430].

5.4.2 Characterization of CQDs

Transmission electron microscopy (TEM)

Transmission electron microscopy (TEM) is broadly used to determine the fine structure of the nanoparticles, such as shape, size, and dispersion. Here, TEM was performed to understand the morphological characterization of two samples derived from white bread.

Figure 5.1 shows the TEM images of the lyophilized white bread samples from both toasting (CQD T1) and hydrothermal techniques (CQD H1) with their size distribution histogram. The presence of spherical carbon quantum dots is visible in both samples, with a slight difference in nanoparticle size. However, almost all the fabricated CQDs are less than 10 nm in diameter and it coincides with previously published reports [431, 432]. The histogram of CQD T1 (toasting method) is left-skewed with smaller particles (2 nm to 4 nm), and the histogram of CQD H1 (hydrothermal method) is bell-shaped, with particle sizes mostly between 3 nm and 6 nm. The average difference between both techniques is approximately 2nm in diameter. The toasting method used higher temperatures for a shorter period, suggesting that increased rates of carbonization restrict the growth of CQD particles. This is demonstrated by the comparatively smaller nanocrystals. On the other hand, the hydrothermal process provided a slower and longer heating profile resulting in slightly larger nanoparticles.

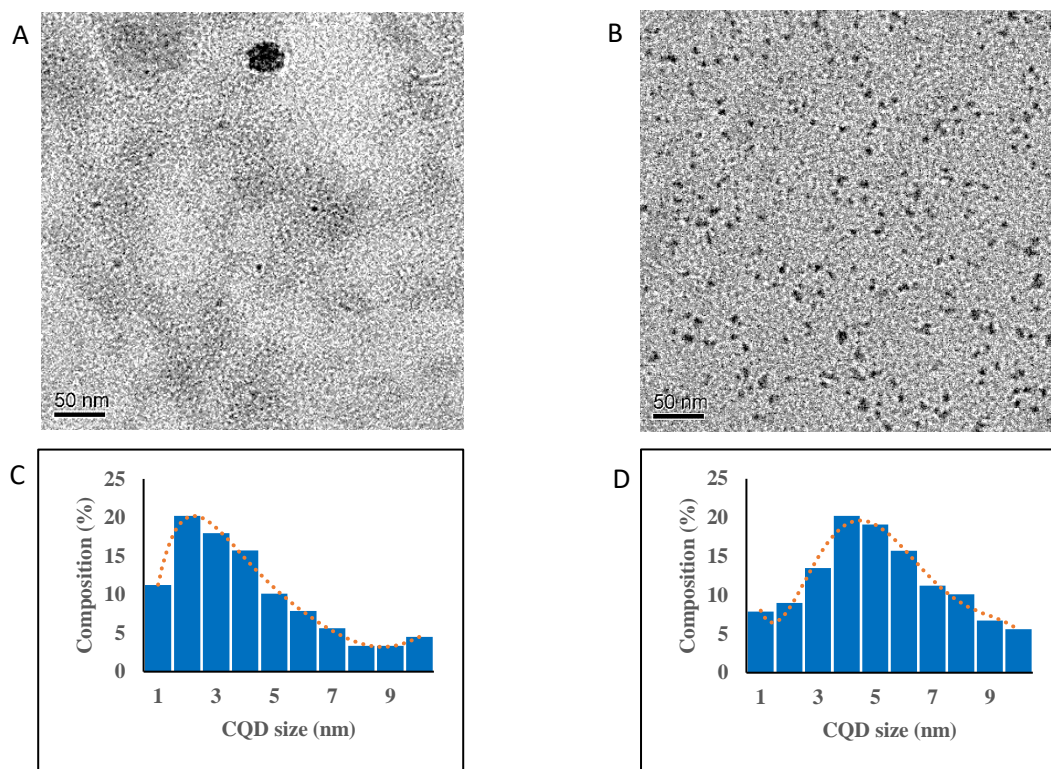


Figure 5.1: TEM images and size distribution histogram of CQD T1 – toasting method (A, C) and CQD H1 – hydrothermal method (B, D), respectively. The distribution histogram is produced from counting 100 particles in each sample

Optical characterization

The remarkable feature of carbon quantum dots is the strong broadband photoluminescence of their colloidal solutions. The emission spectra of the samples were obtained and used in analyzing their photoluminescence. Five excitation wavelengths from 360 nm to 440 nm were used to obtain the emission spectra for all six sample types (Figure 5.2).

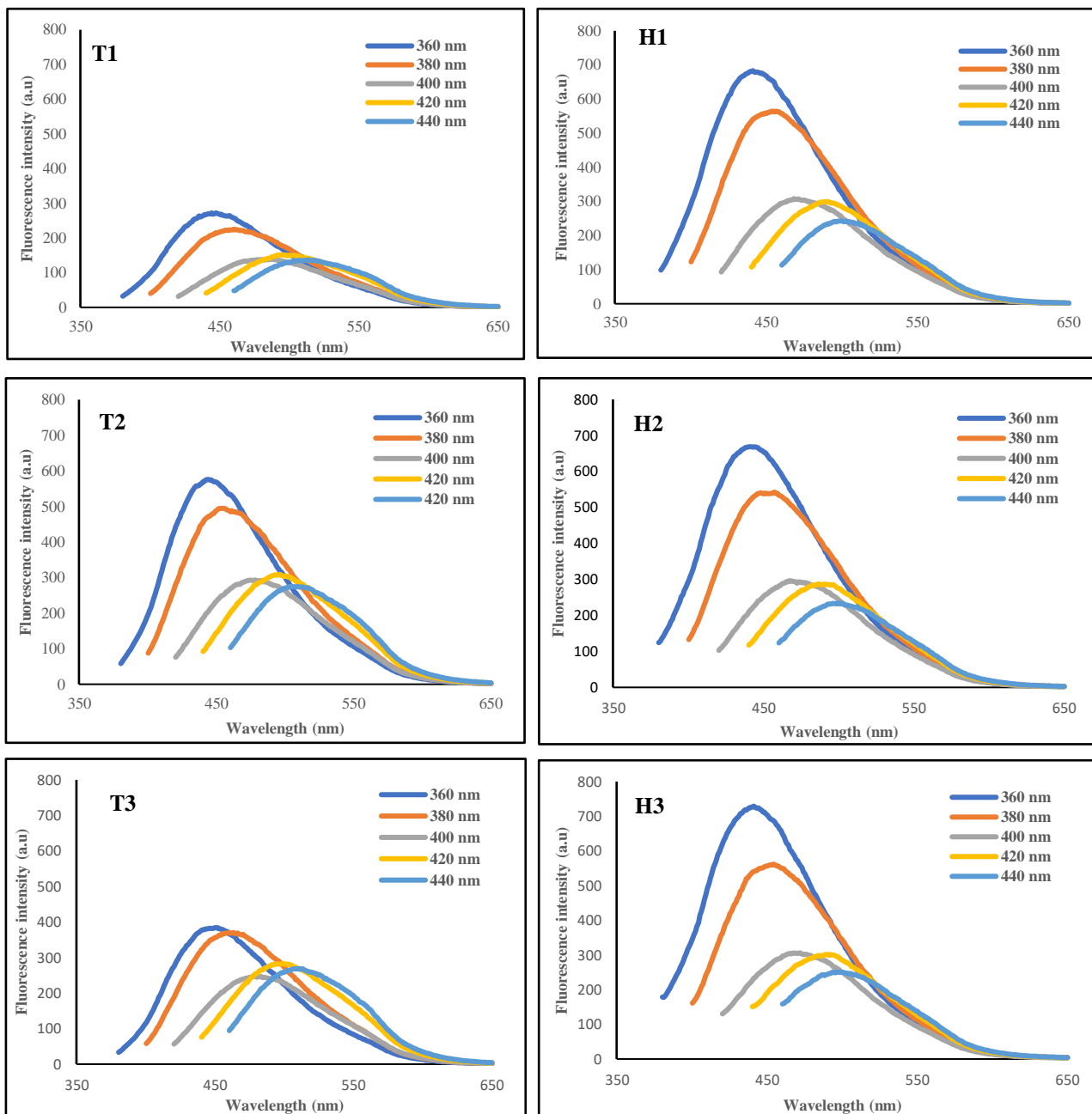


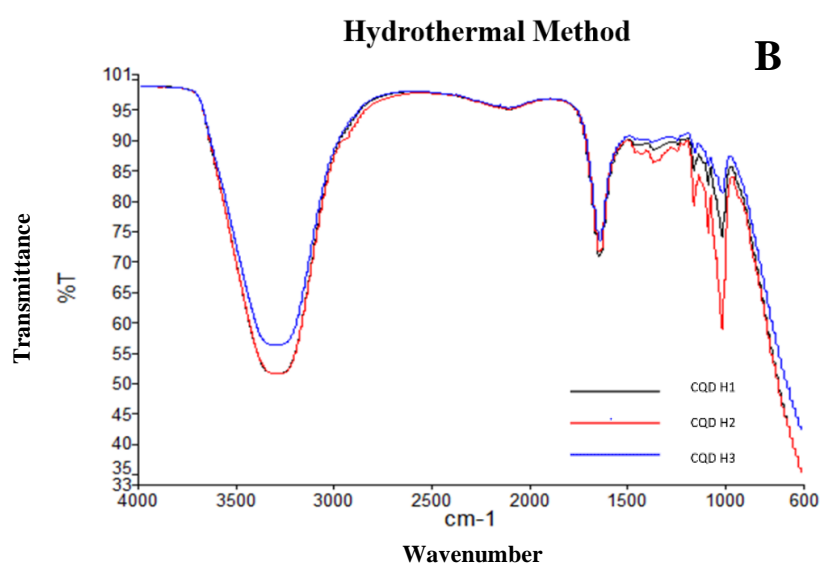
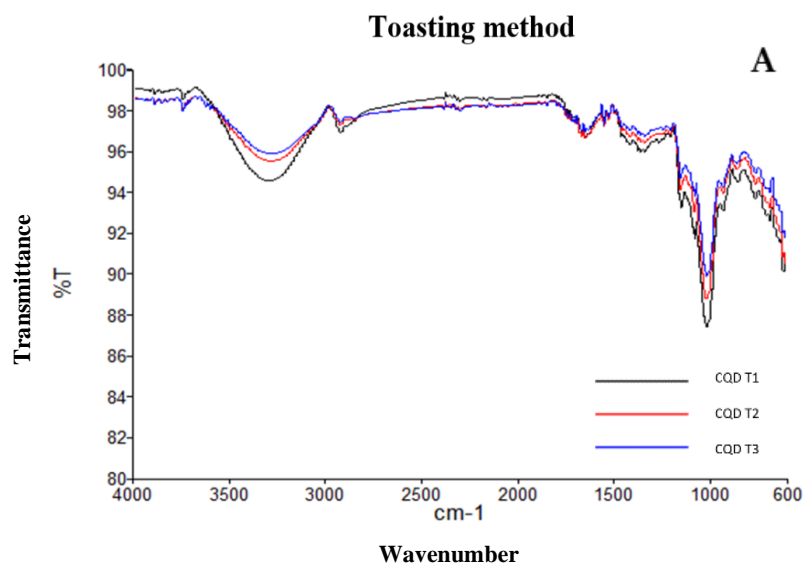
Figure 5.2: Emission spectra of samples. CQD T1 – white bread (T1), CQD T2 – whole meal bread (T2), and CQD T3 - mixed grain bread (T3) are samples from the toasting method, and CQD H1- white bread (H1), CQD H2 – wholemeal bread (H2), and CQD H3 - mixed grain bread (H3) are samples from the hydrothermal method.

It was observed that all samples from both methods were fluorescent over a wide range of excitation wavelengths. For the hydrothermal method, all samples were brighter, and there was only a minimal variation in the photoluminescence among the three types of bread. Considering the samples derived from the toasting method, the emission of the white bread is slightly lower than the other two types of bread. The whole meal bread-derived CQDs exhibited better fluorescence in both fabrication methods compared to the CQDs derived from white bread and multigrain bread. The overall photoluminescence trend of the samples was common, with the peak emission obtained for 360 nm excitation wavelength and showed excitation-dependent emission regardless of the fabrication technique, and this optical property is widely evident in CQDs [71, 433]. The engrossment of multiple discrete electronic states due to the presence of different types of aggregates in ensemble fluorescence spectroscopy leads to huge excitation-dependent shifting of emission spectra of carbon quantum dots. Further, surface-exposed functional groups play a crucial role in determining the extent and nature of aggregation and thus excitation dependent or -independent emission spectra [399]. Even though the emission intensity of the samples from the hydrothermal method is quite better than the samples from the toasting method, their bioimaging capability is comparatively equal and they were proved to be well suitable for bioimaging applications.

Fourier transform infrared spectroscopy (FTIR)

The FTIR spectra of three samples from the toasting method and three samples from the hydrothermal method were shown in two different figures (Figure 3A and Figure

3B, respectively). Additionally, the comparison of two samples, one from the hydrothermal method and another one the from toasting method was shown in Figure 3C.



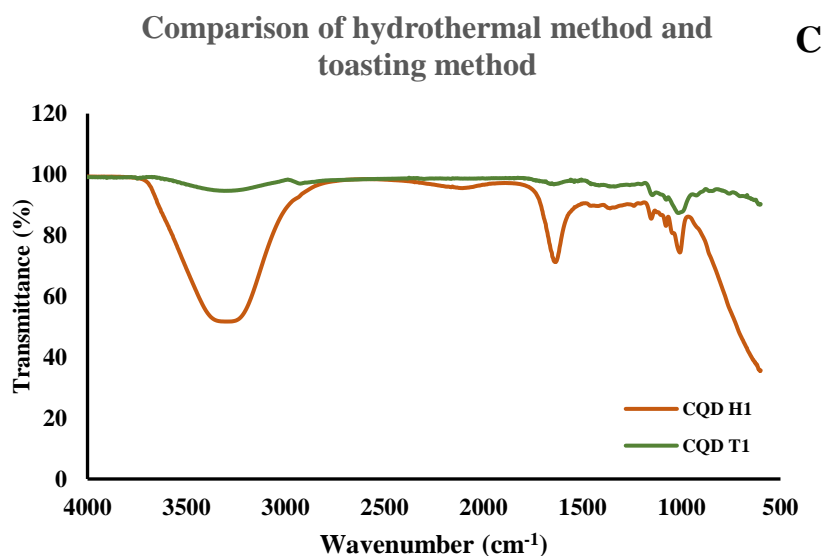


Figure 5.3: FTIR spectra of (A) samples from the toasting method (CQD T1 – white bread, CQD T2 – whole meal bread, CQD T3 – mixed grain bread) and (B) samples from the hydrothermal method (CQD H1 – white bread, CQD H2 – whole meal bread, CQD H3 – mixed grain bread), and (C) Both CQD T1 (white bread from toasting method) and CQD H1 (white bread from hydrothermal method)

The FTIR spectroscopy of three samples from the toasted method (CQD T1, CQD T2, and CQD T3) that are reflected in Figure 3A are almost identical. Similarly, the samples from the hydrothermal method (CQD H1, CQD H2, and CQD H3) exhibit similar FTIR peaks as shown in Figure 3B. However, one sample from each method is compared in Figure 3C to highlight the difference.

In Figures 3A and 3B, the broad FTIR stretch between 3200 and 3600 cm⁻¹ is attributed to the hydroxyl group (-OH). The C=O stretching is sharp in and visible around 1700 cm⁻¹ in Figure 3B, which indicates the existence of -COOH. On the other hand, the less intense peak in the same region of Figure 3A could indicate C=C. The peaks centered at around 2900 and 1300 cm⁻¹ are assigned to stretching and bending vibrations of C-H

bonds, respectively. The peaks in the fingerprint region below 1200cm^{-1} are ascribed to the vibrational absorption band of SP^3 hybridization of C-O bonds. The FTIR spectroscopy analysis of all the samples closely resembled that of a parental carbohydrate molecule [434]. Since no additional chemicals were added during the two fabrication processes, the functional groups were related to hydrocarbons. The comparison between the two samples from different fabrication techniques showed variation. Only the sample from the hydrothermal technique contains a carboxylic acid group. The carboxyl functional group on the surface of CQDs increases their emission and this explains the slight increment in quantum yield measurement [435, 436].

Quantum yield measurement results

Table 5.1. Quantum yield measurements of all six samples

Sample	Quantum Yield (%)
CQD T1	0.03
CQD T2	0.20
CQD T3	0.05
CQD H1	0.33
CQD H2	0.81
CQD H3	0.63

The samples derived from the toasted bread method (CQD T1, CQD T2, and CQD T3) exhibited lower quantum yield compared to the samples from the hydrothermal method (CQD H1, CQD H2, and CQD H3), however, the absolute difference was not significant. The CQD T2 and CQD H2 are fabricated from whole-meal bread, and they possess better QY than the other two types of precursors.

Generally, the quantum yield of CQDs obtained from edible resources are quite low without any additives or surface modification. Though, all the results are less than 1%, a positive trend is observed. The CQDs derived from hydrothermal method showed the highest quantum yield of 0.81% and it was consistent with the FTIR spectra. According to the FTIR spectra, the samples from hydrothermal technique contain carboxylic acid functional group on their surface, but this functional group is absent in the samples derived from toasting method. Hence the enhanced photoluminescence can be explained by the presence of the carboxylic acid functional group and it is in agreement with previously published reports [435, 436]. The main ingredient of the white bread was wheat flour, this wheat flour is mixed with whole grains to produce mixed grain bread and instead of regular wheat flour, whole meal wheat flour was used to produce whole meal bread. This difference also supports the quantum yield of the CQDs.

5.4.3 Bioimaging Application

Imaging cells, tissues, organs, and other biological entities are vital for biomedical research. Organic dyes and inorganic semiconductor-based fluorophores are widely used for cellular imaging and bio-imaging applications. Fluorescence imaging has garnered particular interest with its real-time capability and high sensitivity. Nevertheless, photobleaching, poor water solubility, and toxicity are some of the

obstacles to using conventional dyes (ex: propidium iodide, rhodamine, DAPI) in biological applications [437]. The six CQDs described in this study are synthesized from natural food sources via a green route of synthesis, namely toasting method (CQD T1, CQD T2, and CQD T3) and hydrothermal technique (CQD H1, CQD H2, and CQD H3). They exhibited favorable fluorescence, ultra-small size, photostability, and water solubility, making them promising candidates to test for their bio-imaging capabilities. Earlier, the CQDs derived from bread were tested on C2C12 muscle myoblast cell lines. As the next step, we intended to check if these CQDs are capable of bioimaging cancer cells with the aim of utilizing them as cancer biomarkers. So, all CQDs were tested in two different types of colon cancer cell lines, namely CT-26 and HT-29 derived from mice and humans, respectively. The cells were grown on glass coverslips for 24 hours, followed by the addition of CQDs to a final concentration of 1 mg/mL culture medium. The cells are then incubated in this medium containing CQDs for 24 hrs, after which they are fixed in 10% formalin and imaged using confocal microscopy.

The results showed that CQDs can cross the cell membranes of both mice (CT-26) and humans (HT-29) colon carcinoma cells. Figures 5.4, 5.5, 5.6 and 5.7 showed that cells were lit up brightly by the internalized CQDs when compared to their respective control cells without CQDs. Excellent fluorescent signals were obtained by using both green (excitation peak at 431 nm and an emission peak at 540 nm) and blue (excitation peak at 345 nm and an emission peak at 455 nm) channels of the microscope without any additional staining. CQDs derived by both methods showed comparable results as indicated by the intensity of fluorescent signals.

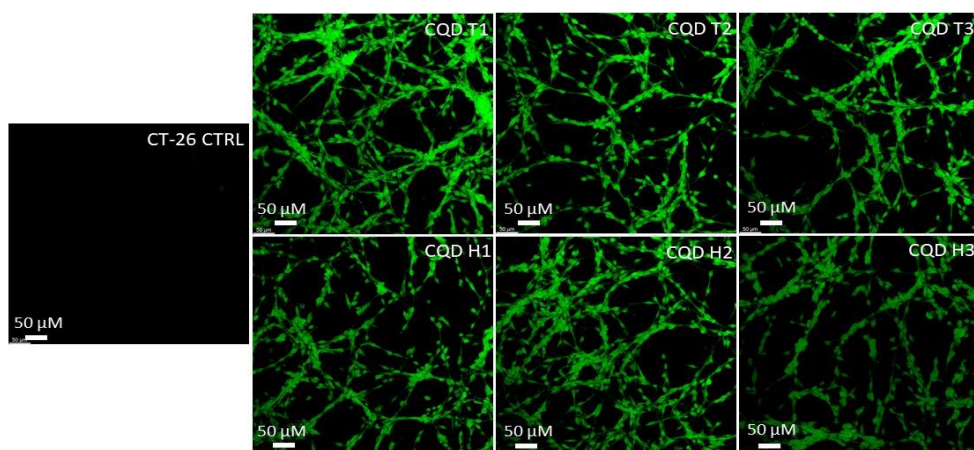


Figure 5.4: Confocal microscopy images of mouse colon cancer cells (CT-26) incubated with CQDs for 24 hours. All images are obtained through the green channel (excitation peak at 431 nm and an emission peak at 540 nm) at 20x magnification.

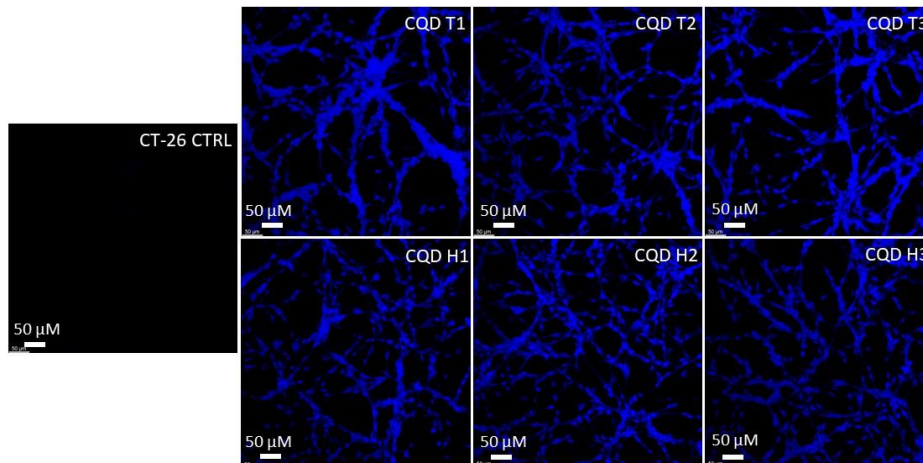


Figure 5.5: Confocal microscopy images of mouse colon cancer cells (CT-26) incubated with CQDs for 24 hours. All images are obtained through the blue channel (excitation peak at 345 nm and an emission peak at 455 nm) at 20x magnification.

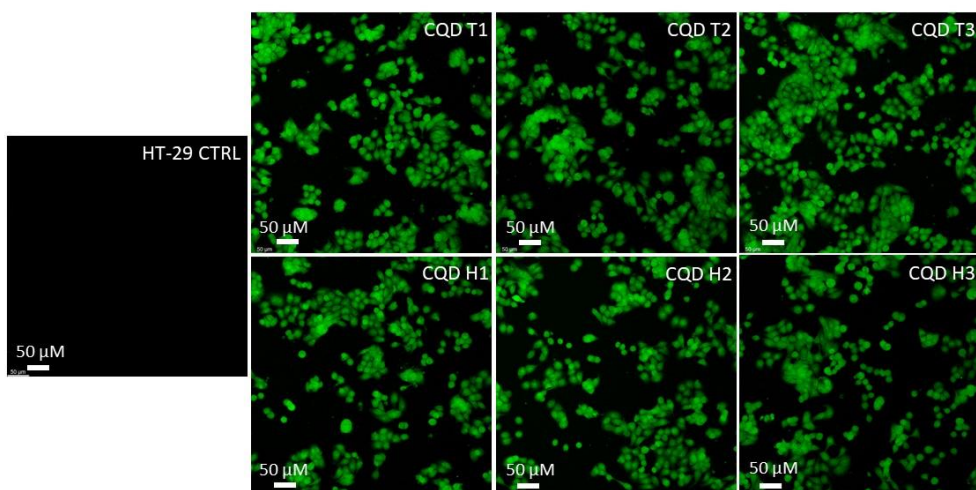


Figure 5.6: Confocal microscopy images of human colon cancer cells (HT-29) incubated with CQDs for 24 hours. All images are obtained through a green (excitation peak at 431 nm and an emission peak at 540 nm) channel at 20x magnification.

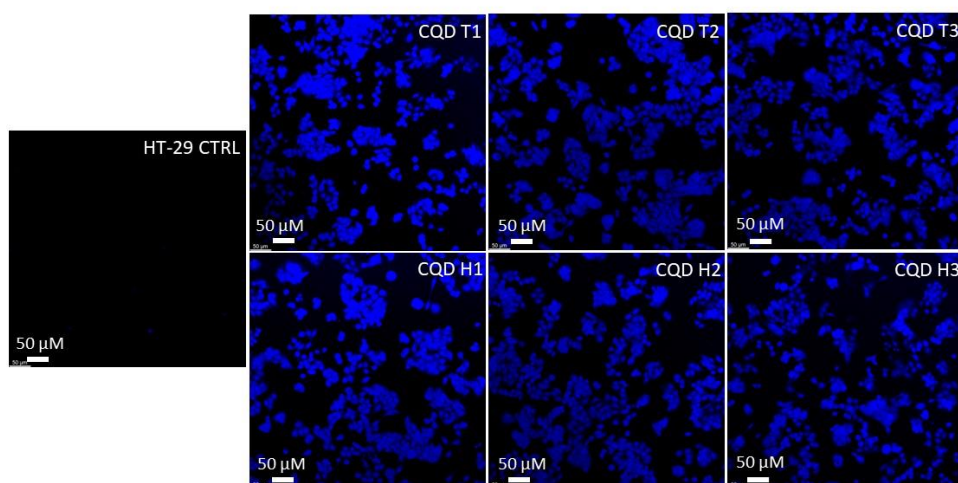


Figure 5.7: Confocal microscopy images of human colon cancer cells (HT-29) incubated with CQDs for 24 hours. All images are obtained through a blue (excitation peak at 345 nm and an emission peak at 455 nm) channel at 20x magnification.

The localization of CQDs inside a cell was investigated to evaluate the efficacy of using the CQDs in imaging applications. To understand this, the CT-26 cells were incubated with CQD H2 for 24 hours, fixed, and counterstained with the nuclear stain propidium iodide. CQD H2 was selected due to its better quantum yield. Cells without CQDs, but in presence of nuclear counterstain, propidium iodide was used as control. It is evident from Figure 5.6 (A, B, and C) that the cells without CQDs stained only the nucleus without any visible cytoplasmic staining. At a magnification of 63x, Figure 5.8 (D, E, and F) shows the prominence of CQDs in the cytoplasm compared to the nucleus. However, possibly due to their ultra-small size, they are also visible in the nuclear region, albeit on a smaller scale compared to the cytoplasmic localization.

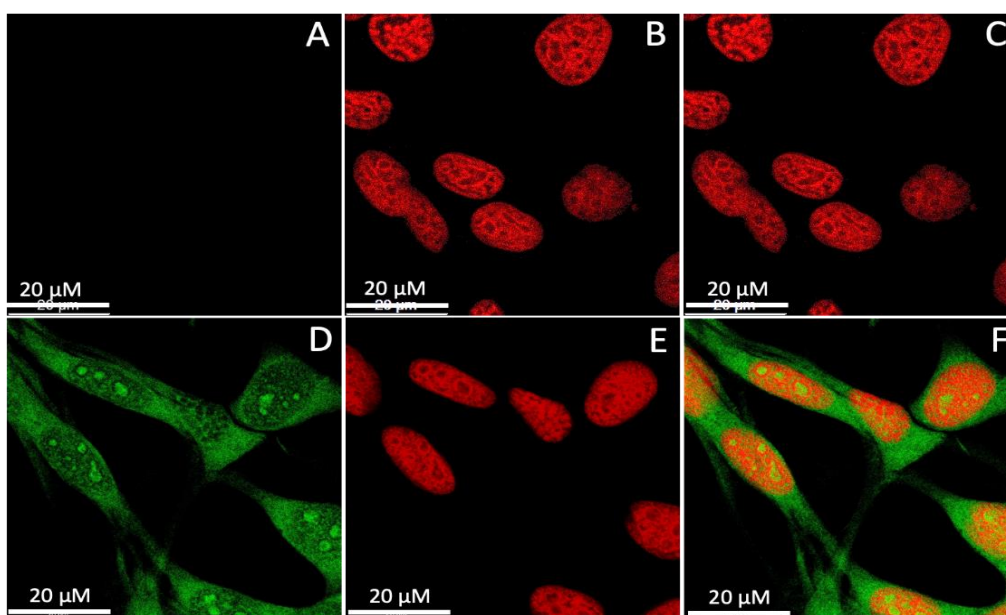


Figure 5.8: Confocal microscopy image of CT26 cells incubated with CQD H2 for 24 hours, fixed and stained with nuclear counterstain propidium iodide. Imaged at 63x magnification. (A and D) Imaged through the green channel (B and E) Imaged through the propidium iodide (red) channel and (C and F) Overlay of images from the green and red channels.

5.4.4 Cytotoxicity of CQDs

Cytotoxicity is one of the major limitations of several fluorescent dyes used for bio-imaging, as cell samples have to be fixed and long-term studies of the same cells cannot be done. CQDs offer an alternative to dyes if they can be shown to have low cytotoxicity. The cytotoxicity of our synthesized CQDs was evaluated using a standard 3-(4,5-dimethylthiazol-2-yl)-2,5-diphenyltetrazolium bromide (MTT) cell viability assay. Both CT-26 and HT-29 cells were incubated with 0-1.5 mg/mL concentrations of as-synthesized CQDs for 24 hours. More than 95% of cells survived even at the highest concentration tested, suggesting our CQDs had low cytotoxicity and hence excellent biocompatibility (Figure 5.9).

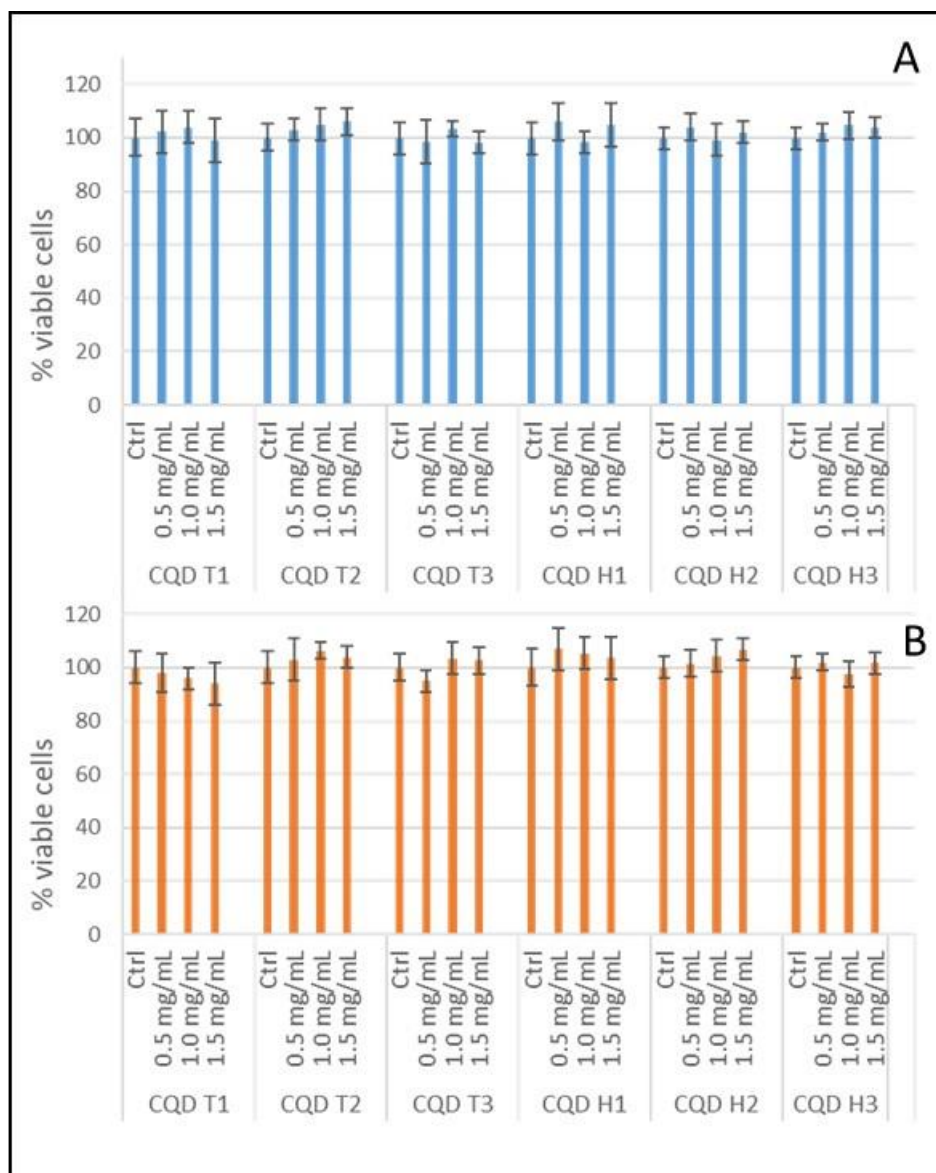


Figure 5.9: MTT assay of CQDs. (A) MTT assay of CT-26 cells with CQD T1, CQD T2, CQD T3, CQD H1, CQD H2 and CQD H3. (B) MTT assay of HT-29 cells with CQD T1, CQD T2, CQD T3, CQD H1, CQD H2, and CQD H3. All CQDs were tested at 0.5, 1.0 and 1.5 mg/mL concentrations.

5.4.5 Internalization of CQD

All six tested CQDs were able to cross the cell membrane barrier and were readily internalized by both types of colon cancer cells tested, namely CT-26 (mouse) and HT-29 (human), as shown by confocal microscopy images. Similar results were obtained for CQDs from various sources by different fabrication techniques [438]. The cytotoxicity of the CQDs was negligible, making them biocompatible and suitable for several biological applications like bio-imaging, bio-sensing, and drug targeting. The CQDs derived by both methods exhibited favorable fluorescence and excellent biocompatibility. The fluorescence images of cells obtained from various bread sources and fabrication methods were very similar. It is well known that confocal microscopy cannot be viewed as a 'black box' for quantitative imaging [439]. Hence attempts to compare the fluorescence intensity based on imaging are less useful. The natural origin and green route of synthesis are added advantages to these CQDs as they perform comparably to CQDs synthesized from chemical precursors and/or via the chemical route of synthesis, making it hazardous to the environment, persons using it and hence limiting the use in biological applications. Even when natural precursors are used, chemical synthesis routes make them less biocompatible. Henceforward the in vitro studies suggest the presented CQDs as excellent candidates for bio-imaging and as possible candidates for biosensors, targeted drug delivery, and disease diagnostics.

5.5 Conclusions

In this work, newly introduced toasting method was compared with the standard hydrothermal technique. The toasting method was a facile and cost-effective route that offers a quicker fabrication process. It didn't require a sophisticated laboratory

equipment, only a household bread toaster was adequate. The creation of carbon-based quantum dots took only 5 minutes in this process. Nevertheless, Hydrothermal technique consumed 4 hours to generate the carbon quantum dots from the reactions inside the autoclave reactor. The time and energy used by this technique were more. However, the quantum yield of CQDs derived via hydrothermal technique were comparatively higher than the CQDs derived from toasting method. While CQDs from hydrothermal technique display 0.81% of quantum yield, CQDs derived from toasting method exhibited only 0.2%. Yet, CQDs derived from both methods were non-cytotoxic and successfully used to image human colon cancer cells and mouse colon cancer cells. They were able to cross the nuclear membrane of the cell and remained in the cytoplasm for sufficient time to image. These CQDs could be potential candidates for bioimage cancer cells without the need for any surface passivation. Among three types of bread, the whole meal bread showed the highest quantum yield. Specially, when it was used in hydrothermal technique, the result was very promising. The following chapter will aim to enhance the quantum yield of these CQDs. It will explore natural additives to carry out this task without using any chemical additives that are commonly used to enhance the quantum yield.

Chapter 6

Quantum yield enhancement of carbon quantum dots using green edible additives

6.1 Abstract

Quantum yield illustrates how efficiently a fluorophore converts the excitation light into fluorescence emission, the higher the quantum yield, the brighter the fluorescence. Carbon quantum dots are naturally fluorescent, and their emission depends on their size, functional groups, and surface defects. Fortunately, the quantum yield of CQDs can be altered via fabrication conditions, chemical doping, and surface modifications. Enhancing the quantum yield will improve the performance of CQDs in the bioimaging sector. In the previous chapter, CQDs were derived from different types of bread, and they exhibited promising photoluminescence. However, the quantum yield of as-produced CQDs was less than 1%. It should be noted that these dots were fabricated using chemical-free fabrication routes. This chapter explored if it is possible to enhance the quantum yield of CQDs using chemical-free routes and natural additives. We aimed to study the chemicals usually employed in typical quantum yield enhancement and replace them with similar natural products. As Ethylenediamine was evidently increased quantum yield, soybean flour which contained amine groups used as an additional precursor with bread. Similarly, acidic medium was noticeably supported quantum yield enhancement, concentrated lemon juice was used to disperse the precursors instead of water. After several trials, the quantum yield of whole meal bread was increased up to 2.31%. The combination of whole meal bread, soybean flour and lemon juice exhibited almost four folds of enhancement in quantum yield. The CQD

samples were characterized and studied using transmission electron microscopy, X-ray diffraction, Fourier transform infrared spectroscopy, and X-ray photoelectron spectroscopy. This study showed that the enhancement of the quantum yield of carbon quantum dots was achievable with natural/edible additives and this chemical-free routes also save time and energy. It is a significant outcome and a good starting point for further development.

6.2 Introduction

The tuneable photoluminescence, alterable quantum yield, and versatile surface functionalization routes are some of the major appealing characteristics of carbon quantum dots. These features allow CQDs to be applied over a diverse range of applications. For bioimaging applications, we require CQDs with better quantum yield and enhanced biocompatibility. Specifically, for real-time continuous imaging across several days, absolute biocompatibility is a necessity. Therefore, the quantum yield of CQDs fabricated through green synthesis routes should be enhanced using chemical-free methods to be safely used for bioimaging.

The quantum yield of CQD is a substantial feature for many optical applications and it is defined as the ratio of the number of photons emitted to the number of photons absorbed [440] by the material. The precursors, fabrication routes, additives, and doping techniques could vary the quantum yield of CQDs. Mostly the CQDs derived from chemical precursors show a high quantum yield. For example, Anthracite and dimethylformamide produced CQDs with a quantum yield of 47% [441]. Similarly, an 80% quantum yield was obtained for the CQDs derived from citric acid and ethylenediamine [442]. Not all CQDs with high quantum yield possess

biocompatibility. As biocompatibility is crucial for biomedical applications, the cytotoxicity of the CQDs is tested. *In vitro* cytotoxicity analysis is generally implemented to check the nanoparticles' toxicity [443]. However, there are concerns such as biodistribution, biodegradability, long-term disposition, and induction of developmental defects that cannot be clearly addressed by these *in vitro* examinations [444, 445]. Therefore, *in vitro* toxicity assessment is inadequate to determine biocompatibility and it's always prudent to use CQDs from natural/edible precursors and green synthesis routes for bioimaging application. Yet, CQDs derived from chemical-free methods possess comparatively low quantum yields, and it is a setback to be used in bioimaging.

Generally, the enhancement of quantum yield takes place with the support of chemicals. Lie, W., et al., reported that the quantum yield of CQDs from fresh tomatoes was 1.77% and when they were modified with EDA and urea, the quantum yield increased to 7.9% and 8.5% respectively [266]. In another instance, ethanol was used to modify the CQDs derived from pineapple peel and a quantum yield of 47% was obtained [446]. There are a few common chemicals used to enhance the quantum yield of CQDs. Mostly the chemicals with amine groups such as Ethylenediamine are used as precursors or nitrogen dopants [447, 448] to obtain the expected quantum yield. Likewise, usage of acids also produces CQDs with better yield. Phosphoric acid, nitric acid and citric acid are generally included during the synthesis or after the synthesis as surface passivation agents [449, 450]. Thus, even the CQDs that derived from natural precursors and chemical-free fabrication methods also treated with chemicals in the purpose of improving quantum yield. Needless to say, these processes decreased their biocompatibility and contested their safety in bioimaging. Therefore, finding natural additives that could raise the quantum yield of CQDs is vital.

In this chapter we explored natural/edible resources to replace chemical additives in quantum yield enhancement process. According to the previous study, the CQDs derived from whole meal bread using hydrothermal technique exhibited a quantum yield of 0.81%. Here in, we proposed to increase this yield by using amine-rich resources that are natural. For this purpose, protein-rich foods containing amino acids are well relevant. Amino acids are compounds which have amine group and carboxylic group that are shown to be supporting quantum yield enhancement. Even though animal-based foods consist of protein, they are not suitable for hydrothermal technique due to the undesirable smell cause by heating. Plant-based foods are advisable for the techniques that involve high temperatures. Initially, green pea flour and soybean flour were selected to be added with bread but based on the quantum yield measurement soybean flour was preferred to continue the research. Protein is one of the prime attributes of soy bean flour and it contains typically greater than 50% protein and can approach 56% on a moisture-free basis [451]. Then, to provide an acidic medium, freshly squeezed lemon juice was used. Lemon juice is a rich natural source of citric acid, and it contains 1.44g of citric acid per ounce [452]. For the purpose of optimization, two different ratios of bread and soybean flour were tried. Also, to check if the surface area causes any difference, whole meal bread flour was tried instead of whole meal bread. The quantum yield of all the samples were analyzed and then the selected samples were further characterized and studied.

The material and method section (section 6.3) details the fabrications of all the samples. It presents the precursors used for each and every sample and their ratios. Then the characterization methods of the selected samples are given. The results obtained from these characterizations are discussed and analyzed in section 6.4. It highlights the enhancement of the quantum yield, and the chapter is concluded in section 6.5.

6.3 Materials and methods

6.3.1 Fabrication of carbon quantum dots

The fabrication of CQDs for this study was handled in several batches. The whole meal bread, whole meal bread flour, green pea flour and lemon juice were the precursors involved in these fabrications in various ratios. Every set of precursors were repeated five times and almost three months were spent to obtain the expected the outcome. Firstly, the CQD sample was fabricated from whole meal bread. Then, soybean flour and green pea flour were mixed with whole meal bread separately and two samples were fabricated. As the quantum yield of the sample that contained soybean flour was better, it was continuously used for further fabrication. For the next level of fabrication, whole meal bread and soybean flour were mixed in 1:4 and 4:1 ratio. Following that, whole meal bread flour and soybean flour were mixed in 1:4 and 4:1 ratio for another set of samples. After the quantum yield of these samples was well analyzed and compared with the basic sample that fabricated from whole meal bread alone, one sample was chosen to refabricate with fresh lemon juice instead of Milli-Q water. The samples were labeled in relation to the precursors and the fabrication methodology of all the samples is given below.

Table 6.1 Details of the fabricated samples

Name of the sample	Precursors
CQD W	Whole meal bread (5g)
CQD WG	Whole meal bread (1g) + green pea flour (4g)
CQD WS	Whole meal bread (1g) + soybean flour (4g)
CQD W4S	Whole meal bread (4g) + soybean flour (1g)
CQD WFS	Whole meal bread flour (1g) + soybean flour (4g)
CQD WF4S	Whole meal bread flour (4g) + soybean flour (1g)
CQD WSL	Whole meal bread (1g) + soybean flour (4g) + lemon juice

CQD W – 5 g (± 0.1 mg) of whole meal bread was dispersed in 30 mL of Milli-Q water by sonication (Soniclean, LABOUIP Technologies, Bayswater, Australia) for 5 minutes and transferred into 50 mL autoclave chambers (Robotdigg equip makers, HK, China) and heated at 180 °C for 4 hours using an oven (RHTOV2HP, Russell Hobbs, Spectrum brands, Victoria, Australia). After the heating, the solutions were allowed to reach room temperature overnight. This solution was then centrifuged (MSE centrifuge, Thomas Scientific, New Jersey, USA) for 5 min at 3000 rpm. The resulting supernatant was filtered using a number 1 (90 mm) filter paper (Whatman, GE Healthcare UK Limited, Amersham, UK). The sample was labelled as CQD W (whole meal bread) and saved in the refrigerator at 4°C.

CQD WG – 1g (± 0.1 mg) of whole meal bread and 4g (± 0.1 mg) of green pea flour (purchased from local supermarket) were dispersed in 30 mL of Milli-Q water by

sonication for 5 minutes and transferred into 50 mL autoclave chambers and heated at 180 °C for 4 hours using an oven. After the heating, the solutions were allowed to reach room temperature overnight. This solution was then centrifuged for 5 min at 3000 rpm. The resulting supernatant was filtered using a number 1 (90 mm) filter paper. The sample was labelled as CQD WG and saved in the refrigerator at 4°C.

CQD WS – 1g (\pm 0.1 mg) of whole meal bread and 4g (\pm 0.1 mg) of soybean flour (purchased from local supermarket) were dispersed in 30 mL of Milli-Q water by sonication for 5 minutes and transferred into 50 mL autoclave chambers and heated at 180 °C for 4 hours using an oven. After the heating, the solutions were allowed to reach room temperature overnight. This solution was then centrifuged for 5 min at 3000 rpm. The resulting supernatant was filtered using a number 1 (90 mm) filter paper. The sample was labelled as CQD WS and saved in the refrigerator at 4°C.

CQD W4S – 4g (\pm 0.1 mg) of whole meal bread and 1g (\pm 0.1 mg) of soybean flour (purchased from local supermarket) were dispersed in 30 mL of Milli-Q water by sonication for 5 minutes and transferred into 50 mL autoclave chambers and heated at 180 °C for 4 hours using an oven. After the heating, the solutions were allowed to reach room temperature overnight. This solution was then centrifuged for 5 min at 3000 rpm. The resulting supernatant was filtered using a number 1 (90 mm) filter paper. The sample was labelled as CQD W4S and saved in the refrigerator at 4°C.

CQD WFS – 1g (\pm 0.1 mg) of whole meal bread and 4g (\pm 0.1 mg) of soybean flour (purchased from local supermarket) were dispersed in 30 mL of Milli-Q water by sonication for 5 minutes and transferred into 50 mL autoclave chambers and heated at 180 °C for 4 hours using an oven. After the heating, the solutions were allowed to reach

room temperature overnight. This solution was then centrifuged for 5 min at 3000 rpm. The resulting supernatant was filtered using a number 1 (90 mm) filter paper. The sample was labelled as CQD WFS and saved in the refrigerator at 4⁰C.

CQD WF4S – 4g (\pm 0.1 mg) of whole meal bread flour and 1g (\pm 0.1 mg) of soybean flour (purchased from local supermarket) were dispersed in 30 mL of Milli-Q water by sonication for 5 minutes and transferred into 50 mL autoclave chambers and heated at 180 ⁰C for 4 hours using an oven. After the heating, the solutions were allowed to reach room temperature overnight. This solution was then centrifuged for 5 min at 3000 rpm. The resulting supernatant was filtered using a number 1 (90 mm) filter paper. The sample was labelled as CQD WF4S and saved in the refrigerator at 4⁰C.

CQD WSL – 1g (\pm 0.1 mg) of whole meal bread and 4g (\pm 0.1 mg) of soybean flour (purchased from local supermarket) were dispersed in 30mL of freshly squeezed pulp-free lemon juice by sonication for 5 minutes and transferred into 50 mL autoclave chambers and heated at 180 ⁰C for 4 hours using an oven. After the heating, the solutions were allowed to reach room temperature overnight. This solution was then centrifuged for 5 min at 3000 rpm. The resulting supernatant was filtered using a number 1 (90 mm) filter paper. The sample was labelled as CQD WSL and saved in the refrigerator at 4⁰C.

6.3.2 Characterization of CQDs

Quantum yield measurement

Fluorescence quantum yield is obtained on a Pico Quant FT300 using an integrated sphere. The quartz cuvette (1cm x 1cm x 5cm) containing the sample solution is

positioned in 'IN mode' with 20-degree tiling, where the 423 nm excitation laser directly transmits through the cuvette. For the measurement of low quantum yield values, an emission attenuator (attenuation level at 100) is applied for less than 445nm, and the correction factors are included in the quantum yield calculation.

Transmission electron microscopy

Transmission electron microscopy (TEM) images were captured using a JEOL 1010 TEM 868 operated at an accelerating voltage of 100 kV. The CQDs were sonicated for 20 min and the resulting supernatant was drop-coated on a carbon TEM grid and dried overnight under ambient conditions for the analysis.

X-ray diffraction

Powder X-ray diffraction (XRD) patterns were collected on a Bruker AXS D8 Discover diffractometer equipped with a Cu K α radiation source ($\lambda = 1.5418 \text{ \AA}$) operating at 40 kV and 35 mA.

Fourier transform infrared spectroscopy

Fourier transform infrared (FTIR) spectra of samples were recorded by an FTIR spectrometer (PerkinElmer, Frontier) with an average of 16 scans per sample and a resolution of 4 cm^{-1} in the range of $4000\text{--}700 \text{ cm}^{-1}$.

X-ray photoelectron spectroscopy

X-ray photoelectron spectroscopy (XPS) was performed using a Thermo Scientific K-Alpha XPS with a monochromate Al 1487 eV 881 K α source. CasaXPS 2.3.23 software was used for peak fitting, and background signal subtraction of each core peak region was compensated for using a Shirley background model.

6.4 Results and discussion

The results obtained from the methodologies are presented and discussed in this section.

6.4.1 Fabrication of CQDs

The quantum yield measurements and bioimaging ability of CQDs derived from whole meal bread was promising. Hence it was selected hopefully to investigate the quantum yield enhancement. Two different additional precursors, namely soybean flour and green pea flour were tried, and soybean flour was selected as it was displaying better quantum yield. Then whole meal bread flour was tried instead of bread pieces. Again, using the quantum yield results as the key performance indicator, whole meal bread was selected to investigate further. Also, two different ratios of whole meal bread and soybean flour were tried to optimize the composition. Finally, the sample with the better quantum yield was selected to fabricate in acidic medium. The hydrothermal method was very convenient to include two or three precursors at once and repeat them as required. All the fabrications were carried out in the absence of any chemicals.

6.4.2 Characterization results of the CQDs

All the seven samples (CQD W, CQD WG, CQD WS, CQD W4S, CQD WFS, CQD WF4S, and CQD WSL) that were derived from whole meal bread, whole meal bread flour, soybean flour, green pea flour and lemon juice were studied for their quantum yield. The trend of quantum yield enhancement was studied, and three samples labelled CQD W, CQD WS, and CQD WSL were chosen for further characterization. Transmission electron microscopy, X-ray diffraction, Fourier transform infrared spectroscopy and x-ray photoelectron spectroscopy were employed to investigate the attributes of the CQDs that displayed significant increment in quantum yield.

Quantum yield measurement results

The quantum yield of samples all the samples were analyzed, and the results are shown in Table 6.2 given below.

Table 6.2: quantum yield measurement of all the samples

Name of the sample	Precursors	Quantum yield (%)
CQD W	Whole meal bread (5g)	0.81
CQD WG	Whole meal bread (1g) + green pea flour (4g)	0.88
CQD WS	Whole meal bread (1g) + soybean flour (4g)	1.42
CQD W4S	Whole meal bread (4g) + soybean flour (1g)	1.10
CQD WFS	Whole meal bread flour (1g) + soybean flour (4g)	0.83
CQD WF4S	Whole meal bread flour (4g) + soybean flour (1g)	0.85
CQD WSL	Whole meal bread (1g) + soybean flour (4g) + lemon juice	2.31

In the process of enhancing the quantum yield of CQDs derived from whole meal bread using natural additives, fabrications were carried out step by step based on the quantum yield results. The quantum yield of the whole meal bread sample, CQD W was 0.81 % and it was aimed to increase by combining various edible resources. In the first combination (CQD WG), the green pea flour showed a slight increment (0.07 %) but on the other hand the quantum yield increment resulted from mixing soybean flour with whole meal bread was very significant (CQD WS). There was an increment of 0.61 % and the quantum yield of the sample exceeded 1 %. When the whole meal bread flour was used with soybean flour to investigate the effect of surface area, only a slight enhancement was observed.

In comparison, the sample derived from whole meal bread showed 20 times more enhancement than the sample derived from whole meal bread flour. Two ratios were tried for both whole meal bread and whole meal bread flour with soybean flour. However, the sample with whole meal bread: soybean flour = 1: 4 (CQD WS) was very favorable. Hence, this sample was refabricated with lemon juice instead of Milli-Q water. The sample derived from whole meal bread, soybean flour and lemon juice exhibited an excellent quantum yield of 2.31 %. To date, it is the highest quantum yield reported for CQDs derived from bread without the addition of any chemicals. To study the enhancement CQD W (whole meal bread), CQD WS (whole meal bread + soybean flour) and CQD WSL (whole meal bread + soybean flour + lemon juice) were further investigated using characterizations.

Transmission electron spectroscopy (TEM)

The transmission electron microscopy images were obtained for three samples (CQD W, CQD WS and CQD WSL) that displayed a systematic enhancement in quantum yield. The morphology and size of the CQDs were observed using TEM and the results are shown in Figure 6.1. The nanoparticles of all three samples looks nearly identical. The average size of the particles is less than 10 nm. Even though the precursors are different, all three CQD samples were derived from the same fabrication techniques and produced under same physical conditions. That's why the particle size didn't differ from each other, But due to the aggregation some nanoparticles look bigger than their true size. The emission and quantum yield can be induced by aggregation, and it can be utilized in bioimaging [453]. It is reported that carbon dots are capable of displayed aggregation induced emission (AIE) [454]. Here, the aggregation of the sample CQD

WSL (whole meal bread + soybean flour + lemon juice) is more than the other two sample and this reinforce its better quantum yield.

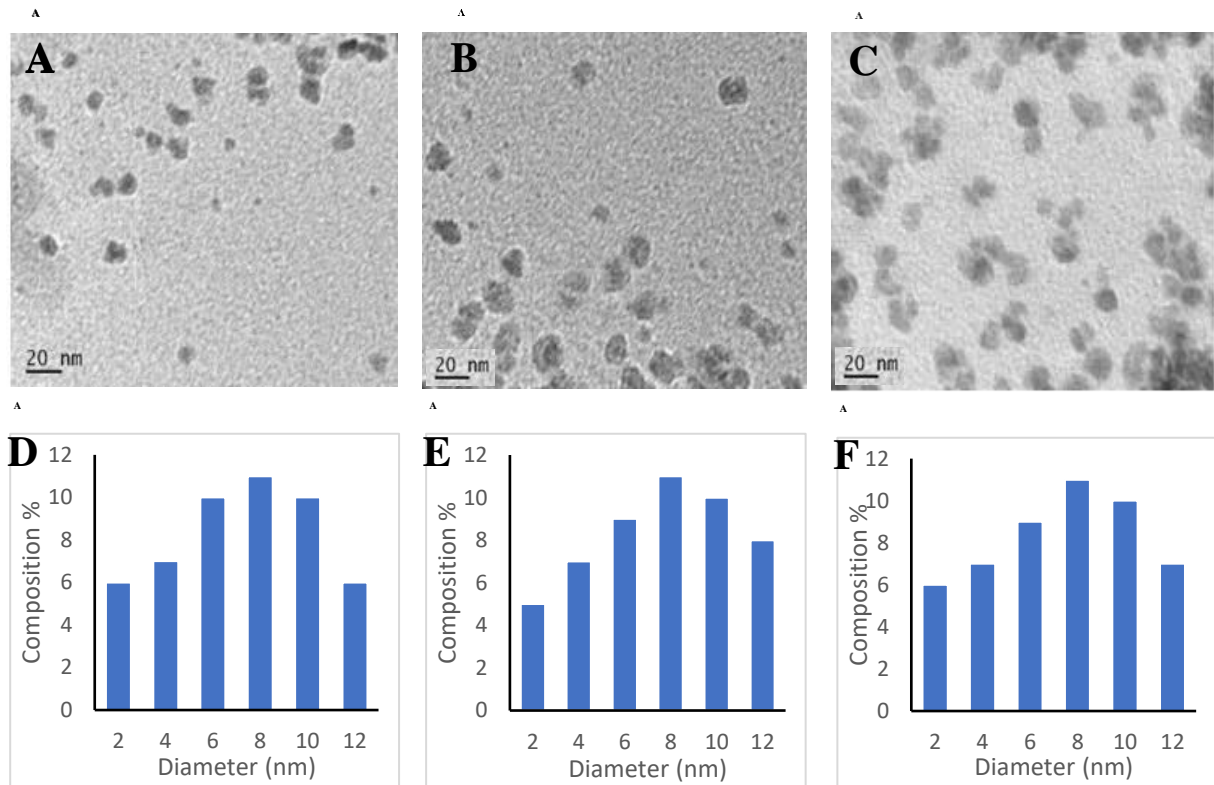


Figure 6.1: TEM images of (A) CQD W (whole meal bread), (B) CQD WS (whole meal bread + soybean flour), and (C) CQD WSL (whole meal bread + soybean flour + lemon juice) and size distribution histograms of (D) CQD W (whole meal bread), (E) CQD WS (whole meal bread + soybean flour), and (F) CQD WSL (whole meal bread + soybean flour + lemon juice). The distribution histograms are produce from counting 50 particles in each sample

X-ray diffraction (XRD)

X-ray diffraction analysis is another technique to determine the crystallographic structure of a material. The XRD spectra of the samples CQD W, CQD WS, and CQD WSL were shown in Figure 6.2. The sample CQD WSL which was fabricated from whole meal bread, soybean flour and lemon juice has a broad peak from 20 to 40 degrees suggesting its amorphous structure. Unlike CQD WSL, other two samples (CQD W and CQD WS) displayed diffraction peaks at $2\theta = 44, 64$ and 81 degrees, implying the formation of crystalline carbon materials in addition to the carbon quantum dots. The broad characteristic peak at $2\theta = 21^\circ$ are due to the graphite carbon [400].

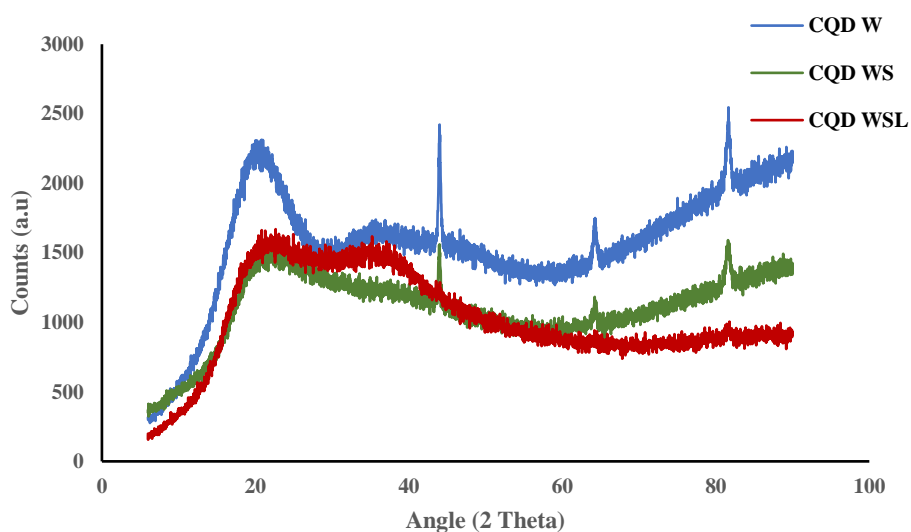


Figure 6.2: X-ray diffraction spectra of CQD W (whole meal bread), CQD WS (whole meal bread + soybean flour), and CQD WSL (whole meal bread + soybean flour + lemon juice)

Fourier transform infrared spectroscopy (FTIR)

FTIR spectroscopy is used to determine the functional groups attached to the CQDs derived from different precursors. The FTIR spectra obtained for the samples CQD W, CQD WS, and CQD WSL were shown in Figure 6.3. In the fingerprint region, sp^3 hybridization of C – O bond was ascribed by the peak at 1050 cm^{-1} . This stretching was stronger in the spectra of CQD W and CQD WS and it was due to the surface oxidation. Even though, the stretching at 1650 cm^{-1} that indicates the C = C bond was common in all three samples, the peak at 1701 cm^{-1} that attributes to the carboxylic group (C = O stretching) was witnessed only in CQD WSL. This surface carboxylic group confirms the enhancement of the quantum yield in CQD SWL [435, 436]. The FTIR results are consistency with the X-ray photoelectron spectroscopy analysis (XPS).

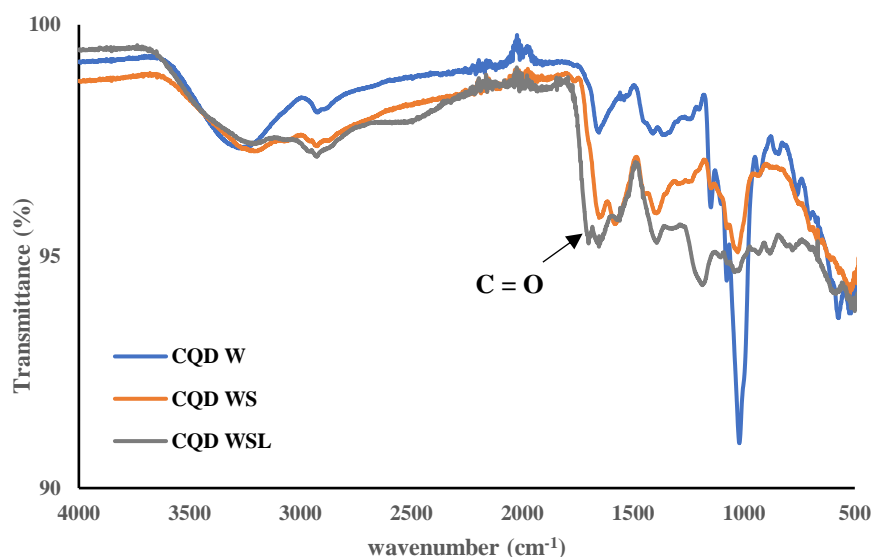


Figure 6.3: FTIR spectra of CQD W (whole meal bread), CQD WS (whole meal bread + soybean flour), and CQD WSL (whole meal bread + soybean flour + lemon juice)

X-ray photoelectron spectroscopy (XPS)

The X-ray photoelectron spectroscopy (XPS) technique is used to analyze the surface chemistry of the CQDs. XPS also reveal elemental composition as well as the chemical and electronic state of an atoms within a material. The common XPS spectra, C 1 s spectra, and O 1 s spectra of CQD samples are shown in figures given below with respective atomic ratios.

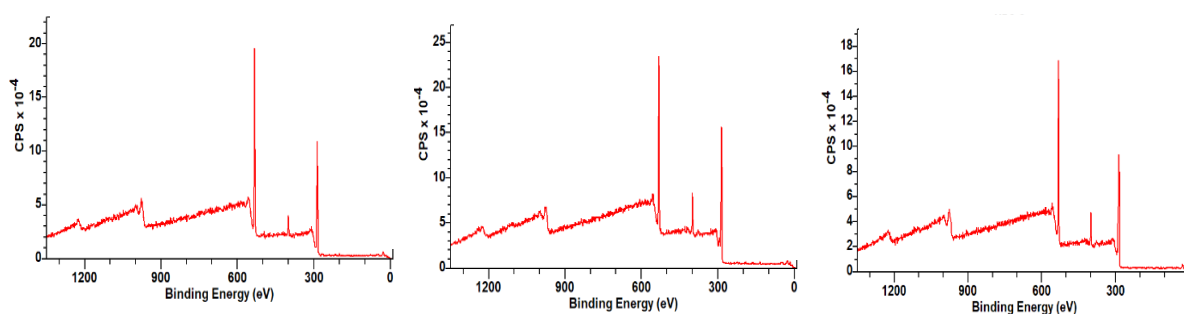


Figure 6.4: XPS spectra of (A) CQD W (whole meal bread), (B) CQD WS (whole meal bread + soybean flour), and (C) CQD WSL (whole meal bread + soybean flour + lemon juice)

Table 6.3: Atomic composition of CQD W (whole meal bread), CQD WS (whole meal bread + soybean flour), and CQD WSL (whole meal bread + soybean flour + lemon juice)

CQD	O (%)	C (%)	N (%)
CQD W	56.76	37.91	5.32
CQD WS	49.76	39.35	10.88
CQD WSL	52.91	32.99	7.87

The XPS results indicated that all three CQD samples were mainly consist of Carbon (C), Oxygen (O), and Nitrogen (N). The atomic ratio of C was around 35% and it was less than the atomic ratio of O. These results suggested complete surface coating. According to the XPS spectra, N was successfully doped on the CQDs without any chemical related technics and generally the quantum yield of N doped CQDs are higher than the undoped ones [136, 455].

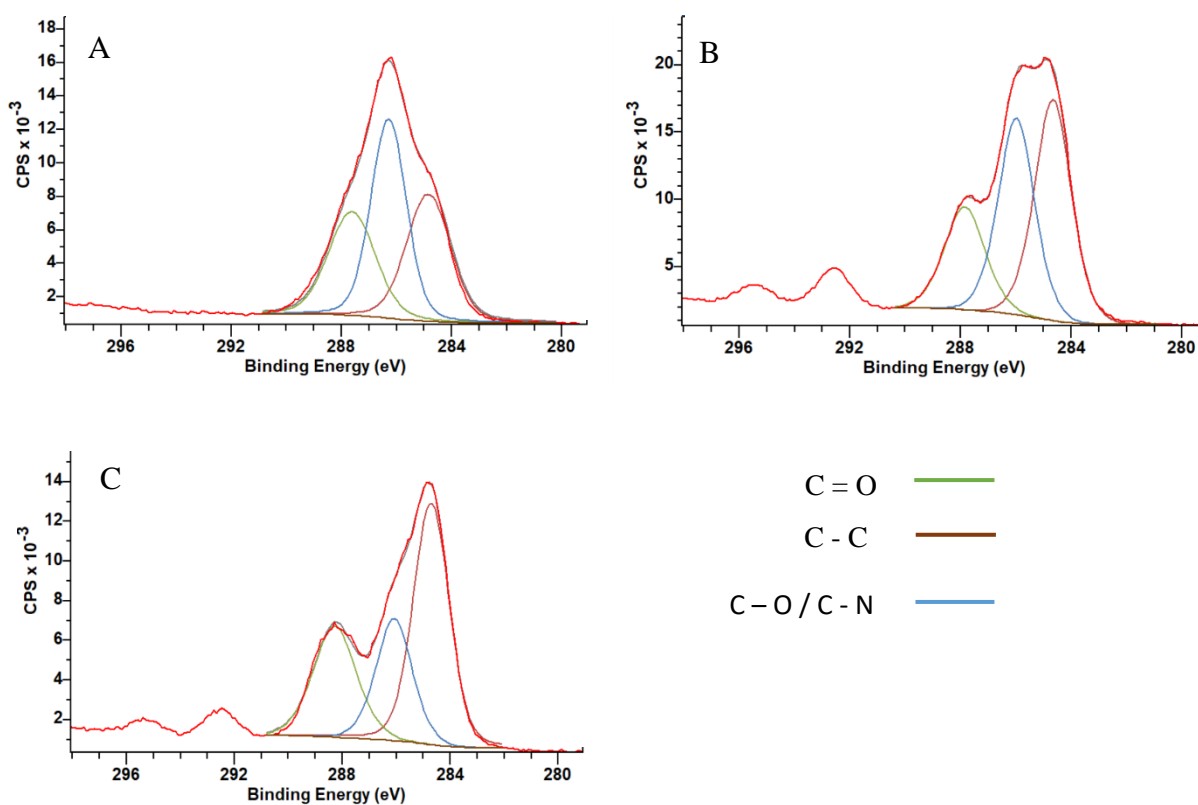


Figure 6.5: C 1s spectra of (A) CQD W (whole meal bread), (B) CQD WS (whole meal bread + soybean flour), and (C) CQD WSL (whole meal bread + soybean flour + lemon juice)

The high-resolution C 1s spectra of three samples are shown in Figure 6.5. It was observed that the spectra exhibited three peaks at 288.32 eV, 283.9 eV, and 286 eV. These were attributed to C = O, C – C, and C – O / C – N bonds respectively.

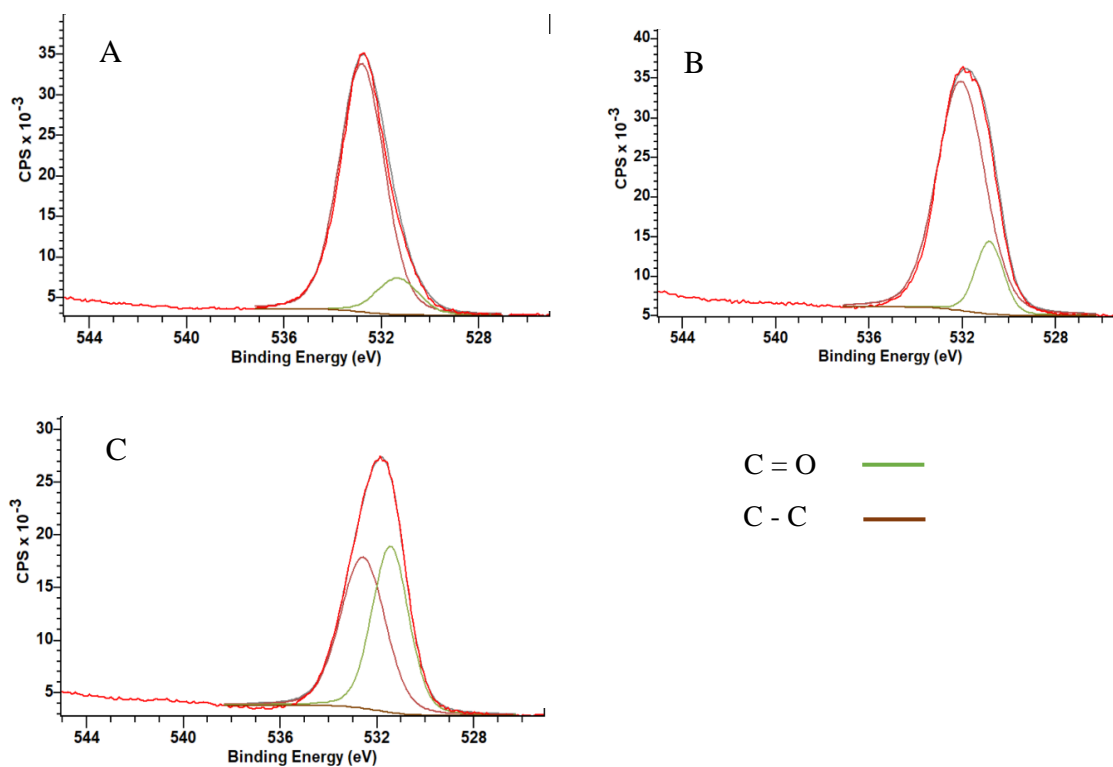


Figure 6.6: O 1s spectra of (A) CQD W (whole meal bread), (B) CQD WS (whole meal bread + soybean flour), and (C) CQD WSL (whole meal bread + soybean flour + lemon juice)

As shown in the figure 6.6, O 1s spectra exhibited two peaks at around 531 eV, and 533 eV. These peaks represented the C = O and C – O bonds respectively. According to the results CQD SWL consist 47 % of C = O and it is four folds of the same bond in CQD W and three folds of the same bond in CQD WS. The C = O which confirms the carboxylic acid group on the surface of CQD SWL the enhanced quantum yield. The

surface oxidation on CQD W and CQD SW is higher than CQD SWL and it is attributed by the C – O bonds (88 % and 85%) on the surface.

According to the characterization results, the Nitrogen was doped on the CQDs by soybean flour and this doping increased the quantum yield. The acid in lemon juice further enhanced the quantum yield and brought it up to 2.31 %. The CQD WSL that was derived from whole meal bread + soybean flour + lemon juice was very distinctive. It's morphology, structure, functional group, and surface chemistry were different from other two samples. Specially the carboxylic functional group on the surface emphasized the enhance quantum yield. Around four folds of increment in quantum yield was achieved using only natural additives. Even though typical chemical methods increase the quantum yield by more than 5 times, this CQDs required to be neutralized and purified prior to biomedical applications which consume time and energy.

6.5 Conclusion

Fabricating CQDs from natural resources is very advantageous for bioimaging application, as the biocompatibility of these CQDs is very high, and they won't affect the live cells. Still, this chemical - free fabrication are not given much attention or appreciation due to the insufficient quantum yield of the derived CQDs. Typically, quantum yield of the CQDs was enhanced using synthetic chemicals, but this approach curtailed the biocompatibility. Again, various purification procedures are required to be performed after the enhancement, to remove the excess chemicals from the CQDs. These processes consumed time and energy and opposed sustainability. Enhancing the quantum yield using green routes without altering the biocompatibility was the main

aim of this chapter. This study investigated if the quantum yield of the CQDs derived from bread can be enhanced without adding any chemicals. Seven samples were fabricated in the absence of any synthetic materials and their quantum yield was measured. A protein-rich resource that contains amino acids, namely soybean flour and lemon juice which is high in citric acid were used to enhance the quantum yield of CQDs derived from whole meal bread. The quantum yield was increased from 0.81% to 2.31% and it was a significant enhancement achieved through chemical-free routes. Accordance with the characterizations, such as Transmission electron spectroscopy, x-ray diffraction analysis, Fourier transform infrared spectroscopy and X-ray photoelectron spectroscopy, these CQDs were amorphous in structure and less than 10 nm in diameter. Only the CQDs with maximum quantum yield contained carboxylic acid functional groups on their surface and this was consistent in both FTIR and XPS characterizations. Evidently, natural additives increased the quantum yield by almost four times. As this result was promising, it could be a good initiation. There are many potential natural resources that can be explored and used for quantum yield enhancement. This exploration will lead towards green, sustainable quantum yield enhancement and more biocompatible CQDs for bioimaging.

Chapter 7

Conclusion and future work

7.1 Thesis summary

This thesis investigated the bioimaging ability of carbon quantum dots derived from bread via chemical-free synthesis routes. The characteristics of CQDs synthesized via the toasting method, muffle furnace method, and hydrothermal method were explored and the efficiency of fabrication techniques was compared. This research also examined the biocompatibility of CQDs derived from bread and their impact on cellular functions. It was also shown that green routes can be used to enhance the CQD's quantum yield.

It was found that the biocompatible CQDs can be fabricated completely chemical-free, and they can be utilized in bioimaging. The bread was identified as a potential precursor, as it produced CQDs with admirable properties. The CQDs fabricated from bread inherited the ability to bioimage C2C12 muscle myoblasts cell lines and differentiated myotubes, human colon cancer cell lines (HT 29), and mouse colon cancer cell lines (CT 26). The C2C12 cells are one of the cell lines that can differentiate into another functional unit. They fused together and formed myotubes which was visualized by CQDs. Colon cancer generally begins without any symptom, and it is a type of cancer that is difficult to diagnose at early stage. Bioimaging of colon cancer cells will promote early detection and treatment procedures.

The toasting method was introduced for the first time to fabricate CQDs from bread. It was discovered that this facile, cost-effective and time-efficient synthesis route can

produce comparable CQDs to the hydrothermal technique. Although, a delay in C2C12 myotube formation was witnessed in the presence of these CQDs at high concentration (1 mg/mL), the cytotoxicity of these CQDs was evaluated by MTT assay and 95 % cell viability was observed even at 1.5 mg/mL concentration. It was proved that the CQDs derived from bread via chemical-free green routes are safe for bioimaging application.

It was shown that the CQDs derived from whole meal bread exhibited better quantum yield than the CQDs derived from white bread and mixed grain bread. The quantum yield of CQDs from whole meal bread was enhanced by using natural additives such as soybean flour and lemon juice. Enhancing the quantum yield was never tried before using only natural resources. Because chemical additives are generally used for this purpose. But in this study, it was proved that the quantum yield can be enhanced by approximately four folds without adding any chemicals.

7.2 General conclusion

Presently, in today's world, we are surrounded by many synthetic chemicals. They are in food, clothes, furniture, toys, and medicines. The manufacturing industry uses chemicals for attractive and profitable outcomes. Even the plants become unsafe due to the excess use of pesticides and insecticides in agriculture. Most of the chemicals can be very harmful to our health and environment. They can cause chronic illnesses, cancer, neurological and developmental diseases, or even death [456, 457]. Eliminating the use of chemicals completely from our life is impractical.

This research successfully produced carbon quantum dots through chemical-free methods and enhanced their quantum yield using the same. As argued throughout the

studies, the absence of chemicals provided better biocompatibility and good suitability for bioimaging. The bread was the primary precursor used in all the chemical-free synthesis routes. Bread is consumed by most of the people, and it is one of the major contributors of food wastage. Bread is the third-highest food wastage contributor to climate change, after dairy and meat. According to Sustainability Victoria, for every loaf of bread that's eaten in the state, almost half a loaf is thrown away. It nearly equates to about 186,000 tonnes or 125 million loaves. This wastage is causing a notable drain on Victoria's natural resources, as water, energy, land, and fuel also go into the production of the bread. This costing was estimated as \$800 million dollars per year [54]. This research found a way to convert this bread waste into a valuable material that can be used in bioimaging application.

This study successfully fabricated fluorescent CQDs from bread without any additives. These CQDs exhibited excitation dependent emission for a wide range of excitation wavelengths from 340 nm to 420 nm. Most of them were less than 10 nm in diameter and well internalized by C2C12 cell lines and differentiated myotubes. 16 hours of incubation with live cells were estimated as sufficient for bioimaging purpose of these CQDs.

Chemical-free and green synthesis techniques were used effectively throughout the research. Other than the precursor no additional materials or solvents except Milli-Q water used in the synthesis. Ignition method, muffle furnace method, toasting method and hydrothermal method produced CQDs without the need of any chemical related assists. The yields (dispersed CQD/starting fine powder, w/w) obtained from toasting method, muffle furnace method, and hydrothermal method are 0.52: 0.54: 0.67 respectively.

A new fabrication technique, namely toasting method, was introduced in this study. It is a form of thermolysis method which was never tried before. The toasting method is a facile, fast, and cost-effective synthesis route to produce CQDs from bread slices. It was a sustainable production method that mainly required a household bread toaster for five minutes of duration. The toasting method was found to be producing comparable CQDs to standardized hydrothermal technique.

For the first time, C2C12 - mouse myoblast cell lines, CT 26 – mouse colon cancer cell lines, and HT 29 – human colon cancer cell lines were imaged using CQDs derived from bread. Without any surface passivation or doping technique, these CQDs were bright enough to illuminate the cells. CQDs were evidently crossed the cell membrane of C2C12 myoblast cells and myotubes formed by the fusion of myoblasts. Like a potential cancer biomarker, these bread derived CQDs imaged the cytoplasm and nucleus of the cancer cells very clearly.

It was discovered that the quantum yield of CQDs could be increased by four times using only natural additives. Instead of chemicals that are rich in amine groups and concentrated acid, natural additives such as soybean flour and fresh lemon juice can be utilized to alter the surface chemistry of CQDs. This was very crucial for retaining the biocompatibility of CQDs and their safe application in bioimaging.

With that has been conveyed, along the way, there were several issues and ambiguities that came to light but could not be completely investigated due to time constraints and the Covid pandemic' lockdowns. The stage 4 lockdown was in place from March 2020 to October 2020 except a few weeks. After a few weeks of snap lockdowns in early 2021, the state was again locked down from August 2021 to December 2021. During

these 13 months of lockdown periods, the laboratory access was completely blocked, and it considerably impacted this research study. However, we managed to carry out the research and produce this thesis with available time and resources.

Hence, the anticipated future works are given below.

7.3 Future work

There are many possible directions for the next stage of the research that can be built upon the finding of this research. Thus, future work can include:

1. Tuning the photoluminescence of CQDs so that the emission is observed in the near-infrared region. Fluorescence imaging in the near-infrared (NIR) region provides much higher signal/noise ratio (SNR) due to low tissue autofluorescence, better tissue penetration and absorption [458]. Generally, NIR emissive CQDs absorb in the visible range instead of ultra-violet (UV) rays. This excitation is very favorable because usage of ultraviolet rays, that pose risk for human health, can be avoided. Hence, in future work, we propose to focus on natural or green fabrication methods that result in CQDs with NIR emission properties.
2. A delay in C2C12 myotube formation was observed in the presence of CQDs at high concentrations. Investigating the cause of this delay is planned for future work. Finding the cause of delay might provide the ability to harness the rate of myotube formation. Advanced techniques such as NGS assay could be used for this upcoming work. This study could be also expanded to other cell lines and

other cellular functions. As various nanoparticles impact the myotube formation in different ways, for example zinc oxide nanoparticles promoted myotube differentiation [459], this outcome requires further investigation. We intended to explore the cause of delay in myotube formation in the future.

3. Exploring more green routes to enhance the quantum yield of biocompatible CQDs. As it was found that natural additives could enhance the quantum yield by almost four times, further natural additives with similar or better attributes should be explored. Other than including additives with the precursor, modifying the fabrication process also will influence the quantum yield of the produced CQDs. More filtration techniques could be used to remove the impurities and separate the nanoparticles based on their size. Enhancing the quantum yield using only natural additives was never tried before, so we planned to investigate the ability of various natural resources in quantum yield enhancement.
4. Bio conjugating CQDs with human proteins to detect the inflammation. C-reactive protein, which is produced inside the liver, is released as soon as any infection affect the human body. Likewise, there are many inflammation markers that convey the ill health. Detecting these inflammation markers by bio conjugating with CQDs and bioimaging them, will aid in early detection of disease. Hence by studying the surface chemistry of both the CQDs and the proteins, suitable techniques can be developed for bioconjugation. We proposed to focus on bio conjugating CQDs with human proteins in future work.

5. Developing a hand-held device that can detect the infected part of the body using stand-off bioimaging. Identifying the specific point of inflammation could avoid delay in treatment or even unnecessary surgeries. A portable device that can excite the CQDs conjugated with biomarker and receive the emission would be helpful to distinguish the effected part from the healthy. This can be used during surgical procedures as well. Hence, in the near future, we expected to develop a device using CQDs to detect the inflammation.

References

1. McNamara, G., M.J. Difilippantonio, and T. Ried, *Microscopy and image analysis*. Current Protocols in Human Genetics, 2005. **46**(1): p. 4.4. 1-4.4. 34.
2. Lahoti, H.S. and S.D. Jogdand, *Bioimaging: Evolution, Significance, and Deficit*. Cureus, 2022. **14**(9).
3. Tuguntaev, R.G., et al., *Bioimaging guided pharmaceutical evaluations of nanomedicines for clinical translations*. Journal of Nanobiotechnology, 2022. **20**(1): p. 1-31.
4. Weissleder, R. and M. Nahrendorf, *Advancing biomedical imaging*. Proceedings of the National Academy of Sciences, 2015. **112**(47): p. 14424-14428.
5. Fasbender, S., et al., *Uptake dynamics of graphene quantum dots into primary human blood cells following in vitro exposure*. RSC advances, 2017. **7**(20): p. 12208-12216.
6. Lee, J.-E., et al., *Target delivery and cell imaging using hyaluronic acid-functionalized graphene quantum dots*. Molecular pharmaceutics, 2013. **10**(10): p. 3736-3744.
7. Nurunnabi, M., et al., *In vivo biodistribution and toxicology of carboxylated graphene quantum dots*. ACS nano, 2013. **7**(8): p. 6858-6867.
8. Siddique, S. and J.C. Chow, *Application of nanomaterials in biomedical imaging and cancer therapy*. Nanomaterials, 2020. **10**(9): p. 1700.
9. Kaslin, J., et al., *Distinct roles of neuroepithelial-like and radial glia-like progenitor cells in cerebellar regeneration*. Development, 2017. **144**(8): p. 1462-1471.
10. Jhonsi, M.A., *Carbon quantum dots for bioimaging*. State of the Art in Nano-bioimaging, 2018: p. 35-53.
11. Fu, Y., J. Zhang, and J.R. Lakowicz, *Metal-enhanced fluorescence of single green fluorescent protein (GFP)*. Biochemical and biophysical research communications, 2008. **376**(4): p. 712-717.
12. Misteli, T. and D.L. Spector, *Applications of the green fluorescent protein in cell biology and biotechnology*. Nature biotechnology, 1997. **15**(10): p. 961-964.
13. Lorian, V., *Differences between in vitro and in vivo studies*. Antimicrobial agents and chemotherapy, 1988. **32**(10): p. 1600-1601.
14. Jonathan Dornell, *In Vivo vs In Vitro: Definition, Pros and Cons*. Technology networks, 2021.
15. Xu, X., et al., *Electrophoretic analysis and purification of fluorescent single-walled carbon nanotube fragments*. Journal of the American Chemical Society, 2004. **126**(40): p. 12736-12737.
16. Ding, H., et al., *Luminescent carbon quantum dots and their application in cell imaging*. New Journal of Chemistry, 2013. **37**(8): p. 2515-2520.
17. Zhu, Z., et al., *Surface charge controlled nucleoli selective staining with nanoscale carbon dots*. PloS one, 2019. **14**(5).
18. Chandra, S., et al., *Tuning of photoluminescence on different surface functionalized carbon quantum dots*. RSC advances, 2012. **2**(9): p. 3602-3606.
19. Li, X., et al., *Preparation of carbon quantum dots with tunable photoluminescence by rapid laser passivation in ordinary organic solvents*. Chemical Communications, 2010. **47**(3): p. 932-934.
20. Qu, Z., et al., *Synthesis of bifunctional carbon quantum dots for bioimaging and anti-inflammation*. Nanotechnology, 2020. **31**(17): p. 175102.

21. Atchudan, R., et al., *Sustainable synthesis of carbon quantum dots from banana peel waste using hydrothermal process for in vivo bioimaging*. *Physica E: Low-dimensional Systems and Nanostructures*, 2021. **126**: p. 114417.
22. Wu, F., et al., *Facile synthesis of N-rich carbon quantum dots from porphyrins as efficient probes for bioimaging and biosensing in living cells*. *International journal of nanomedicine*, 2017. **12**: p. 7375.
23. Li, Y., et al., *Theranostic carbon dots with innovative NIR-II emission for in vivo renal-excreted optical imaging and photothermal therapy*. *ACS applied materials & interfaces*, 2019. **11**(5): p. 4737-4744.
24. Liu, J., et al., *One-step hydrothermal synthesis of nitrogen-doped conjugated carbonized polymer dots with 31% efficient red emission for in vivo imaging*. *Small*, 2018. **14**(15): p. 1703919.
25. Tao, H., et al., *In vivo NIR fluorescence imaging, biodistribution, and toxicology of photoluminescent carbon dots produced from carbon nanotubes and graphite*. *Small*, 2012. **8**(2): p. 281-290.
26. Gao, X., et al., *In vivo cancer targeting and imaging with semiconductor quantum dots*. *Nature biotechnology*, 2004. **22**(8): p. 969-976.
27. Zhang, Y., et al., *Fluorescent probes for "off-on" highly sensitive detection of Hg²⁺ and L-cysteine based on nitrogen-doped carbon dots*. *Talanta*, 2016. **152**: p. 288-300.
28. Sharma, V., P. Tiwari, and S.M. Mobin, *Sustainable carbon-dots: recent advances in green carbon dots for sensing and bioimaging*. *Journal of Materials Chemistry B*, 2017. **5**(45): p. 8904-8924.
29. Luo, P.G., et al., *Carbon-based quantum dots for fluorescence imaging of cells and tissues*. *Rsc Advances*, 2014. **4**(21): p. 10791-10807.
30. Bu, D., et al., *An immunosensor designed for polybrominated biphenyl detection based on fluorescence resonance energy transfer (FRET) between carbon dots and gold nanoparticles*. *Sensors and Actuators B: Chemical*, 2014. **195**: p. 540-548.
31. Zhao, X., et al., *Graphene quantum dots in biomedical applications: recent advances and future challenges*, in *Handbook of Nanomaterials in Analytical Chemistry*. 2020, Elsevier. p. 493-505.
32. Huang, H., et al., *One-pot green synthesis of nitrogen-doped carbon nanoparticles as fluorescent probes for mercury ions*. *RSC Advances*, 2013. **3**(44): p. 21691-21696.
33. Wang, N., et al., *Green preparation of carbon dots with papaya as carbon source for effective fluorescent sensing of Iron (III) and Escherichia coli*. *Biosensors and Bioelectronics*, 2016. **85**: p. 68-75.
34. Atchudan, R., T.N.J.I. Edison, and Y.R. Lee, *Nitrogen-doped carbon dots originating from unripe peach for fluorescent bioimaging and electrocatalytic oxygen reduction reaction*. *Journal of colloid and interface science*, 2016. **482**: p. 8-18.
35. Liu, L., et al., *Synthesis of carbon dots from pear juice for fluorescence detection of Cu²⁺ ion in water*. *Journal of nanoscience and nanotechnology*, 2018. **18**(8): p. 5327-5332.
36. Sahu, S., et al., *Simple one-step synthesis of highly luminescent carbon dots from orange juice: application as excellent bio-imaging agents*. *Chemical communications*, 2012. **48**(70): p. 8835-8837.
37. Mehta, V.N., S. Jha, and S.K. Kailasa, *One-pot green synthesis of carbon dots by using Saccharum officinarum juice for fluorescent imaging of bacteria (Escherichia coli) and yeast (Saccharomyces cerevisiae) cells*. *Materials Science and Engineering: C*, 2014. **38**: p. 20-27.
38. Hoan, B.T., P.D. Tam, and V.-H. Pham, *Green synthesis of highly luminescent carbon quantum dots from lemon juice*. *Journal of Nanotechnology*, 2019. **2019**.

39. Liu, Y., et al., *Green synthesis of fluorescent carbon dots from carrot juice for in vitro cellular imaging*. Carbon Letters (Carbon Lett.), 2017. **21**: p. 61-67.
40. Jin, H., et al., *Carrot-derived carbon dots modified with polyethyleneimine and Nile blue for ratiometric two-photon fluorescence turn-on sensing of sulfide anion in biological fluids*. Talanta, 2017. **169**: p. 141-148.
41. Alam, A.-M., et al., *Synthesis of carbon quantum dots from cabbage with down-and up-conversion photoluminescence properties: excellent imaging agent for biomedical applications*. Green Chemistry, 2015. **17**(7): p. 3791-3797.
42. Shen, J., et al., *Facile synthesis of fluorescence carbon dots from sweet potato for Fe³⁺ sensing and cell imaging*. Materials Science and Engineering: C, 2017. **76**: p. 856-864.
43. Tyagi, A., et al., *Green synthesis of carbon quantum dots from lemon peel waste: applications in sensing and photocatalysis*. RSC advances, 2016. **6**(76): p. 72423-72432.
44. Boruah, A., et al., *Blue-emitting fluorescent carbon quantum dots from waste biomass sources and their application in fluoride ion detection in water*. Journal of Photochemistry and Photobiology B: Biology, 2020. **209**: p. 111940.
45. Zhou, J., et al., *Facile synthesis of fluorescent carbon dots using watermelon peel as a carbon source*. Materials Letters, 2012. **66**(1): p. 222-224.
46. university, G. *What is Green Manufacturing and Why is It Important?* 2016; Available from: <https://www.goodwin.edu/enews/what-is-green-manufacturing/>.
47. Jagannathan, M., et al., *Green synthesis of white light emitting carbon quantum dots: Fabrication of white fluorescent film and optical sensor applications*. Journal of Hazardous Materials, 2021. **416**: p. 125091.
48. Thambiraj, S. and R. Shankaran, *Green synthesis of highly fluorescent carbon quantum dots from sugarcane bagasse pulp*. Applied Surface Science, 2016. **390**: p. 435-443.
49. Yang, Z., et al., *Nitrogen-doped, carbon-rich, highly photoluminescent carbon dots from ammonium citrate*. Nanoscale, 2014. **6**(3): p. 1890-1895.
50. Jiang, K., et al., *Bright-yellow-emissive N-doped carbon dots: preparation, cellular imaging, and bifunctional sensing*. ACS applied materials & interfaces, 2015. **7**(41): p. 23231-23238.
51. Dimos, K., *Carbon quantum dots: surface passivation and functionalization*. Current Organic Chemistry, 2016. **20**(6): p. 682-695.
52. Mulvihill, M.J., et al., *Green chemistry and green engineering: a framework for sustainable technology development*. Annual review of environment and resources, 2011. **36**(1): p. 271-293.
53. Demirci, A.S., I. Palabiyik, and T. Gumus, *Bread wastage and recycling of waste bread by producing biotechnological products*. Journal of Biotechnology, 2016(231): p. S13.
54. *Victorians urged not to throw out bread*, in *The west australian*. 2021.
55. Perrotti, V., et al., *Biocompatibility of dental biomaterials*, in *Biocompatibility of Dental Biomaterials*. 2017, Woodhead Publishing. p. 1-7.
56. Schmalz, G., *Strategies to improve biocompatibility of dental materials*. Current Oral Health Reports, 2014. **1**(4): p. 222-231.
57. Bucevičius, J., et al., *Enhancing the biocompatibility of rhodamine fluorescent probes by a neighbouring group effect*. Chemical science, 2020. **11**(28): p. 7313-7323.
58. Edvinsson, T., *Optical quantum confinement and photocatalytic properties in two-, one- and zero-dimensional nanostructures*. Royal society open science, 2018. **5**(9): p. 180387.
59. García de Arquer, F.P., et al., *Semiconductor quantum dots: Technological progress and future challenges*. Science, 2021. **373**(6555): p. eaaz8541.

60. Ekimov, A.I. and A.A. Onushchenko, *Quantum size effect in three-dimensional microscopic semiconductor crystals*. JETP Lett, 1981. **34**(6): p. 345-349.
61. Hyun, B.-R., et al., *Near-infrared fluorescence imaging with water-soluble lead salt quantum dots*. The Journal of Physical Chemistry B, 2007. **111**(20): p. 5726-5730.
62. Bell, G., et al., *Direct growth of CdSe semiconductor quantum dots in glass matrix by femtosecond laser beam*. Applied Physics Letters, 2016. **108**(6): p. 063112.
63. Pal, B.N., et al., *'Giant' CdSe/CdS core/shell nanocrystal quantum dots as efficient electroluminescent materials: strong influence of shell thickness on light-emitting diode performance*. Nano letters, 2012. **12**(1): p. 331-336.
64. Leschkes, K.S., et al., *Photosensitization of ZnO nanowires with CdSe quantum dots for photovoltaic devices*. Nano letters, 2007. **7**(6): p. 1793-1798.
65. Dondapati, H., D. Ha, and A. Pradhan, *Enhanced photocurrent in solution processed electronically coupled CdSe nanocrystals thin films*. Applied Physics Letters, 2013. **103**(12): p. 121114.
66. Talgorn, E., et al., *Supercrystals of CdSe quantum dots with high charge mobility and efficient electron transfer to TiO₂*. ACS nano, 2010. **4**(3): p. 1723-1731.
67. Robel, I., et al., *Quantum dot solar cells. Harvesting light energy with CdSe nanocrystals molecularly linked to mesoscopic TiO₂ films*. Journal of the American Chemical Society, 2006. **128**(7): p. 2385-2393.
68. Jang, H.S., et al., *White light-emitting diodes with excellent color rendering based on organically capped CdSe quantum dots and Sr₃SiO₅: Ce³⁺, Li⁺ phosphors*. Advanced Materials, 2008. **20**(14): p. 2696-2702.
69. Takagahara, T. and K. Takeda, *Theory of the quantum confinement effect on excitons in quantum dots of indirect-gap materials*. Physical Review B, 1992. **46**(23): p. 15578.
70. Weller, H., *Colloidal semiconductor q-particles: chemistry in the transition region between solid state and molecules*. Angewandte Chemie International Edition in English, 1993. **32**(1): p. 41-53.
71. Mintz, K.J., Y. Zhou, and R.M. Leblanc, *Recent development of carbon quantum dots regarding their optical properties, photoluminescence mechanism, and core structure*. Nanoscale, 2019. **11**(11): p. 4634-4652.
72. Josh, D., *Quantum dots - A new era of technology*, in IETE SF MEC. 2020.
73. Brus, L., *Electronic wave functions in semiconductor clusters: experiment and theory*. The Journal of Physical Chemistry, 1986. **90**(12): p. 2555-2560.
74. Hardman, R., *A toxicologic review of quantum dots: toxicity depends on physicochemical and environmental factors*. Environmental health perspectives, 2006. **114**(2): p. 165-172.
75. Pelley, J.L., A.S. Daar, and M.A. Saner, *State of academic knowledge on toxicity and biological fate of quantum dots*. Toxicological sciences, 2009. **112**(2): p. 276-296.
76. Tsoi, K.M., et al., *Are quantum dots toxic? Exploring the discrepancy between cell culture and animal studies*. Accounts of chemical research, 2013. **46**(3): p. 662-671.
77. Kumari, A. and R.R. Singh, *Encapsulation of highly confined CdSe quantum dots for defect free luminescence and improved stability*. Physica E: Low-dimensional Systems and Nanostructures, 2017. **89**: p. 77-85.
78. Wu, T. and M. Tang, *Toxicity of quantum dots on respiratory system*. Inhalation toxicology, 2014. **26**(2): p. 128-139.
79. Derfus, A.M., W.C. Chan, and S.N. Bhatia, *Probing the cytotoxicity of semiconductor quantum dots*. Nano letters, 2004. **4**(1): p. 11-18.
80. Liu, W., et al., *CdSe quantum dot (QD)-induced morphological and functional impairments to liver in mice*. PloS one, 2011. **6**(9): p. e24406.
81. Parak, W.J., et al., *Cell motility and metastatic potential studies based on quantum dot imaging of phagokinetic tracks*. Advanced Materials, 2002. **14**(12): p. 882-885.

82. Green, M. and E. Howman, *Semiconductor quantum dots and free radical induced DNA nicking*. Chemical communications, 2005(1): p. 121-123.
83. Filali, S., F. Pirot, and P. Miossec, *Biological applications and toxicity minimization of semiconductor quantum dots*. Trends in biotechnology, 2020. **38**(2): p. 163-177.
84. Liu, W., et al., *Temperature-dependent photoluminescence of ZnCuInS/ZnSe/ZnS quantum dots*. The Journal of Physical Chemistry C, 2013. **117**(38): p. 19288-19294.
85. Xie, P., et al., *Advanced carbon nanomaterials for state-of-the-art flexible supercapacitors*. Energy Storage Materials, 2021. **36**: p. 56-76.
86. Cayuela, A., et al., *Semiconductor and carbon-based fluorescent nanodots: the need for consistency*. Chemical Communications, 2016. **52**(7): p. 1311-1326.
87. Wang, Y., et al., *Synthesis of N, S-doped carbon quantum dots for use in organic solar cells as the ZnO modifier to eliminate the light-soaking effect*. ACS applied materials & interfaces, 2018. **11**(2): p. 2243-2253.
88. Boakye-Yiadom, K.O., et al., *Carbon dots: Applications in bioimaging and theranostics*. International journal of pharmaceutics, 2019. **564**: p. 308-317.
89. Sun, Y.-P., et al., *Quantum-sized carbon dots for bright and colorful photoluminescence*. Journal of the American Chemical Society, 2006. **128**(24): p. 7756-7757.
90. Wu, M., et al., *Scalable synthesis of organic-soluble carbon quantum dots: superior optical properties in solvents, solids, and LEDs*. Nanoscale, 2017. **9**(35): p. 13195-13202.
91. Kuo, T.-R., et al., *One-pot green hydrothermal synthesis of fluorescent nitrogen-doped carbon nanodots for in vivo bioimaging*. Analytical and bioanalytical chemistry, 2016. **408**(1): p. 77-82.
92. Li, C.-H., et al., *Fluorescence-guided probes of aptamer-targeted gold nanoparticles with computed tomography imaging accesses for in vivo tumor resection*. Scientific reports, 2015. **5**: p. 15675.
93. Liu, W., et al., *Carbon dots: surface engineering and applications*. Journal of Materials Chemistry B, 2016. **4**(35): p. 5772-5788.
94. Singh, R., et al., *Progress in microwave-assisted synthesis of quantum dots (graphene/carbon/semiconducting) for bioapplications: a review*. Materials Today Chemistry, 2019. **12**: p. 282-314.
95. Zheng, X.T., et al., *Glowing graphene quantum dots and carbon dots: properties, syntheses, and biological applications*. small, 2015. **11**(14): p. 1620-1636.
96. Ahmed, S.R., et al., *Nanozymatic detection of thiocyanate through accelerating the growth of ultra-small gold nanoparticles/graphene quantum dots hybrids*. Food Chemistry, 2022: p. 132152.
97. Zhang, J., et al., *Scale-up synthesis of fragrant nitrogen-doped carbon dots from bee pollens for bioimaging and catalysis*. Advanced Science, 2015. **2**(4): p. 1500002.
98. Anwar, S., et al., *Recent advances in synthesis, optical properties, and biomedical applications of carbon dots*. ACS Applied Bio Materials, 2019. **2**(6): p. 2317-2338.
99. Mehta, V.N., et al., *One-step hydrothermal approach to fabricate carbon dots from apple juice for imaging of mycobacterium and fungal cells*. Sensors and Actuators B: Chemical, 2015. **213**: p. 434-443.
100. Feng, X., et al., *Easy synthesis of photoluminescent N-doped carbon dots from winter melon for bio-imaging*. RSC Adv 5: 31250–31254. 2015.
101. Kasibabu, B.S.B., et al., *One-step synthesis of fluorescent carbon dots for imaging bacterial and fungal cells*. Analytical Methods, 2015. **7**(6): p. 2373-2378.
102. Oza, G., et al., *A green route towards highly photoluminescent and cytocompatible carbon dot synthesis and its separation using sucrose density gradient centrifugation*. Journal of fluorescence, 2015. **25**(1): p. 9-14.

103. Kasibabu, B.S.B., et al., *Imaging of bacterial and fungal cells using fluorescent carbon dots prepared from carica papaya juice*. Journal of fluorescence, 2015. **25**(4): p. 803-810.
104. Wang, G., et al., *Facile and highly effective synthesis of controllable lattice sulfur-doped graphene quantum dots via hydrothermal treatment of durian*. ACS applied materials & interfaces, 2018. **10**(6): p. 5750-5759.
105. Atchudan, R., et al., *Indian gooseberry-derived tunable fluorescent carbon dots as a promise for in vitro/in vivo multicolor bioimaging and fluorescent ink*. Acs Omega, 2018. **3**(12): p. 17590-17601.
106. Xue, M., et al., *Green preparation of fluorescent carbon dots from lychee seeds and their application for the selective detection of methylene blue and imaging in living cells*. Journal of Materials Chemistry B, 2015. **3**(33): p. 6783-6789.
107. Jiao, X.-Y., et al., *The synthesis of fluorescent carbon dots from mango peel and their multiple applications*. Colloids and Surfaces A: Physicochemical and Engineering Aspects, 2019. **577**: p. 306-314.
108. Dias, C., et al., *Biocompatibility and bioimaging potential of fruit-based carbon dots*. Nanomaterials, 2019. **9**(2): p. 199.
109. Raji, K., V. Ramanan, and P. Ramamurthy, *Facile and green synthesis of highly fluorescent nitrogen-doped carbon dots from jackfruit seeds and its applications towards the fluorimetric detection of Au 3+ ions in aqueous medium and in in vitro multicolor cell imaging*. New Journal of Chemistry, 2019. **43**(29): p. 11710-11719.
110. Bandi, R., et al., *Facile and green synthesis of fluorescent carbon dots from onion waste and their potential applications as sensor and multicolour imaging agents*. RSC advances, 2016. **6**(34): p. 28633-28639.
111. Zhao, S., et al., *Green synthesis of bifunctional fluorescent carbon dots from garlic for cellular imaging and free radical scavenging*. ACS applied materials & interfaces, 2015. **7**(31): p. 17054-17060.
112. Li, C.-L., et al., *Carbon dots prepared from ginger exhibiting efficient inhibition of human hepatocellular carcinoma cells*. Journal of Materials Chemistry B, 2014. **2**(28): p. 4564-4571.
113. Wang, W.-J., et al., *Green preparation of carbon dots for intracellular pH sensing and multicolor live cell imaging*. Journal of Materials Chemistry B, 2016. **4**(44): p. 7130-7137.
114. Liu, Y., et al., *Green synthesis of fluorescent carbon dots from carrot juice for in vitro cellular imaging*. Carbon letters, 2017. **21**: p. 61-67.
115. Singh, V., et al., *Biocompatible fluorescent carbon quantum dots prepared from beetroot extract for in vivo live imaging in C. elegans and BALB/c mice*. Journal of Materials Chemistry B, 2018. **6**(20): p. 3366-3371.
116. Vasimalai, N., et al., *Green synthesis of fluorescent carbon dots from spices for in vitro imaging and tumour cell growth inhibition*. Beilstein journal of nanotechnology, 2018. **9**(1): p. 530-544.
117. D'Angelis do ES Barbosa, C., et al., *Carbon dots (C-dots) from cow manure with impressive subcellular selectivity tuned by simple chemical modification*. Chemistry—A European Journal, 2015. **21**(13): p. 5055-5060.
118. Wang, J., C.F. Wang, and S. Chen, *Amphiphilic egg-derived carbon dots: Rapid plasma fabrication, pyrolysis process, and multicolor printing patterns*. Angewandte Chemie International Edition, 2012. **51**(37): p. 9297-9301.
119. D'souza, S.L., et al., *Synthesis of fluorescent nitrogen-doped carbon dots from dried shrimps for cell imaging and boldine drug delivery system*. RSC advances, 2016. **6**(15): p. 12169-12179.

120. Wang, D., et al., *Luminescent properties of milk carbon dots and their sulphur and nitrogen doped analogues*. RSC advances, 2014. **4**(93): p. 51658-51665.
121. Song, Y., et al., *Highly photoluminescent carbon dots derived from linseed and their applications in cellular imaging and sensing*. Journal of Materials Chemistry B, 2018. **6**(19): p. 3181-3187.
122. Yu, C., et al., *A facile, green synthesis of highly fluorescent carbon nanoparticles from oatmeal for cell imaging*. Journal of Materials Chemistry C, 2015. **3**(37): p. 9514-9518.
123. Chen, W., et al., *Synthesis of graphene quantum dots from natural polymer starch for cell imaging*. Green chemistry, 2018. **20**(19): p. 4438-4442.
124. Wei, J., et al., *Dual functional carbon dots derived from cornflour via a simple one-pot hydrothermal route*. Materials Letters, 2014. **123**: p. 107-111.
125. Wang, Z., et al., *Large-scale and controllable synthesis of graphene quantum dots from rice husk biomass: a comprehensive utilization strategy*. ACS applied materials & interfaces, 2016. **8**(2): p. 1434-1439.
126. Hsu, P.-C., et al., *Synthesis and analytical applications of photoluminescent carbon nanodots*. Green Chemistry, 2012. **14**(4): p. 917-920.
127. Hu, Y., et al., *Waste frying oil as a precursor for one-step synthesis of sulfur-doped carbon dots with pH-sensitive photoluminescence*. Carbon, 2014. **77**: p. 775-782.
128. Xue, M., et al., *Green synthesis of stable and biocompatible fluorescent carbon dots from peanut shells for multicolor living cell imaging*. New Journal of Chemistry, 2016. **40**(2): p. 1698-1703.
129. Amin, N., et al., *Green and cost-effective synthesis of carbon dots from date kernel and their application as a novel switchable fluorescence probe for sensitive assay of Zoledronic acid drug in human serum and cellular imaging*. Analytica chimica acta, 2018. **1030**: p. 183-193.
130. Huang, C., et al., *Synthesis of carbon quantum dot nanoparticles derived from byproducts in bio-refinery process for cell imaging and in vivo bioimaging*. Nanomaterials, 2019. **9**(3): p. 387.
131. Singh, V., et al., *Chickpea peel waste as sustainable precursor for synthesis of fluorescent carbon nanotubes for bioimaging application*. Carbon Letters, 2021. **31**(1): p. 117-123.
132. Anthony, A.M., et al., *Ultra-radiant photoluminescence of glutathione rigidified reduced carbon quantum dots (r-CQDs) derived from ice-biryani for in vitro and in vivo bioimaging applications*. Colloids and Surfaces A: Physicochemical and Engineering Aspects, 2020. **586**: p. 124266.
133. Huang, G., et al., *Photoluminescent carbon dots derived from sugarcane molasses: synthesis, properties, and applications*. RSC advances, 2017. **7**(75): p. 47840-47847.
134. Irmania, N., et al., *Manganese-doped green tea-derived carbon quantum dots as a targeted dual imaging and photodynamic therapy platform*. Journal of Biomedical Materials Research Part B: Applied Biomaterials, 2020. **108**(4): p. 1616-1625.
135. Abbas, A., L.T. Mariana, and A.N. Phan, *Biomass-waste derived graphene quantum dots and their applications*. Carbon, 2018. **140**: p. 77-99.
136. Liao, J., Z. Cheng, and L. Zhou, *Nitrogen-doping enhanced fluorescent carbon dots: green synthesis and their applications for bioimaging and label-free detection of Au³⁺ ions*. ACS Sustainable Chemistry & Engineering, 2016. **4**(6): p. 3053-3061.
137. Dehvari, K., et al., *Sonochemical-assisted green synthesis of nitrogen-doped carbon dots from crab shell as targeted nanoprobe for cell imaging*. Journal of the Taiwan Institute of Chemical Engineers, 2019. **95**: p. 495-503.

138. Liu, R., et al., *A facile microwave-hydrothermal approach towards highly photoluminescent carbon dots from goose feathers*. RSC advances, 2015. **5**(6): p. 4428-4433.
139. Feng, J., et al., *Green preparation of nitrogen-doped carbon dots derived from silkworm chrysalis for cell imaging*. Journal of Materials Chemistry B, 2016. **4**(3): p. 387-393.
140. Wang, H., et al., *Presence of fluorescent carbon nanoparticles in baked lamb: their properties and potential application for sensors*. Journal of agricultural and food chemistry, 2017. **65**(34): p. 7553-7559.
141. Vickers, N.J., *Animal communication: when i'm calling you, will you answer too?* Current biology, 2017. **27**(14): p. R713-R715.
142. Ye, Q., et al., *Formation of N, S-codoped fluorescent carbon dots from biomass and their application for the selective detection of mercury and iron ion*. Spectrochimica Acta Part A: Molecular and Biomolecular Spectroscopy, 2017. **173**: p. 854-862.
143. Tai, D., C. Liu, and J. Liu, *Facile synthesis of fluorescent carbon dots from shrimp shells and using the carbon dots to detect chromium (VI)*. Spectroscopy Letters, 2019. **52**(3-4): p. 194-199.
144. Wang, B., et al., *Synthesis of catalytically active multielement-doped carbon dots and application for colorimetric detection of glucose*. Sensors and Actuators B: Chemical, 2018. **255**: p. 2601-2607.
145. Cong, S., et al., *Biocompatible fluorescent carbon dots derived from roast duck for in vitro cellular and in vivo C. elegans bio-imaging*. Methods, 2019. **168**: p. 76-83.
146. Devi, P., et al., *Waste derivitized blue luminescent carbon quantum dots for selenite sensing in water*. Talanta, 2017. **170**: p. 49-55.
147. Zhang, Z., W. Sun, and P. Wu, *Highly photoluminescent carbon dots derived from egg white: facile and green synthesis, photoluminescence properties, and multiple applications*. ACS Sustainable Chemistry & Engineering, 2015. **3**(7): p. 1412-1418.
148. Sui, G., et al., *Preparation and characterization of g-C₃N₄/Ag-TiO₂ ternary hollowsphere nanoheterojunction catalyst with high visible light photocatalytic performance*. Journal of Alloys and Compounds, 2020. **823**: p. 153851.
149. Baig, M.M.F. and Y.-C. Chen, *Bright carbon dots as fluorescence sensing agents for bacteria and curcumin*. Journal of colloid and interface science, 2017. **501**: p. 341-349.
150. Pramanik, S., et al., *Egg-shell derived carbon dots for base pair selective DNA binding and recognition*. Physical Chemistry Chemical Physics, 2018. **20**(31): p. 20476-20488.
151. Maddu, A., R. Meliafatmah, and E. Rustami, *Enhancing Photocatalytic Degradation of Methylene Blue Using ZnO/Carbon Dots Nanocomposite Derived From Coffee Grounds*. Polish Journal of Environmental Studies, 2021. **30**(1).
152. Wang, L., et al., *Facile synthesis of fluorescent graphene quantum dots from coffee grounds for bioimaging and sensing*. Chemical Engineering Journal, 2016. **300**: p. 75-82.
153. Chen, K., et al., *On-off-on fluorescent carbon dots from waste tea: Their properties, antioxidant and selective detection of CrO₄²⁻, Fe³⁺, ascorbic acid and L-cysteine in real samples*. Spectrochimica Acta Part A: Molecular and Biomolecular Spectroscopy, 2019. **213**: p. 228-234.
154. Hu, Z., X.-Y. Jiao, and L. Xu, *The N, S co-doped carbon dots with excellent luminescent properties from green tea leaf residue and its sensing of gefitinib*. Microchemical Journal, 2020. **154**: p. 104588.
155. Shi, L., et al., *Green-fluorescent nitrogen-doped carbon nanodots for biological imaging and paper-based sensing*. Analytical Methods, 2017. **9**(14): p. 2197-2204.

156. Song, P., et al., *A multianalyte fluorescent carbon dots sensing system constructed based on specific recognition of Fe (III) ions*. RSC advances, 2017. **7**(46): p. 28637-28646.
157. Rahbari, R., et al., *A novel L1 retrotransposon marker for HeLa cell line identification*. Biotechniques, 2009. **46**(4): p. 277-284.
158. Scherer, W.F., J.T. Syverton, and G.O. Gey, *Studies on the propagation in vitro of poliomyelitis viruses: IV. Viral multiplication in a stable strain of human malignant epithelial cells (strain HeLa) derived from an epidermoid carcinoma of the cervix*. The Journal of experimental medicine, 1953. **97**(5): p. 695-710.
159. Saboowala, H.K., *What HeLa Cells aka Immortal Cells Are and Why They Are Important. An Example of Racism in Medicine*. 2022: Dr. Hakim Saboowala.
160. Capes-Davis, A., et al., *Check your cultures! A list of cross-contaminated or misidentified cell lines*. International journal of cancer, 2010. **127**(1): p. 1-8.
161. Batts, D.W., *Cancer cells killed Henrietta Lacks—then made her immortal*. Retrieved from: https://www.pilotonline.com/news/health/article_17bd351a-f606-54fb-a499-b6a84cb3a286.html, 2010.
162. Puck, T.T. and P.I. Marcus, *A rapid method for viable cell titration and clone production with HeLa cells in tissue culture: the use of X-irradiated cells to supply conditioning factors*. Proceedings of the National Academy of Sciences, 1955. **41**(7): p. 432-437.
163. Bulzomi, P., et al., *The pro-apoptotic effect of quercetin in cancer cell lines requires ERβ-dependent signals*. Journal of cellular physiology, 2012. **227**(5): p. 1891-1898.
164. Tan, X., et al., *A NIR heptamethine dye with intrinsic cancer targeting, imaging and photosensitizing properties*. Biomaterials, 2012. **33**(7): p. 2230-2239.
165. Pene, F., et al., *Toward theragnostics*. Critical care medicine, 2009. **37**(1): p. S50-S58.
166. Bräuner, T. and D.F. Hülser, *Tumor cell invasion and gap junctional communication. 2, Normal and malignant cells confronted in multicell spheroids*. 1990.
167. Xie, Z., et al., *Multi-input RNAi-based logic circuit for identification of specific cancer cells*. Science, 2011. **333**(6047): p. 1307-1311.
168. Arjomandnejad, M., et al., *HeLa cell line xenograft tumor as a suitable cervical cancer model: growth kinetic characterization and immunohistochemistry array*. Archives of Iranian Medicine, 2014. **17**(4): p. 0-0.
169. Masters, J.R., *HeLa cells 50 years on: the good, the bad and the ugly*. Nature Reviews Cancer, 2002. **2**(4): p. 315-319.
170. Turner, T., *Development of the polio vaccine: a historical perspective of Tuskegee University's role in mass production and distribution of HeLa cells*. Journal of health care for the poor and underserved, 2012. **23**(4 0): p. 5.
171. Brownlee, K.A., *Statistics of the 1954 polio vaccine trials*. Journal of the American Statistical Association, 1955. **50**(272): p. 1005-1013.
172. Parker, J.S., et al., *Canine and feline parvoviruses can use human or feline transferrin receptors to bind, enter, and infect cells*. Journal of Virology, 2001. **75**(8): p. 3896-3902.
173. Acrani, G.O., et al., *Apoptosis induced by Oropouche virus infection in HeLa cells is dependent on virus protein expression*. Virus Research, 2010. **149**(1): p. 56-63.
174. Hou, S.Y., S.-Y. Wu, and C.-M. Chiang, *Transcriptional activity among high and low risk human papillomavirus E2 proteins correlates with E2 DNA binding*. Journal of Biological Chemistry, 2002. **277**(47): p. 45619-45629.
175. Del Puerto, H.L., et al., *Canine distemper virus induces apoptosis in cervical tumor derived cell lines*. Virology journal, 2011. **8**(1): p. 1-7.

176. Mondor, I., S. Ugolini, and Q.J. Sattentau, *Human immunodeficiency virus type 1 attachment to HeLa CD4 cells is CD4 independent and gp120 dependent and requires cell surface heparans*. Journal of virology, 1998. **72**(5): p. 3623-3634.
177. Wechsler, S.L., et al., *Measles virus-specified polypeptide synthesis in two persistently infected HeLa cell lines*. Journal of Virology, 1979. **31**(3): p. 677-684.
178. Li, L., et al., *Attenuation of Zika virus by passage in human HeLa cells*. Vaccines, 2019. **7**(3): p. 93.
179. Smith, V., *Wonder woman: The life, death, and life after death of Henrietta Lacks, unwitting heroine of modern medical science*. Baltimore City Paper, 2002. **17**.
180. Skloot, R., *The immortal life of Henrietta Lacks*. 2017: Broadway Paperbacks.
181. Xu, J., et al., *Formation of fluorescent carbon nanodots from kitchen wastes and their application for detection of Fe³⁺*. Luminescence, 2015. **30**(4): p. 420-424.
182. Xu, Y., et al., *Enhanced-quantum yield sulfur/nitrogen co-doped fluorescent carbon nanodots produced from biomass Enteromorpha prolifera: synthesis, posttreatment, applications and mechanism study*. Scientific reports, 2017. **7**(1): p. 1-12.
183. Huang, H., et al., *Facile and green synthesis of photoluminescent carbon nanoparticles for cellular imaging*. New Journal of Chemistry, 2014. **38**(2): p. 784-789.
184. Ding, H., et al., *Facile synthesis of red-emitting carbon dots from pulp-free lemon juice for bioimaging*. Journal of Materials Chemistry B, 2017. **5**(26): p. 5272-5277.
185. Fan, L., et al., *Highly sensitive photoelectrochemical aptasensor based on MoS₂ quantum dots/TiO₂ nanotubes for detection of atrazine*. Sensors and Actuators B: Chemical, 2021. **334**: p. 129652.
186. Line, C., *Human alveolar adenocarcinoma cell line-General Information*. Retrieved January, 2012. **3**.
187. Giard, D.J., et al., *In vitro cultivation of human tumors: establishment of cell lines derived from a series of solid tumors*. Journal of the National Cancer Institute, 1973. **51**(5): p. 1417-1423.
188. Foster, K.A., et al., *Characterization of the A549 cell line as a type II pulmonary epithelial cell model for drug metabolism*. Experimental cell research, 1998. **243**(2): p. 359-366.
189. Korsnes, M.S. and R. Korsnes, *Single-cell tracking of A549 lung cancer cells exposed to a marine toxin reveals correlations in pedigree tree profiles*. Frontiers in oncology, 2018. **8**: p. 260.
190. Andrei, L., et al., *Advanced technological tools to study multidrug resistance in cancer*. Drug Resistance Updates, 2020. **48**: p. 100658.
191. Thomas, L., et al., *Respiratory syncytial virus-induced RANTES production from human bronchial epithelial cells is dependent on nuclear factor- κ B nuclear binding and is inhibited by adenovirus-mediated expression of inhibitor of κ B α* . The Journal of Immunology, 1998. **161**(2): p. 1007-1016.
192. Lin, Y., M. Zhang, and P.F. Barnes, *Chemokine production by a human alveolar epithelial cell line in response to Mycobacterium tuberculosis*. Infection and immunity, 1998. **66**(3): p. 1121-1126.
193. Foss, J.F., D.G. Bohl, and T.J. Hicks, *The pulse width modulated-constant temperature anemometer*. Measurement Science and Technology, 1996. **7**(10): p. 1388.
194. Wu, Z.L., et al., *One-pot hydrothermal synthesis of highly luminescent nitrogen-doped amphoteric carbon dots for bioimaging from Bombyx mori silk-natural proteins*. Journal of Materials Chemistry B, 2013. **1**(22): p. 2868-2873.
195. Aden, D.P., et al., *Controlled synthesis of HBsAg in a differentiated human liver carcinoma-derived cell line*. Nature, 1979. **282**(5739): p. 615-616.

196. López-Terrada, D., et al., *Hep G2 is a hepatoblastoma-derived cell line*. Human pathology, 2009. **40**(10): p. 1512.
197. Ihrke, G., et al., *WIF-B cells: an in vitro model for studies of hepatocyte polarity*. The Journal of Cell Biology, 1993. **123**(6): p. 1761-1775.
198. Moscato, S., et al., *Poly (vinyl alcohol)/gelatin hydrogels cultured with HepG2 cells as a 3D model of hepatocellular carcinoma: a morphological study*. Journal of functional biomaterials, 2015. **6**(1): p. 16-32.
199. Suryawanshi, S.B., et al., *Consensus Pharmacophore Modeling Analysis for Human Cellular Cytotoxicity (Hepg2) Activity of 2-Anilino 4-Amino Substituted Quinazolines*. Journal of Current Pharma Research, 2019. **9**(2): p. 2727-2733.
200. Mersch-Sundermann, V., et al., *Use of a human-derived liver cell line for the detection of cytoprotective, antigenotoxic and cogenotoxic agents*. Toxicology, 2004. **198**(1-3): p. 329-340.
201. Shi, C., et al., *N, S-self-doped carbon quantum dots from fungus fibers for sensing tetracyclines and for bioimaging cancer cells*. Materials Science and Engineering: C, 2019. **105**: p. 110132.
202. Li, W., et al., *Simple and green synthesis of nitrogen-doped photoluminescent carbonaceous nanospheres for bioimaging*. Angewandte Chemie International Edition, 2013. **52**(31): p. 8151-8155.
203. Wang, Z., F. Liu, and C. Lu, *Evolution of biogenic amine concentrations in foods through their induced chemiluminescence inactivation of layered double hydroxide nanosheet colloids*. Biosensors and Bioelectronics, 2014. **60**: p. 237-243.
204. Lu, M., et al., *Green preparation of versatile nitrogen-doped carbon quantum dots from watermelon juice for cell imaging, detection of Fe³⁺ ions and cysteine, and optical thermometry*. Journal of Molecular Liquids, 2018. **269**: p. 766-774.
205. Lee, A.V., S. Oesterreich, and N.E. Davidson, *MCF-7 cells—changing the course of breast cancer research and care for 45 years*. JNCI: Journal of the National Cancer Institute, 2015. **107**(7).
206. Soule, H., et al., *A human cell line from a pleural effusion derived from a breast carcinoma*. Journal of the national cancer institute, 1973. **51**(5): p. 1409-1416.
207. Cass, G., *A History of the Michigan Cancer Foundation, the Beginnings & Growth of Detroit's Anticancer Movement*. Detroit: Michigan Cancer Foundation, 1990.
208. Tadesse, A., et al., *Fluorescent-nitrogen-doped carbon quantum dots derived from citrus lemon juice: green synthesis, mercury (II) ion sensing, and live cell imaging*. ACS omega, 2020. **5**(8): p. 3889-3898.
209. Arkan, E., et al., *Green synthesis of carbon dots derived from walnut oil and an investigation of their cytotoxic and apoptogenic activities toward cancer cells*. Advanced pharmaceutical bulletin, 2018. **8**(1): p. 149.
210. Devi, P., S. Saini, and K.-H. Kim, *The advanced role of carbon quantum dots in nanomedical applications*. Biosensors and Bioelectronics, 2019. **141**: p. 111158.
211. Tian, L., et al., *Nanosized carbon particles from natural gas soot*. Chemistry of materials, 2009. **21**(13): p. 2803-2809.
212. Liu, R., et al., *An aqueous route to multicolor photoluminescent carbon dots using silica spheres as carriers*. Angewandte Chemie International Edition, 2009. **48**(25): p. 4598-4601.
213. Deng, J., et al., *Electrochemical synthesis of carbon nanodots directly from alcohols*. Chemistry—A European Journal, 2014. **20**(17): p. 4993-4999.
214. Yuan, F., et al., *Shining carbon dots: synthesis and biomedical and optoelectronic applications*. Nano Today, 2016. **11**(5): p. 565-586.
215. Liu, M.L., et al., *Carbon dots: synthesis, formation mechanism, fluorescence origin and sensing applications*. Green chemistry, 2019. **21**(3): p. 449-471.

216. Yoo, D., et al., *Carbon dots as an effective fluorescent sensing platform for metal ion detection*. *Nanoscale research letters*, 2019. **14**(1): p. 1-13.
217. Luo, J., et al., *Hydrothermal synthesis of bright blue-emitting carbon dots for bioimaging and fluorescent determination of baicalein*. *Optical Materials*, 2021. **113**: p. 110796.
218. Zheng, M., et al., *Self-targeting fluorescent carbon dots for diagnosis of brain cancer cells*. *ACS nano*, 2015. **9**(11): p. 11455-11461.
219. Canevari, T.C., et al., *High performance electrochemical sensors for dopamine and epinephrine using nanocrystalline carbon quantum dots obtained under controlled chronoamperometric conditions*. *Electrochimica Acta*, 2016. **209**: p. 464-470.
220. Eskalen, H., et al., *Microwave-assisted ultra-fast synthesis of carbon quantum dots from linter: Fluorescence cancer imaging and human cell growth inhibition properties*. *Industrial Crops and Products*, 2020. **147**: p. 112209.
221. Wan, J.-Y., et al., *Ionic liquid-assisted thermal decomposition synthesis of carbon dots and graphene-like carbon sheets for optoelectronic application*. *RSC advances*, 2016. **6**(66): p. 61292-61300.
222. Shang, W., et al., *Facile one pot pyrolysis synthesis of carbon quantum dots and graphene oxide nanomaterials: all carbon hybrids as eco-environmental lubricants for low friction and remarkable wear-resistance*. *Tribology International*, 2018. **118**: p. 373-380.
223. Namdari, P., B. Negahdari, and A. Eatemadi, *Synthesis, properties and biomedical applications of carbon-based quantum dots: An updated review*. *Biomedicine & Pharmacotherapy*, 2017. **87**: p. 209-222.
224. Crista, D., J.C. Esteves da Silva, and L. Pinto da Silva, *Evaluation of different bottom-up routes for the fabrication of carbon dots*. *Nanomaterials*, 2020. **10**(7): p. 1316.
225. Mittal, S.S., et al. *Carbon Quantum Dot-Polypyrrole Nanocomposite for Supercapacitor Electrodes*. in *IOP Conference Series: Materials Science and Engineering*. 2019. IOP Publishing.
226. Kasprzyk, W., et al., *Luminescence phenomena of carbon dots derived from citric acid and urea—a molecular insight*. *Nanoscale*, 2018. **10**(29): p. 13889-13894.
227. Xie, Y., et al., *One-step hydrothermal synthesis of fluorescence carbon quantum dots with high product yield and quantum yield*. *Nanotechnology*, 2019. **30**(8): p. 085406.
228. Baragau, I.-A., et al., *Efficient continuous hydrothermal flow synthesis of carbon quantum dots from a targeted biomass precursor for on-off metal ions nanosensing*. *ACS Sustainable Chemistry & Engineering*, 2021. **9**(6): p. 2559-2569.
229. Paikaray, S., *A simple hydrothermal synthesis of luminescent carbon quantum dots from different molecular precursors*. 2013.
230. Shabbir, H., et al., *Milk-Derived Carbon Quantum Dots: Study of Biological and Chemical Properties Provides Evidence of Toxicity*. *Molecules*, 2022. **27**(24): p. 8728.
231. Gan, Y.X., et al., *Hydrothermal synthesis of nanomaterials*. 2020, Hindawi.
232. Xue, B., et al., *Photoluminescent lignin hybridized carbon quantum dots composites for bioimaging applications*. *International journal of biological macromolecules*, 2019. **122**: p. 954-961.
233. Qian, J., et al., *Aconitic acid derived carbon dots: Conjugated interaction for the detection of folic acid and fluorescence targeted imaging of folate receptor overexpressed cancer cells*. *Sensors and Actuators B: Chemical*, 2018. **262**: p. 444-451.
234. Gawande, M.B., et al., *Microwave-assisted chemistry: synthetic applications for rapid assembly of nanomaterials and organics*. *Accounts of chemical research*, 2014. **47**(4): p. 1338-1348.

235. Sun, J., W. Wang, and Q. Yue, *Review on microwave-matter interaction fundamentals and efficient microwave-associated heating strategies*. *Materials*, 2016. **9**(4): p. 231.
236. Lu, S., et al., *Synthesis of dual functional gallic-acid-based carbon dots for bioimaging and antitumor therapy*. *Biomaterials science*, 2019. **7**(8): p. 3258-3265.
237. Jaiswal, A., S.S. Ghosh, and A. Chattopadhyay, *One step synthesis of C-dots by microwave mediated caramelization of poly (ethylene glycol)*. *Chemical communications*, 2012. **48**(3): p. 407-409.
238. Xia, C., et al., *Evolution and synthesis of carbon dots: from carbon dots to carbonized polymer dots*. *Advanced Science*, 2019. **6**(23): p. 1901316.
239. Kumar, S., et al., *Biofunctionalized two-dimensional Ti₃C₂ MXenes for ultrasensitive detection of cancer biomarker*. *Biosensors and Bioelectronics*, 2018. **121**: p. 243-249.
240. Nallayagari, A., et al., *Tuneable properties of carbon quantum dots by different synthetic methods*. *Journal of Nanostructure in Chemistry*, 2021: p. 1-16.
241. JiaXF, L., WangEK. *One-pot greensynthesis of optically pH-sensitive carbon dots with upconversion luminescence*. *Nanoscale* 2012. **4**: p. 5572-5.
242. Azam, N., M. Najabat Ali, and T. Javaid Khan, *Carbon quantum dots for biomedical applications: review and analysis*. *Frontiers in Materials*, 2021. **8**: p. 700403.
243. Jorns, M. and D. Pappas, *A review of fluorescent carbon dots, their synthesis, physical and chemical characteristics, and applications*. *Nanomaterials*, 2021. **11**(6): p. 1448.
244. Liu, H., T. Ye, and C. Mao, *Fluorescent carbon nanoparticles derived from candle soot*. *Angewandte chemie*, 2007. **119**(34): p. 6593-6595.
245. Hu, S., et al., *Chemical regulation of carbon quantum dots from synthesis to photocatalytic activity*. *Chemistry—An Asian Journal*, 2013. **8**(5): p. 1035-1041.
246. Qu, S., et al., *A biocompatible fluorescent ink based on water-soluble luminescent carbon nanodots*. *Angewandte Chemie international edition*, 2012. **51**(49): p. 12215-12218.
247. Wang, R., et al., *Recent progress in carbon quantum dots: synthesis, properties and applications in photocatalysis*. *Journal of Materials Chemistry A*, 2017. **5**(8): p. 3717-3734.
248. Molaei, M.J., *A review on nanostructured carbon quantum dots and their applications in biotechnology, sensors, and chemiluminescence*. *Talanta*, 2019. **196**: p. 456-478.
249. Cao, L., et al., *Photoluminescence properties of graphene versus other carbon nanomaterials*. *Accounts of Chemical Research*, 2013. **46**(1): p. 171-180.
250. Lin, L. and S. Zhang, *Creating high yield water soluble luminescent graphene quantum dots via exfoliating and disintegrating carbon nanotubes and graphite flakes*. *Chemical communications*, 2012. **48**(82): p. 10177-10179.
251. Bao, L., et al., *Electrochemical tuning of luminescent carbon nanodots: from preparation to luminescence mechanism*. *Advanced materials*, 2011. **23**(48): p. 5801-5806.
252. Qu, D., et al., *Highly luminescent S, N co-doped graphene quantum dots with broad visible absorption bands for visible light photocatalysts*. *Nanoscale*, 2013. **5**(24): p. 12272-12277.
253. !!! INVALID CITATION !!! [2-5].
254. Molaei, M.J., *Principles, mechanisms, and application of carbon quantum dots in sensors: a review*. *Analytical Methods*, 2020. **12**(10): p. 1266-1287.
255. Wang, X., et al., *A mini review on carbon quantum dots: preparation, properties, and electrocatalytic application*. *Frontiers in Chemistry*, 2019. **7**: p. 671.

256. Zhu, S., et al., *The photoluminescence mechanism in carbon dots (graphene quantum dots, carbon nanodots, and polymer dots): current state and future perspective*. Nano research, 2015. **8**(2): p. 355-381.
257. Atkins, P., J. De Paula, and J. Keeler, *Molecular Spectroscopy. Atkins' Physical Chemistry*. 2018, Oxford: Oxford University Press.
258. Würth, C., et al., *Relative and absolute determination of fluorescence quantum yields of transparent samples*. Nature protocols, 2013. **8**(8): p. 1535-1550.
259. Faulkner, D.O., et al., *Measurement of absolute photoluminescence quantum yields using integrating spheres—Which way to go?* Laser & Photonics Reviews, 2012. **6**(6): p. 802-806.
260. Porres, L., et al., *Absolute measurements of photoluminescence quantum yields of solutions using an integrating sphere*. Journal of fluorescence, 2006. **16**(2): p. 267-273.
261. Sun, Y., et al., *The cost-effective preparation of green fluorescent carbon dots for bioimaging and enhanced intracellular drug delivery*. Nanoscale research letters, 2020. **15**(1): p. 1-9.
262. Hua, X.-W., Y.-W. Bao, and F.-G. Wu, *Fluorescent carbon quantum dots with intrinsic nucleolus-targeting capability for nucleolus imaging and enhanced cytosolic and nuclear drug delivery*. ACS applied materials & interfaces, 2018. **10**(13): p. 10664-10677.
263. Yuan, B., et al., *Highly efficient carbon dots with reversibly switchable green–red emissions for trichromatic white light-emitting diodes*. ACS applied materials & interfaces, 2018. **10**(18): p. 16005-16014.
264. Yuan, F., et al., *Highly efficient and stable white LEDs based on pure red narrow bandwidth emission triangular carbon quantum dots for wide-color gamut backlight displays*. Nano Research, 2019. **12**(7): p. 1669-1674.
265. Sk, M.P., et al., *Presence of amorphous carbon nanoparticles in food caramels*. Scientific reports, 2012. **2**(1): p. 1-5.
266. Liu, W., et al., *Highly crystalline carbon dots from fresh tomato: UV emission and quantum confinement*. Nanotechnology, 2017. **28**(48): p. 485705.
267. Qi, H., et al., *Biomass-derived nitrogen-doped carbon quantum dots: highly selective fluorescent probe for detecting Fe³⁺ ions and tetracyclines*. Journal of colloid and interface science, 2019. **539**: p. 332-341.
268. Qiang, R., et al., *Synthesis of carbon quantum dots with green luminescence from potato starch*. New Journal of Chemistry, 2019. **43**(27): p. 10826-10833.
269. Ren, X., et al., *A new approach in functionalization of carbon nanoparticles for optoelectronically relevant carbon dots and beyond*. Carbon, 2019. **141**: p. 553-560.
270. Dang, D.K., et al., *One pot solid-state synthesis of highly fluorescent N and S co-doped carbon dots and its use as fluorescent probe for Ag⁺ detection in aqueous solution*. Sensors and Actuators B: Chemical, 2018. **255**: p. 3284-3291.
271. Hou, Y., et al., *One-pot electrochemical synthesis of functionalized fluorescent carbon dots and their selective sensing for mercury ion*. Analytica Chimica Acta, 2015. **866**: p. 69-74.
272. LIU, J.-H., et al., *Cytotoxicity evaluations of fluorescent carbon nanoparticles*. Nano Life, 2010. **1**(01n02): p. 153-161.
273. Zhao, F., et al., *Cellular uptake, intracellular trafficking, and cytotoxicity of nanomaterials*. small, 2011. **7**(10): p. 1322-1337.
274. Li, H., et al., *Nucleic acid detection using carbon nanoparticles as a fluorescent sensing platform*. Chemical Communications, 2011. **47**(3): p. 961-963.

275. Zhao, H.X., et al., *Highly selective detection of phosphate in very complicated matrixes with an off-on fluorescent probe of europium-adjusted carbon dots*. Chemical Communications, 2011. **47**(9): p. 2604-2606.
276. Dong, Y., et al., *Polyamine-functionalized carbon quantum dots for chemical sensing*. Carbon, 2012. **50**(8): p. 2810-2815.
277. Yin, J.-Y., et al., *Hyperbranched polymer functionalized carbon dots with multistimuli-responsive property*. ACS Macro Letters, 2013. **2**(11): p. 1033-1037.
278. Alcantar, N.A., E.S. Aydil, and J.N. Israelachvili, *Polyethylene glycol-coated biocompatible surfaces*. Journal of Biomedical Materials Research: An Official Journal of The Society for Biomaterials, The Japanese Society for Biomaterials, and The Australian Society for Biomaterials and the Korean Society for Biomaterials, 2000. **51**(3): p. 343-351.
279. Bjugstad, K., et al., *Biocompatibility of poly (ethylene glycol)-based hydrogels in the brain: An analysis of the glial response across space and time*. Journal of Biomedical Materials Research Part A, 2010. **95**(1): p. 79-91.
280. Nie, H., et al., *Carbon dots with continuously tunable full-color emission and their application in ratiometric pH sensing*. Chemistry of Materials, 2014. **26**(10): p. 3104-3112.
281. Iida, T., et al., *Overall interaction of cytosolic proteins with the PEI/DNA complex*. Journal of controlled release, 2007. **118**(3): p. 364-369.
282. Moghimi, S.M., et al., *A two-stage poly (ethylenimine)-mediated cytotoxicity: implications for gene transfer/therapy*. Molecular therapy, 2005. **11**(6): p. 990-995.
283. Kircheis, R., L. Wightman, and E. Wagner, *Design and gene delivery activity of modified polyethylenimines*. Advanced drug delivery reviews, 2001. **53**(3): p. 341-358.
284. Pierrat, P., et al., *Efficient in vitro and in vivo pulmonary delivery of nucleic acid by carbon dot-based nanocarriers*. Biomaterials, 2015. **51**: p. 290-302.
285. Bae, Y.H. and K. Park, *Targeted drug delivery to tumors: myths, reality and possibility*. Journal of controlled release, 2011. **153**(3): p. 198.
286. Gratton, S.E., et al., *The effect of particle design on cellular internalization pathways*. Proceedings of the National Academy of Sciences, 2008. **105**(33): p. 11613-11618.
287. Lee, E.S., et al., *Super pH-sensitive multifunctional polymeric micelle for tumor pH specific TAT exposure and multidrug resistance*. Journal of Controlled Release, 2008. **129**(3): p. 228-236.
288. Huang, X., et al., *Effect of injection routes on the biodistribution, clearance, and tumor uptake of carbon dots*. ACS nano, 2013. **7**(7): p. 5684-5693.
289. Xiao, W., et al., *Design of a Cellular-Uptake-Shielding "Plug and Play" Template for Photo Controllable Drug Release*. Advanced Materials, 2011. **23**(31): p. 3526-3530.
290. Lee, Y., et al., *Charge-conversion ternary polyplex with endosome disruption moiety: a technique for efficient and safe gene delivery*. Angewandte Chemie, 2008. **120**(28): p. 5241-5244.
291. Mintzer, M.A. and E.E. Simanek, *Nonviral vectors for gene delivery*. Chemical reviews, 2009. **109**(2): p. 259-302.
292. Fischer, D., et al., *In vitro cytotoxicity testing of polycations: influence of polymer structure on cell viability and hemolysis*. Biomaterials, 2003. **24**(7): p. 1121-1131.
293. Ge, Z. and S. Liu, *Functional block copolymer assemblies responsive to tumor and intracellular microenvironments for site-specific drug delivery and enhanced imaging performance*. Chemical Society Reviews, 2013. **42**(17): p. 7289-7325.
294. Jin, E., et al., *Acid-active cell-penetrating peptides for in vivo tumor-targeted drug delivery*. Journal of the American Chemical Society, 2013. **135**(2): p. 933-940.

295. Kou, L., et al., *The endocytosis and intracellular fate of nanomedicines: Implication for rational design*. Asian Journal of Pharmaceutical Sciences, 2013. **8**(1): p. 1-10.
296. Liu, Y., et al., *The Influence on Cell Cycle and Cell Division by Various Cadmium-Containing Quantum Dots*. Small, 2013. **9**(14): p. 2440-2451.
297. Li, F., D. Yang, and H. Xu, *Non-metal-heteroatom-doped carbon dots: synthesis and properties*. Chemistry—A European Journal, 2019. **25**(5): p. 1165-1176.
298. Li, L. and T. Dong, *Photoluminescence tuning in carbon dots: surface passivation or/and functionalization, heteroatom doping*. Journal of Materials Chemistry C, 2018. **6**(30): p. 7944-7970.
299. Jana, J. and T. Pal, *An account of doping in carbon dots for varied applications*. Natural Resources & Engineering, 2017. **2**(1): p. 5-12.
300. Park, Y., et al., *Improving the functionality of carbon nanodots: doping and surface functionalization*. Journal of Materials Chemistry A, 2016. **4**(30): p. 11582-11603.
301. Atabaev, T.S., *Doped carbon dots for sensing and bioimaging applications: A minireview*. Nanomaterials, 2018. **8**(5): p. 342.
302. Wolfbeis, O.S., *An overview of nanoparticles commonly used in fluorescent bioimaging*. Chemical Society Reviews, 2015. **44**(14): p. 4743-4768.
303. Lin, L., et al., *Metal ions doped carbon quantum dots: Synthesis, physicochemical properties, and their applications*. TrAC Trends in Analytical Chemistry, 2018. **103**: p. 87-101.
304. Liu, S., et al., *Hydrothermal treatment of grass: a low-cost, green route to nitrogen-doped, carbon-rich, photoluminescent polymer nanodots as an effective fluorescent sensing platform for label-free detection of Cu (II) ions*. Advanced materials, 2012. **24**(15): p. 2037-2041.
305. Dey, S., et al., *New methods of synthesis and varied properties of carbon quantum dots with high nitrogen content*. Journal of Materials Research, 2014. **29**(3): p. 383-391.
306. Wang, L., et al., *Aqueous phase synthesis of highly luminescent, nitrogen-doped carbon dots and their application as bioimaging agents*. Langmuir, 2014. **30**(47): p. 14270-14275.
307. Niu, J. and H. Gao, *Synthesis and drug detection performance of nitrogen-doped carbon dots*. Journal of luminescence, 2014. **149**: p. 159-162.
308. Dong, Y., et al., *Carbon-based dots co-doped with nitrogen and sulfur for high quantum yield and excitation-independent emission*. Angewandte Chemie International Edition, 2013. **52**(30): p. 7800-7804.
309. Teng, X., et al., *Green synthesis of nitrogen-doped carbon dots from konjac flour with "off-on" fluorescence by Fe 3+ and L-lysine for bioimaging*. Journal of Materials Chemistry B, 2014. **2**(29): p. 4631-4639.
310. Qian, Z., et al., *Highly luminescent N-doped carbon quantum dots as an effective multifunctional fluorescence sensing platform*. Chemistry—A European Journal, 2014. **20**(8): p. 2254-2263.
311. Shan, X., et al., *B-doped carbon quantum dots as a sensitive fluorescence probe for hydrogen peroxide and glucose detection*. Analyst, 2014. **139**(10): p. 2322-2325.
312. Bourlinos, A.B., et al., *Green and simple route toward boron doped carbon dots with significantly enhanced non-linear optical properties*. Carbon, 2015. **83**: p. 173-179.
313. Zuo, G., et al., *Large emission red-shift of carbon dots by fluorine doping and their applications for red cell imaging and sensitive intracellular Ag+ detection*. The Journal of Physical Chemistry C, 2017. **121**(47): p. 26558-26565.
314. Zuo, G., et al., *Fluorine-doped cationic carbon dots for efficient gene delivery*. ACS Applied Nano Materials, 2018. **1**(5): p. 2376-2385.

315. Zhou, J., et al., *Facile synthesis of P-doped carbon quantum dots with highly efficient photoluminescence*. Rsc Advances, 2014. **4**(11): p. 5465-5468.
316. Sarkar, S., et al., *Amino acid functionalized blue and phosphorous-doped green fluorescent carbon dots as bioimaging probe*. RSC Advances, 2015. **5**(81): p. 65913-65921.
317. Hola, K., et al., *Photoluminescence effects of graphitic core size and surface functional groups in carbon dots: COO⁻ induced red-shift emission*. Carbon, 2014. **70**: p. 279-286.
318. Li, N., et al., *Biodistribution study of carbogenic dots in cells and in vivo for optical imaging*. Journal of Nanoparticle Research, 2012. **14**(10): p. 1-9.
319. Ray, S., et al., *Fluorescent carbon nanoparticles: synthesis, characterization, and bioimaging application*. The Journal of Physical Chemistry C, 2009. **113**(43): p. 18546-18551.
320. Wang, Y., et al., *Carbon dots of different composition and surface functionalization: cytotoxicity issues relevant to fluorescence cell imaging*. Experimental Biology and Medicine, 2011. **236**(11): p. 1231-1238.
321. Havrdova, M., et al., *Toxicity of carbon dots—Effect of surface functionalization on the cell viability, reactive oxygen species generation and cell cycle*. Carbon, 2016. **99**: p. 238-248.
322. Ju, L., et al., *Quantum dot-related genotoxicity perturbation can be attenuated by PEG encapsulation*. Mutation Research/Genetic Toxicology and Environmental Mutagenesis, 2013. **753**(1): p. 54-64.
323. Yang, S.-T., et al., *Carbon dots as nontoxic and high-performance fluorescence imaging agents*. The Journal of Physical Chemistry C, 2009. **113**(42): p. 18110-18114.
324. Zhao, Q.-L., et al., *Facile preparation of low cytotoxicity fluorescent carbon nanocrystals by electrooxidation of graphite*. Chemical Communications, 2008(41): p. 5116-5118.
325. Wang, Y., et al., *Aptamer biosensor based on fluorescence resonance energy transfer from upconverting phosphors to carbon nanoparticles for thrombin detection in human plasma*. Analytical chemistry, 2011. **83**(21): p. 8130-8137.
326. Dong, Y., et al., *Polyamine-functionalized carbon quantum dots as fluorescent probes for selective and sensitive detection of copper ions*. Analytical chemistry, 2012. **84**(14): p. 6220-6224.
327. Yang, S.-T., et al., *Carbon dots for optical imaging in vivo*. Journal of the American Chemical Society, 2009. **131**(32): p. 11308-11309.
328. Wang, X., et al., *Bandgap-like strong fluorescence in functionalized carbon nanoparticles*. Angewandte Chemie International Edition, 2010. **49**(31): p. 5310-5314.
329. Cao, L., et al., *Carbon dots for multiphoton bioimaging*. Journal of the American Chemical Society, 2007. **129**(37): p. 11318-11319.
330. Farshbaf, M., et al., *Carbon quantum dots: recent progresses on synthesis, surface modification and applications*. Artificial cells, nanomedicine, and biotechnology, 2018. **46**(7): p. 1331-1348.
331. Xin Ting Zheng, A.A., Kathy Qian Luo , and Peng Chen, *Glowing Graphene Quantum Dots and Carbon Dots: Properties, Syntheses, and Biological Applications*. Small, 2015. **11**(14): p. 1620-1636.
332. M.J.Molaei, *A review on nanostructured carbon quantum dots and their application in biotechnology, sensors, and chemiluminescence*. Talanta, 2018. **196**: p. 456-478.
333. Molaei, M.J., *Carbon quantum dots and their biomedical and therapeutic applications :a riview*. RSC Advances, 2019. **9**: p. 6460-6481.

334. Himmelstoß, S.F. and T. Hirsch, *A critical comparison of lanthanide based upconversion nanoparticles to fluorescent proteins, semiconductor quantum dots, and carbon dots for use in optical sensing and imaging*. *Methods and Applications in Fluorescence*, 2019. **7**(2): p. 022002.
335. Miao, P., et al., *Recent advances in carbon nanodots: synthesis, properties and biomedical applications*. *Nanoscale*, 2015. **7**(5): p. 1586-1595.
336. Qianchun Zhang, X.Z., Linchun Bao, Yun Wu, Li Jiang, Yuguo Zheng,, *The Application of Green-Synthesis-Derived Carbon Quantum Dots to Bioimaging and the Analysis of Mercury(II)*. *Hindawi - Journal of analytical methods of Chemistry*, 2019. **2019**: p. 9.
337. Xin Ren, F.Z., *Synthesis of N-Doped Micropore Carbon Quantum Dots with High Quantum Yield and Dual-Wavelength Photoluminescence Emission from Biomass for Cellular Imaging*. *Nanomaterials*, 2019. **9**: p. 495.
338. Xu, Y., et al., *Nitrogen-doped carbon dots: a facile and general preparation method, photoluminescence investigation, and imaging applications*. *Chemistry—A European Journal*, 2013. **19**(7): p. 2276-2283.
339. Zheng, L., P. Qi, and D. Zhang, *Identification of bacteria by a fluorescence sensor array based on three kinds of receptors functionalized carbon dots*. *Sensors and Actuators B: Chemical*, 2019. **286**: p. 206-213.
340. Yang, Y.Z., et al., *pH-induced aggregation of hydrophilic carbon dots for fluorescence detection of acidic amino acid and intracellular pH imaging*. *Materials Science and Engineering: C*, 2020. **108**: p. 110401.
341. Zhong, J., et al., *Blood compatible heteratom-doped carbon dots for bio-imaging of human umbilical vein endothelial cells*. *Chinese Chemical Letters*, 2020. **31**(3): p. 769-773.
342. Shi, X., et al., *Red emissive carbon dots with dual targetability for imaging polarity in living cells*. *Sensors and Actuators B: Chemical*, 2020. **306**: p. 127582.
343. Wang, N., et al., *Deep eutectic solvent-assisted preparation of nitrogen/chloride-doped carbon dots for intracellular biological sensing and live cell imaging*. *ACS applied materials & interfaces*, 2018. **10**(9): p. 7901-7909.
344. Xue, M., et al., *Dual functionalized natural biomass carbon dots from lychee exocarp for cancer cell targetable near-infrared fluorescence imaging and photodynamic therapy*. *Nanoscale*, 2018. **10**(38): p. 18124-18130.
345. Ramanan, V., et al., *Outright green synthesis of fluorescent carbon dots from eutrophic algal blooms for in vitro imaging*. *ACS Sustainable Chemistry & Engineering*, 2016. **4**(9): p. 4724-4731.
346. Hamd-Ghadareh, S., et al., *An amplified comparative fluorescence resonance energy transfer immunosensing of CA125 tumor marker and ovarian cancer cells using green and economic carbon dots for bio-applications in labeling, imaging and sensing*. *Biosensors and Bioelectronics*, 2017. **96**: p. 308-316.
347. Gao, G., et al., *On-off-on fluorescent nanosensor for Fe³⁺ detection and cancer/normal cell differentiation via silicon-doped carbon quantum dots*. *Carbon*, 2018. **134**: p. 232-243.
348. Li, H., et al., *Recent advances in carbon dots for bioimaging applications*. *Nanoscale Horizons*, 2020. **5**(2): p. 218-234.
349. Meena, R., et al., *Fluorescent carbon dots driven from ayurvedic medicinal plants for cancer cell imaging and phototherapy*. *Heliyon*, 2019. **5**(9): p. e02483.
350. Lin, H., et al., *Bone marrow mesenchymal stem cells: Aging and tissue engineering applications to enhance bone healing*. *Biomaterials*, 2019. **203**: p. 96-110.
351. Gonzales, K.A.U. and E. Fuchs, *Skin and its regenerative powers: an alliance between stem cells and their niche*. *Developmental cell*, 2017. **43**(4): p. 387-401.

352. Nucci, L.P., et al., *Stem cells labeled with superparamagnetic iron oxide nanoparticles in a preclinical model of cerebral ischemia: a systematic review with meta-analysis*. Stem cell research & therapy, 2015. **6**(1): p. 1-13.
353. Shang, W., et al., *The uptake mechanism and biocompatibility of graphene quantum dots with human neural stem cells*. Nanoscale, 2014. **6**(11): p. 5799-5806.
354. Zhang, M., et al., *Facile synthesis of water-soluble, highly fluorescent graphene quantum dots as a robust biological label for stem cells*. Journal of materials chemistry, 2012. **22**(15): p. 7461-7467.
355. Shao, D., et al., *Carbon dots for tracking and promoting the osteogenic differentiation of mesenchymal stem cells*. Biomaterials science, 2017. **5**(9): p. 1820-1827.
356. Zhou, N., et al., *A novel fluorescent retrograde neural tracer: cholera toxin B conjugated carbon dots*. Nanoscale, 2015. **7**(38): p. 15635-15642.
357. Huang, X., et al., *YP 25 Sun, S. Lee and XY Chen*. ACS Nano, 2013. **7**: p. 5684-5693.
358. Licciardello, N., et al., *Biodistribution studies of ultrasmall silicon nanoparticles and carbon dots in experimental rats and tumor mice*. Nanoscale, 2018. **10**(21): p. 9880-9891.
359. Singh, A., et al., *Multifunctional photonics nanoparticles for crossing the blood–brain barrier and effecting optically trackable brain theranostics*. Advanced functional materials, 2016. **26**(39): p. 7057-7066.
360. Qian, M., et al., *Highly crystalline multicolor carbon nanodots for dual-modal imaging-guided photothermal therapy of glioma*. ACS applied materials & interfaces, 2018. **10**(4): p. 4031-4040.
361. Ruan, S., et al., *A simple one-step method to prepare fluorescent carbon dots and their potential application in non-invasive glioma imaging*. Nanoscale, 2014. **6**(17): p. 10040-10047.
362. Zheng, M., et al., *Self-targeting fluorescent carbon dots for diagnosis of brain cancer cells*. ACS Nano 9: 11455–11461. 2015.
363. Lu, S., et al., *Hydrothermal synthesis of nitrogen-doped carbon dots with real-time live-cell imaging and blood–brain barrier penetration capabilities*. International journal of nanomedicine, 2016. **11**: p. 6325.
364. Borisova, T., et al., *Neuromodulatory properties of fluorescent carbon dots: effect on exocytotic release, uptake and ambient level of glutamate and GABA in brain nerve terminals*. The International Journal of Biochemistry & Cell Biology, 2015. **59**: p. 203-215.
365. Hu, Q., et al., *Green synthesis of fluorescent nitrogen/sulfur-doped carbon dots and investigation of their properties by HPLC coupled with mass spectrometry*. RSC Advances, 2014. **4**(35): p. 18065-18073.
366. Li, H., et al., *Synthesis of fluorescent carbon nanoparticles directly from active carbon via a one-step ultrasonic treatment*. Materials Research Bulletin, 2011. **46**(1): p. 147-151.
367. Wang, F., et al., *Highly luminescent organosilane-functionalized carbon dots*. Advanced Functional Materials, 2011. **21**(6): p. 1027-1031.
368. Dong, Y., et al., *Blue luminescent graphene quantum dots and graphene oxide prepared by tuning the carbonization degree of citric acid*. Carbon, 2012. **50**(12): p. 4738-4743.
369. Tang, L., et al., *Deep ultraviolet photoluminescence of water-soluble self-passivated graphene quantum dots*. ACS nano, 2012. **6**(6): p. 5102-5110.
370. Yan, F., et al., *The fluorescence mechanism of carbon dots, and methods for tuning their emission color: A review*. Microchimica Acta, 2019. **186**(8): p. 1-37.

371. Li, X., et al., *Engineering surface states of carbon dots to achieve controllable luminescence for solid-luminescent composites and sensitive Be²⁺ detection*. Scientific reports, 2014. **4**(1): p. 1-8.
372. Kumar, P., et al., *A review on advancements in carbon quantum dots and their application in photovoltaics*. RSC advances, 2022. **12**(8): p. 4714-4759.
373. Zuo, P., et al., *A review on syntheses, properties, characterization and bioanalytical applications of fluorescent carbon dots*. Microchimica Acta, 2016. **183**(2): p. 519-542.
374. Shinde, D.B. and V.K. Pillai, *Electrochemical preparation of luminescent graphene quantum dots from multiwalled carbon nanotubes*. Chemistry—A European Journal, 2012. **18**(39): p. 12522-12528.
375. Zhao, C., et al., *Synthesis of BiOBr/carbon quantum dots microspheres with enhanced photoactivity and photostability under visible light irradiation*. Applied Catalysis A: General, 2016. **527**: p. 127-136.
376. Bishnoi, A., S. Kumar, and N. Joshi, *Wide-angle X-ray diffraction (WAXRD): technique for characterization of nanomaterials and polymer nanocomposites*, in *Microscopy methods in nanomaterials characterization*. 2017, Elsevier. p. 313-337.
377. Liu, R., et al., *Bottom-up fabrication of photoluminescent graphene quantum dots with uniform morphology*. Journal of the American Chemical Society, 2011. **133**(39): p. 15221-15223.
378. Mao, L.-H., et al., *Facile access to white fluorescent carbon dots toward light-emitting devices*. Industrial & Engineering Chemistry Research, 2014. **53**(15): p. 6417-6425.
379. Bourlinos, A.B., et al., *Surface functionalized carbogenic quantum dots*. small, 2008. **4**(4): p. 455-458.
380. Keeler, J., *Understanding NMR spectroscopy, chapter 2*. University of California, Irvine, retrieved, 2007.
381. Hornak, J., *The Basics of NMR-A non-technical overview of NMR theory, equipment, and techniques*. 2018.
382. Kundu, A., et al., *Facile approach to synthesize highly fluorescent multicolor emissive carbon dots via surface functionalization for cellular imaging*. Journal of colloid and interface science, 2018. **513**: p. 505-514.
383. Peng, J., et al., *Graphene quantum dots derived from carbon fibers*. Nano letters, 2012. **12**(2): p. 844-849.
384. Griffiths, P.R., *Fourier transform infrared spectrometry*. Science, 1983. **222**(4621): p. 297-302.
385. Tougaard, S.M., *X-ray Photoelectron Spectroscopy-Elsevier Reference Module in Chemistry, Molecular Sciences and Chemical Engineering*, in *Elsevier Reference Module in Chemistry, Molecular Sciences and Chemical Engineering*. 2013, Elsevier.
386. Anastas, P.T., *Green engineering and sustainability*. 2003, ACS Publications.
387. Sharma, V., et al., *Green, sustainable, and economical synthesis of fluorescent nitrogen-doped carbon quantum dots for applications in optical displays and light-emitting diodes*. Materials Today Sustainability, 2022. **19**: p. 100184.
388. Liu, Y., et al., *Selective and sensitive chemosensor for lead ions using fluorescent carbon dots prepared from chocolate by one-step hydrothermal method*. Sensors and Actuators B: Chemical, 2016. **237**: p. 597-604.
389. Zhang, Z., et al., *Carbon quantum dots: synthesis, characterization, and assessment of cytocompatibility*. Journal of Materials Science: Materials in Medicine, 2015. **26**(7): p. 1-7.
390. Lai, Z., et al., *Green synthesis of fluorescent carbon dots from cherry tomatoes for highly effective detection of trifluralin herbicide in soil samples*. ChemistrySelect, 2020. **5**(6): p. 1956-1960.

391. Saxena, M. and S. Sarkar, *Fluorescence imaging of human erythrocytes by carbon nanoparticles isolated from food stuff and their fluorescence enhancement by blood plasma*. *Materials Express*, 2013. **3**(3): p. 201-209.
392. Roodbar Shojaei, T., et al., *Multivariable optimization of carbon nanoparticles synthesized from waste facial tissues by artificial neural networks, new material for downstream quenching of quantum dots*. *Journal of Materials Science: Materials in Electronics*, 2019. **30**(3): p. 3156-3165.
393. Wang, R.-C., J.-T. Lu, and Y.-C. Lin, *High-performance nitrogen doped carbon quantum dots: facile green synthesis from waste paper and broadband photodetection by coupling with ZnO nanorods*. *Journal of Alloys and Compounds*, 2020. **813**: p. 152201.
394. Olmos-Moya, P.M., et al., *High added value functionalized carbon quantum dots synthesized from orange peels by assisted microwave solvothermal method and their performance as photosensitizer of mesoporous TiO₂ photoelectrodes*. *Carbon*, 2022. **187**: p. 216-229.
395. Adams, L. and K. Fagbenro-Owoseni, *Tunable carbon quantum dots from starch via microwave assisted carbonization*. 2017.
396. Van Ewijk, S., J.A. Stegemann, and P. Ekins, *Global life cycle paper flows, recycling metrics, and material efficiency*. *Journal of Industrial Ecology*, 2018. **22**(4): p. 686-693.
397. Lim, S.Y., W. Shen, and Z. Gao, *Carbon quantum dots and their applications*. *Chemical Society Reviews*, 2015. **44**(1): p. 362-381.
398. Pan, L., et al., *Truly fluorescent excitation-dependent carbon dots and their applications in multicolor cellular imaging and multidimensional sensing*. *Advanced materials*, 2015. **27**(47): p. 7782-7787.
399. Sharma, A., et al., *Origin of excitation dependent fluorescence in carbon nanodots*. *The journal of physical chemistry letters*, 2016. **7**(18): p. 3695-3702.
400. Chaudhary, S., et al., *Potential prospects for carbon dots as a fluorescence sensing probe for metal ions*. *RSC advances*, 2016. **6**(93): p. 90526-90536.
401. De, B. and N. Karak, *A green and facile approach for the synthesis of water soluble fluorescent carbon dots from banana juice*. *Rsc Advances*, 2013. **3**(22): p. 8286-8290.
402. Vogel, R., et al., *High-resolution single particle zeta potential characterisation of biological nanoparticles using tunable resistive pulse sensing*. *Scientific reports*, 2017. **7**(1): p. 1-13.
403. Nimesh, S., R. Chandra, and N. Gupta, *Advances in nanomedicine for the delivery of therapeutic nucleic acids*. 2017: Woodhead Publishing.
404. Heinrichs, A., *Stains and fluorescent dyes*. *Nature Cell Biology*, 2009. **11**(1): p. S7-S7.
405. Forterre, A., et al., *Proteomic analysis of C2C12 myoblast and myotube exosome-like vesicles: a new paradigm for myoblast-myotube cross talk?* *PloS one*, 2014. **9**(1).
406. Dehghani, A., et al., *Collagen derived carbon quantum dots for cell imaging in 3D scaffolds via two-photon spectroscopy*. *Carbon*, 2018. **131**: p. 238-245.
407. McKee, C. and G.R. Chaudhry, *Advances and challenges in stem cell culture*. *Colloids and Surfaces B: Biointerfaces*, 2017. **159**: p. 62-77.
408. Xu, Y., et al., *Reduced carbon dots versus oxidized carbon dots: photo- and electrochemiluminescence investigations for selected applications*. *Chemistry–A European Journal*, 2013. **19**(20): p. 6282-6288.
409. Arumugam, S.S., et al., *Facile preparation of fluorescent carbon quantum dots from denatured sour milk and its multifunctional applications in the fluorometric determination of gold ions, in vitro bioimaging and fluorescent polymer film*. *Journal of Photochemistry and Photobiology A: Chemistry*, 2020. **401**: p. 112788.

410. Guo, J., et al., *Photoluminescent hybrids of cellulose nanocrystals and carbon quantum dots as cytocompatible probes for in vitro bioimaging*. *Biomacromolecules*, 2017. **18**(7): p. 2045-2055.
411. Kaur, N., et al., "*Vigna radiata*" based green C-dots: photo-triggered theranostics, fluorescent sensor for extracellular and intracellular iron (III) and multicolor live cell imaging probe. *Sensors and Actuators B: Chemical*, 2019. **291**: p. 275-286.
412. Priyadarshini, E., et al., *Antifungal efficacy of Au@ carbon dots nanoconjugates against opportunistic fungal pathogen, Candida albicans*. *Colloids and Surfaces B: Biointerfaces*, 2018. **163**: p. 355-361.
413. Kumarathasan, P., et al., *Cytotoxicity of carbon nanotube variants: a comparative in vitro exposure study with A549 epithelial and J774 macrophage cells*. *Nanotoxicology*, 2015. **9**(2): p. 148-161.
414. Ouyang, S., X. Hu, and Q. Zhou, *Envelopment–internalization synergistic effects and metabolic mechanisms of graphene oxide on single-cell Chlorella vulgaris are dependent on the nanomaterial particle size*. *ACS Applied Materials & Interfaces*, 2015. **7**(32): p. 18104-18112.
415. Chen, M., et al., *Toxicity of carbon nanomaterials to plants, animals and microbes: Recent progress from 2015-present*. *Chemosphere*, 2018. **206**: p. 255-264.
416. Yan, J., et al., *The effect of surface charge on the cytotoxicity and uptake of carbon quantum dots in human umbilical cord derived mesenchymal stem cells*. *Colloids and Surfaces B: Biointerfaces*, 2018. **171**: p. 241-249.
417. Dhawan, A. and V. Sharma, *Toxicity assessment of nanomaterials: methods and challenges*. *Analytical and bioanalytical chemistry*, 2010. **398**(2): p. 589-605.
418. Li, W., et al., *Phytotoxicity, uptake, and translocation of fluorescent carbon dots in mung bean plants*. *ACS applied materials & interfaces*, 2016. **8**(31): p. 19939-19945.
419. Chen, J., et al., *The effect and fate of water-soluble carbon nanodots in maize (Zea mays L.)*. *Nanotoxicology*, 2016. **10**(6): p. 818-828.
420. Yaffe, D. and O. Saxel, *Serial passaging and differentiation of myogenic cells isolated from dystrophic mouse muscle*. *Nature*, 1977. **270**(5639): p. 725-727.
421. K. Anpalagan, K., et al., *Bioimaging of C2C12 Muscle Myoblasts Using Fluorescent Carbon Quantum Dots Synthesized from Bread*. *Nanomaterials*, 2020. **10**(8): p. 1575.
422. Stockert, J.C., et al., *Tetrazolium salts and formazan products in Cell Biology: Viability assessment, fluorescence imaging, and labeling perspectives*. *Acta histochemica*, 2018. **120**(3): p. 159-167.
423. Karakkat, J.V., et al., *The metabolic sensor PASK is a histone 3 kinase that also regulates H3K4 methylation by associating with H3K4 MLL2 methyltransferase complex*. *Nucleic acids research*, 2019. **47**(19): p. 10086-10103.
424. Nie, X., et al., *An appropriate loading control for western blot analysis in animal models of myocardial ischemic infarction*. *Biochemistry and biophysics reports*, 2017. **12**: p. 108-113.
425. Reza, M.T., *Upgrading biomass by hydrothermal and chemical conditioning*. 2013: University of Nevada, Reno.
426. Zhu, L., et al., *Mild Acidolysis-Assisted Hydrothermal Carbonization of Lignin for Simultaneous Preparation of Green and Blue Fluorescent Carbon Quantum Dots*. *ACS Sustainable Chemistry & Engineering*, 2022. **10**(30): p. 9888-9898.
427. Berge, N.D., et al., *Hydrothermal carbonization of municipal waste streams*. *Environmental science & technology*, 2011. **45**(13): p. 5696-5703.
428. Bandura, A.V. and S.N. Lvov, *The ionization constant of water over wide ranges of temperature and density*. *Journal of physical and chemical reference data*, 2006. **35**(1): p. 15-30.

429. Kesberg, A.I. and D. Schleheck, *Improved protocol for recovery of bacterial DNA from water filters: Sonication and backflushing of commercial syringe filters*. Journal of microbiological methods, 2013. **93**(1): p. 55-57.
430. de Yro, P.A.N., et al. *Hydrothermal synthesis of carbon quantum dots from biowaste for bio-imaging*. in *AIP conference proceedings*. 2019. AIP Publishing LLC.
431. Khan, Z.M., et al., *Hydrothermal treatment of red lentils for the synthesis of fluorescent carbon quantum dots and its application for sensing Fe³⁺*. Optical Materials, 2019. **91**: p. 386-395.
432. Shen, T., et al., *Hydrothermal synthesis of carbon quantum dots using different precursors and their combination with TiO₂ for enhanced photocatalytic activity*. Ceramics International, 2018. **44**(10): p. 11828-11834.
433. Sun, Z., et al., *Origin of green luminescence in carbon quantum dots: specific emission bands originate from oxidized carbon groups*. New Journal of Chemistry, 2018. **42**(6): p. 4603-4611.
434. Wiercigroch, E., et al., *Raman and infrared spectroscopy of carbohydrates: A review*. Spectrochimica Acta Part A: Molecular and Biomolecular Spectroscopy, 2017. **185**: p. 317-335.
435. Li, M., et al., *Fingerprinting photoluminescence of functional groups in graphene oxide*. Journal of Materials Chemistry, 2012. **22**(44): p. 23374-23379.
436. Kubo, T., T. Isobe, and M. Senna, *Enhancement of photoluminescence of ZnS: Mn nanocrystals modified by surfactants with phosphate or carboxyl groups via a reverse micelle method*. Journal of Luminescence, 2002. **99**(1): p. 39-45.
437. Das, P., et al., *Tailor made magnetic nanolights: Fabrication to cancer theranostics applications*. Nanoscale Advances, 2021.
438. Azam, N., M. Najabat Ali, and T. Javaid Khan, *Carbon Quantum Dots for Biomedical Applications: Review and Analysis*. Frontiers in Materials, 2021: p. 272.
439. Jonkman, J., C.M. Brown, and R.W. Cole, *Quantitative confocal microscopy: beyond a pretty picture*, in *Methods in cell biology*. 2014, Elsevier. p. 113-134.
440. Sommer, M.E., et al., *Structure-based biophysical analysis of the interaction of rhodopsin with G protein and arrestin*, in *Methods in enzymology*. 2015, Elsevier. p. 563-608.
441. Li, M., et al., *Solvothermal conversion of coal into nitrogen-doped carbon dots with singlet oxygen generation and high quantum yield*. Chemical Engineering Journal, 2017. **320**: p. 570-575.
442. Zhu, S., et al., *Highly photoluminescent carbon dots for multicolor patterning, sensors, and bioimaging*. Angewandte Chemie, 2013. **125**(14): p. 4045-4049.
443. Oliveira, A.C.N., et al., *Counter ions and constituents combination affect DODAX: MO nanocarriers toxicity in vitro and in vivo*. Toxicology research, 2016. **5**(4): p. 1244-1255.
444. Rizzo, L.Y., et al., *In vivo nanotoxicity testing using the zebrafish embryo assay*. Journal of Materials Chemistry B, 2013. **1**(32): p. 3918-3925.
445. Bar-Ilan, O., et al., *Toxicity assessments of multisized gold and silver nanoparticles in zebrafish embryos*. Small, 2009. **5**(16): p. 1897-1910.
446. Vandarkuzhali, S.A.A., et al., *Pineapple peel-derived carbon dots: applications as sensor, molecular keypad lock, and memory device*. ACS omega, 2018. **3**(10): p. 12584-12592.
447. Niu, W.-J., et al., *Ethylenediamine-assisted hydrothermal synthesis of nitrogen-doped carbon quantum dots as fluorescent probes for sensitive biosensing and bioimaging*. Sensors and Actuators B: Chemical, 2015. **218**: p. 229-236.

448. Zheng, J., et al., *An efficient synthesis and photoelectric properties of green carbon quantum dots with high fluorescent quantum yield*. *Nanomaterials*, 2020. **10**(1): p. 82.
449. Wu, M., et al., *Preparation of functionalized water-soluble photoluminescent carbon quantum dots from petroleum coke*. *Carbon*, 2014. **78**: p. 480-489.
450. Lin, X., et al., *Encapsulation of strongly fluorescent carbon quantum dots in metal-organic frameworks for enhancing chemical sensing*. *Analytical chemistry*, 2014. **86**(2): p. 1223-1228.
451. Porter, M.A. and A.M. Jones, *Variability in soy flour composition*. *Journal of the American Oil Chemists' Society*, 2003. **80**(6): p. 557-562.
452. Penniston, K.L., et al., *Quantitative assessment of citric acid in lemon juice, lime juice, and commercially-available fruit juice products*. *Journal of Endourology*, 2008. **22**(3): p. 567-570.
453. Zhang, X., et al., *Surfactant modification of aggregation-induced emission material as biocompatible nanoparticles: Facile preparation and cell imaging*. *Nanoscale*, 2013. **5**(1): p. 147-150.
454. Gao, M.X., et al., *A surfactant-assisted redox hydrothermal route to prepare highly photoluminescent carbon quantum dots with aggregation-induced emission enhancement properties*. *Chemical Communications*, 2013. **49**(73): p. 8015-8017.
455. Liu, J., et al., *One-step preparation of nitrogen-doped and surface-passivated carbon quantum dots with high quantum yield and excellent optical properties*. *Rsc Advances*, 2014. **4**(15): p. 7648-7654.
456. *Living healthily in a chemical world*. The European Environment Agency, 2020.
457. Cohen, A. and F. vom Saal, *Non-toxic: Guide to Living Healthy in a Chemical World*. 2020: Dr Weil's Healthy Living Guides.
458. Liu, T.-M., et al., *Revisiting the classification of NIR-absorbing/emitting nanomaterials for in vivo bioapplications*. *NPG Asia Materials*, 2016. **8**(8): p. e295-e295.
459. Ramalingam, V. and I. Hwang, *Zinc oxide nanoparticles promoting the formation of myogenic differentiation into myotubes in mouse myoblast C2C12 cells*. *Journal of Industrial and Engineering Chemistry*, 2020. **83**: p. 315-322.
460. Heremans, H., et al., *In vitro cultivation of human tumor tissues II. Morphological and virological characterization of three cell lines*. *Oncology*, 1978. **35**(6): p. 246-252.
461. Clark, M.J., et al., *U87MG decoded: the genomic sequence of a cytogenetically aberrant human cancer cell line*. *PLoS genetics*, 2010. **6**(1): p. e1000832.
462. Sheets, R., *History and Characterization of the Vero Cell Line for Vaccines and Related Biological Products Advisory Committee*. FDA. www.fda.gov/ohrms/dockets/ac/00/backgrd/3616b1a.pdf, 2000.
463. Yasumura, Y., *The research for the SV40 by means of tissue culture technique*. *Nippon Rinsho*, 1963. **21**(6): p. 1201-1219.
464. Shimizu, B., *In Seno K. Koyama H, Kuroki T, Manual of selected cultured cell lines for bioscience and biotechnology (in Japanese)*, Tokyo, Kyoritsu Shuppan, 1993: p. 299-300.
465. Osada, N., et al., *The genome landscape of the african green monkey kidney-derived vero cell line*. *DNA research*, 2014. **21**(6): p. 673-683.
466. Ooi, A., et al., *A guide to transient expression of membrane proteins in HEK-293 cells for functional characterization*. *Frontiers in physiology*, 2016. **7**: p. 300.
467. Ryan, M.J., et al., *HK-2: an immortalized proximal tubule epithelial cell line from normal adult human kidney*. *Kidney international*, 1994. **45**(1): p. 48-57.
468. Tan, X., et al., *Differences of four catechins in cell cycle arrest and induction of apoptosis in LoVo cells*. *Cancer letters*, 2000. **158**(1): p. 1-6.

469. Lea, T., *Caco-2 cell line*. The impact of food bioactives on health, 2015: p. 103-111.
470. Fogh, J., J.M. Fogh, and T. Orfeo, *One hundred and twenty-seven cultured human tumor cell lines producing tumors in nude mice*. Journal of the National Cancer Institute, 1977. **59**(1): p. 221-226.
471. Hidalgo, I.J., T.J. Raub, and R.T. Borchardt, *Characterization of the human colon carcinoma cell line (Caco-2) as a model system for intestinal epithelial permeability*. Gastroenterology, 1989. **96**(2): p. 736-749.
472. Artursson, P., *Epithelial transport of drugs I. A model for studying the transport of drugs (β -blocking agents) over an intestinal epithelial cell line (Caco-2)*. J. Pharm. Sci, 1990. **79**: p. 476-482.
473. Torres, F.M., et al., *Pre-Plated Cell Lines for ADMETox Applications in the Pharmaceutical Industry*. Current Protocols in Toxicology, 2015. **65**(1): p. 23.8. 1-23.8. 23.
474. Shukla, D., et al., *Sandalwood-derived carbon quantum dots as bioimaging tools to investigate the toxicological effects of malachite green in model organisms*. Chemosphere, 2020. **248**: p. 125998.
475. Cloutier, M., et al., *Long-term stability of hydrogenated DLC coatings: Effects of aging on the structural, chemical and mechanical properties*. Diamond and related materials, 2014. **48**: p. 65-72.
476. Strickberger, M.W., B.K. Hall, and B. Hallgrimsson, *Strickberger's Evolution: the integration of genes, organisms and populations*. 2008: Jones and Bartlett.
477. Morisaki, J.H., J.E. Heuser, and L.D. Sibley, *Invasion of *Toxoplasma gondii* occurs by active penetration of the host cell*. Journal of cell science, 1995. **108**(6): p. 2457-2464.
478. Niller, H.H. and J. Minarovits, *Patho-epigenetics of infectious diseases caused by intracellular bacteria*. Patho-epigenetics of infectious disease, 2016: p. 107-130.
479. Curtiss, R., *Bacterial infectious disease control by vaccine development*. The Journal of clinical investigation, 2002. **110**(8): p. 1061-1066.
480. Scannapieco, F.A., *Role of oral bacteria in respiratory infection*. Journal of periodontology, 1999. **70**(7): p. 793-802.
481. Slonczewski, J.L. and J.W. Foster, *Microbiology: An evolving science: Third international student edition*. 2013: WW Norton & Company.
482. Sanchez-Perez, A., et al., *Considerations on bacterial nucleoids*. 2017.
483. Bobik, T.A., *Polyhedral organelles compartmenting bacterial metabolic processes*. Applied Microbiology and Biotechnology, 2006. **70**(5): p. 517-525.
484. Yeates, T.O., et al., *Protein-based organelles in bacteria: carboxysomes and related microcompartments*. Nature Reviews Microbiology, 2008. **6**(9): p. 681-691.
485. Kerfeld, C.A., et al., *Protein structures forming the shell of primitive bacterial organelles*. Science, 2005. **309**(5736): p. 936-938.
486. Gitai, Z., *The new bacterial cell biology: moving parts and subcellular architecture*. Cell, 2005. **120**(5): p. 577-586.
487. Shih, Y.-L. and L. Rothfield, *The bacterial cytoskeleton*. Microbiology and Molecular Biology Reviews, 2006. **70**(3): p. 729-754.
488. Norris, V., et al., *Functional taxonomy of bacterial hyperstructures*. Microbiology and Molecular Biology Reviews, 2007. **71**(1): p. 230-253.
489. Lee, D.-E., et al., *Multifunctional nanoparticles for multimodal imaging and theragnosis*. Chemical Society Reviews, 2012. **41**(7): p. 2656-2672.
490. Seo, M.-D., et al., *HaCaT keratinocytes and primary epidermal keratinocytes have different transcriptional profiles of cornified envelope-associated genes to T helper cell cytokines*. Biomolecules & therapeutics, 2012. **20**(2): p. 171.

491. Wang, X., et al., *Green preparation of fluorescent carbon quantum dots from cyanobacteria for biological imaging*. *Polymers*, 2019. **11**(4): p. 616.
492. He, M., et al., *Material and optical properties of fluorescent carbon quantum dots fabricated from lemon juice via hydrothermal reaction*. *Nanoscale Research Letters*, 2018. **13**(1): p. 1-7.
493. Atchudan, R., et al., *Green synthesized multiple fluorescent nitrogen-doped carbon quantum dots as an efficient label-free optical nanoprobe for in vivo live-cell imaging*. *Journal of Photochemistry and Photobiology A: Chemistry*, 2019. **372**: p. 99-107.
494. Surendran, P., et al., *Facile preparation of high fluorescent carbon quantum dots from orange waste peels for nonlinear optical applications*. *Luminescence*, 2020. **35**(2): p. 196-202.
495. Zhu, C., J. Zhai, and S. Dong, *Bifunctional fluorescent carbon nanodots: green synthesis via soy milk and application as metal-free electrocatalysts for oxygen reduction*. *Chemical communications*, 2012. **48**(75): p. 9367-9369.
496. Gao, S., et al., *A green one-arrow-two-hawks strategy for nitrogen-doped carbon dots as fluorescent ink and oxygen reduction electrocatalysts*. *Journal of Materials Chemistry A*, 2014. **2**(18): p. 6320-6325.
497. Qin, X., et al., *Green, low-cost synthesis of photoluminescent carbon dots by hydrothermal treatment of willow bark and their application as an effective photocatalyst for fabricating Au nanoparticles–reduced graphene oxide nanocomposites for glucose detection*. *Catalysis Science & Technology*, 2013. **3**(4): p. 1027-1035.
498. Yang, L., et al., *Facile Synthesis of Fluorescent Nitrogen-Doped Carbon Quantum Dots Using Scindapsus as a Carbon Source*. *physica status solidi (a)*, 2019. **216**(4): p. 1800404.
499. Du, W., et al., *Green synthesis of fluorescent carbon quantum dots and carbon spheres from pericarp*. *Science China Chemistry*, 2015. **58**(5): p. 863-870.

Appendix

Human bone osteosarcoma cells (MG63), brain epithelial glioblastoma cells (U87), kidney cell lines (Vero, HEK293, HK2), and Colon carcinoma cell lines (LoVo, Caco-2)

The MG-63 is a cell line that has fibroblast morphology isolated from the bone of a White, 14-year-old male patient with osteosarcoma [460]. The U87 cell line has an epithelial morphology and was obtained from a 44-year-old female patient in 1966 at Uppsala University [461]. In contrast, Vero cells are a lineage of cells used in cell cultures and was isolated from kidney epithelial cells extracted from an African green monkey [462]. The lineage was developed on 27 March 1962, by Yasumura and Kawakita at the Chiba University in Chiba, Japan [463]. The original cell line was named 'Vero' after an abbreviation of *verda reno*, which means 'green kidney' in Esperanto, while Vero itself means 'truth' in Esperanto [464]. Vero cells were used for many purposes including screening for the toxicity of *Escherichia coli* [465]. The HEK293 cell line which comprises of immortalized human embryonic kidney cells is one of the most extensively used cell lines in research. Since its isolation in the 1970s from a female fetus, this robust and fast-growing cell line and its derivatives have been used widely in receptor signalling, cancer research, and large-scale protein production. Currently, they are also commonly used in CRISPR-based genome engineering studies. The morphology of HEK293 cell is epithelial. However, the exact characteristic of cell that was originally isolated from the fetal kidney is unknown, as the cells were not completely characterized before they were immortalized. Embryonic kidneys primarily comprise of endothelial, epithelial and fibroblast cells, hence HEK293 are most likely one of these cell types. However, it has been figured out that they were, in fact, neuronal

cells, based on the presence of certain mRNA and gene products [466]. The HK-2 cells are derived from a normal, human adult male kidney and these cell line has applications in toxicology research [467]. The LoVo is a cell line isolated in 1971 from the large intestine of a White, 56-year-old, male with grade IV Dukes C colorectal cancer patient. LoVo cells can be used for cancer, toxicology, and immuno-oncology research [468]. The Caco-2 is an immortalized cell line of human colorectal adenocarcinoma cells. It was mainly used as a model of the intestinal epithelial barrier [469]. Caco-2 cells has the ability to spontaneously differentiate into a heterogeneous mixture of intestinal epithelial cells. It was developed in 1977 by Jorgen Fogh at the Sloan-Kettering Institute for Cancer Research [470]. The Caco-2 cells are most generally used not as individual cells, but as a confluent monolayer on a cell culture insert filter (e.g., Trans well). When cultured in this format, the cells differentiate to create a polarized epithelial cell monolayer that provides a physical and biochemical barrier to the passage of ions and small molecules [471, 472]. The Caco-2 monolayer is well utilized across the pharmaceutical industry as an in vitro model of the human small intestinal mucosa to study the absorption of orally administered drugs with various kits such as the “Caco Ready” [473].

Sahu et al. used orange juice to derive green CQDs and utilized them in imaging studies using L929 and human osteosarcoma (MG-63) cell lines. The quantum efficiency of the emissions of these CQDs at 455nm was 26% [473]. Recently, CQDs fabricated hydrothermally from sandalwood precursors exhibited good fluorescence in both cytoplasm and nucleus of MG63 cells [474]. The CQDs synthesized using biomass precursors produced by the palm oil also used for imaging in the Vero cell-line [475]. Another batch of CQDs from onion waste were utilized in HEK-293 and HeLa cells imaging [110]. The Bioimaging of LN-229 and HK-2 cell-lines were performed by the

CQDs produced from cinnamon, red chili, turmeric, and black pepper precursors. In this study, it was reported that the uptake in cancer cells is higher than non-cancerous cells. Hence these CQDs can be used to identify cancer cells [116]. The fluorescent CQDs with 4.5nm in size produced from pear, avocado and kiwi fruit precursors have been used for imaging of epithelial human kidney cells HK-2 and epithelial human colorectal adenocarcinoma Caco-2 cell-lines [108]. The CQDs with a lower quantum efficiency compared to the other green-CQDs were produced via the hydrothermal method using bee pollens and used in LoVo human colon carcinoma cell-line imaging [97].

Bacteria and other cell lines

The bacteria is a free-living organisms, often consisting of one biological cell. They comprise a large domain of prokaryotic micro-organisms and typically a few micrometres in length. Bacterias were among the first life systems to appear on Earth around 4 billion years ago [476], and exist in most of its habitats. Humans and most of the other animals have millions of bacteria in and on their bodies. Most bacterias are in the gut, and there are many on the skin. Generally, most of the bacteria in and on the body are harmless and some of them are beneficial for health due to their participation in the protective effects of the immune system [477], particularly the ones in the gut. However, several species of bacteria are pathogenic and cause infectious diseases, including cholera, syphilis, anthrax, leprosy, tuberculosis, tetanus and bubonic plague [478, 479]. The most common fatal bacterial diseases that affect human around the globe are respiratory infections [480]. The bacterial cell is encircled by a cell membrane, which is made mainly of phospholipids. This membrane covers the contents

of the cell and acts as a barrier to withheld the nutrients, proteins and other important components of the cytoplasm within the cell [481]. Bacterias are not like eukaryotic cells, they generally don't have large membrane-bound structures in their cytoplasm such as a nucleus, mitochondria, chloroplasts and the other organelles as present in eukaryotic cells [482]. However, some bacteria contain protein-bound organelles in the cytoplasm that compartmentalize forms of bacterial metabolism [483, 484], such as the carboxysome [485]. Moreover, bacteria have a multi-component cytoskeleton to regulate the localization of proteins and nucleic acids within the cell, and to control the process of cell division [486-488].

The CQDs synthesized via the hydrothermal method from *Carica papaya* juice precursor were used for imaging of *Fusarium avenaceum* and *Pseudomonas aeruginosa* cells [488, 489]. Mehta et al. Performed bioimaging of *Mycobacterium tuberculosis*, *Pseudomonas aeruginosa* and *Magnaporthe oryzae* using CQDs derived from apple juice [99]. The bioimaging of *Escherichia coli* and *S. Cerevisiae* cells were carried out with CQDs obtained from sugar cane juice and potato precursors [37]. Besides Milk-based CQDs were also used for bioimaging of human liver cancer cell lines (SMMC-7721) [120]. Dehghani et al. performed the bioimaging of RL-14 human fetal ventricular cardiomyocytes cells fixed in a luminescent 3D printed scaffold using collagen-based CQDs [406]. Another study using CQDs with high quantum efficiency demonstrated visualization of HaCaT cells with cabbage-based CQDs [41]. HaCaT cells are the immortalized human keratinocytes and have been widely used to investigate the epidermal homeostasis and its pathophysiology [490]. Recently, a reserach has been published on Cyanobacteria biomass derivative CQDs that create a vivid distinction between cytoplasm and nucleus on the pheochromocytoma PC12 cell-

line [491]. In a study for plant cells imaging, CQDs derived from lemon juice were used [492].

In the imaging study using *Caenorhabditis elegans* as a model, consistent fluorescence in the gut tissues of the worms was evident without showing any sign of toxic effects on the nematodes. The CQDs utilized in this study were fabricated using the beetroot extract precursor [115]. In another case, CQDs were synthesized using *Phyllanthus acidus* precursor were used for high-contrast *Caenorhabditis elegans* bioimaging and in-vivo studies demonstrated that the Nitrogen doped CQDs displayed excellent biocompatibility [493].

Although, some studies declared that CQDs derived from natural resources can be used for bioimaging with the hydrothermal method but have not been experimented with cell-line. In these form of studies, orange waste peel [267, 494], soy milk [495], willow bark, and leaves [496, 497], *Scindapsus* leaves [498] and orange pericarp [499] were reported as carbon sources.

Now, the techniques that convert these precursors into carbon quantum dots are reviewed in the following section.